Geochemical and Photochemical Constraints on S[IV] Concentrations in Natural Waters on Prebiotic Earth

Sukrit Ranjan[1], Khaled Abdelazim[2], Gabriella G Lozano[2], Sangita Mandal[3], Cindy Y Zhou[4], Corinna L Kufner[2], Zoe R Todd[5], Nita Sahai[6], and Dimitar D Sasselov[2]

[1]University of Arizona
[2]Harvard University
[3]National Institute of Science Education and Research
[4]Boston University
[5]University of Washington
[6]University of Akron

May 25, 2023

Abstract

Sulfur is important to planetary habitability, but the early sulfur cycle is poorly understood. In particular, S[IV] species (HSO_3^-, SO_3^{2-}), derived from volcanogenic SO_2, are critically invoked in recent proposals for origins-of-life chemistry and also influence atmospheric sulfur haze formation, but their abundance in early natural waters is unclear. Here, we combine new laboratory constraints on the kinetics of S[IV] disproportionation with a novel aqueous photochemistry model to estimate the concentrations of S[IV] in natural waters on prebiotic Earth. We show that S[IV] disproportionation is slow in pH[?]7 waters, with timescale T[?]1 year at room temperature, meaning that S[IV] was present in prebiotic natural waters. However, we also show that photolysis of S[IV] limits [S[IV]]$<$ 100 μM in global-mean steady state. Marine S[IV] was sub-saturation with respect to atmospheric SO_2, meaning that climate-altering, UV-attenuating sulfur hazes did not persist on prebiotic Earth. [S[IV]] was much lower in natural waters compared to the concentrations generally invoked in laboratory simulations of origins-of-life chemistry ([?]10 mM), meaning further work is needed to confirm whether S[IV]-dependent prebiotic chemistries discovered in the lab could have realistically functioned in nature. [S[IV]][?]1 μM in terrestrial waters for: (1) SO_2 outgassing [?]20× modern, (2) pond depths <10 cm, or (3) UV-attenuating agents present in early waters or the prebiotic atmosphere. Our work illustrates the synergy between planetary science, geochemistry and synthetic organic chemistry experiments in understanding the emergence and maintenance of life on early Earth.

NOTE: MANUSCRIPT IN REVISION (this version v1). SI FOLLOWS MAIN TEXT. COMMENTS, CRITICISM & QUESTIONS SOLICITED AT sukrit@arizona.edu**.**

Geochemical and Photochemical Constraints on S[IV] Concentrations in Natural Waters on Prebiotic Earth

Sukrit Ranjan[1,2,3,4,5], Khaled Abdelazim[6], Gabriella G. Lozano[7], Sangita Mandal[8], Cindy Y. Zhou[9], Corinna L. Kufner[7], Zoe R. Todd[10], Nita Sahai[11], Dimitar D. Sasselov[7]

[1]Lunar & Planetary Laboratory/Department of Planetary Sciences, University of Arizona, Tucson, AZ 85721, USA
[2]Blue Marble Space Institute of Science, Seattle, WA 98104, USA
[3]School of Earth and Planetary Sciences, National Institute of Science Education and Research, HBNI, Jatni 752050, Odisha, India
[4]Department of Physics and Astronomy & Center for Interdisciplinary Exploration and Research in Astrophysics, Northwestern University, Evanston, IL 60201, USA
[5]Department of Earth, Atmospheric and Planetary Sciences, Massachusetts Institute of Technology, Cambridge, MA 02139, USA
[6]Department of Chemistry and Chemical Biology, Harvard University, Cambridge, MA 02138, USA
[7]Harvard-Smithsonian Center for Astrophysics, Cambridge, MA 02138, USA
[8]School of Chemical Sciences, National Institute of Science Education and Research, HBNI, Jatni 752050, Odisha, India
[9]Department of Biochemistry and Molecular Biology, Boston University, Boston, MA 02215, USA
[10]Department of Earth and Space Sciences, University of Washington, Seattle, WA 98195, USA
[11]Department of Geosciences; Department of Biology; and Integrated Bioscience Program, School of Polymer Science and Polymer Engineering, University of Akron, Akron, OH 44325, USA

Key Points:

- We use new experiments and modeling to constrain S[IV] (sulfite) concentrations in marine and terrestrial waters on prebiotic Earth.
- We show that S[IV] was a prebiotic reagent, but its concentration were limited to < 100 μM by photolysis in early natural waters.
- Our work shows the need to characterize the sensitivity of proposed chemical pathways for the origin of life to S[IV] abundance.

Corresponding author: Sukrit Ranjan, sukrit@arizona.edu

Abstract

Sulfur is important to planetary habitability, but the early sulfur cycle is poorly understood. In particular, S[IV] species (HSO_3^-, SO_3^{2-}), derived from volcanogenic SO_2, are critically invoked in recent proposals for origins-of-life chemistry and also influence atmospheric sulfur haze formation, but their abundance in early natural waters is unclear. Here, we combine new laboratory constraints on the kinetics of S[IV] disproportionation with a novel aqueous photochemistry model to estimate the concentrations of S[IV] in natural waters on prebiotic Earth. We show that S[IV] disproportionation is slow in pH$\geq$ 7 waters, with timescale T$\geq$ 1 year at room temperature, meaning that S[IV] was present in prebiotic natural waters. However, we also show that photolysis of S[IV] limits [S[IV]]$<$ 100 μM in global-mean steady state. Marine S[IV] was sub-saturation with respect to atmospheric SO_2, meaning that climate-altering, UV-attenuating sulfur hazes did not persist on prebiotic Earth. [S[IV]] was much lower in natural waters compared to the concentrations generally invoked in laboratory simulations of origins-of-life chemistry ($\geq$ 10 mM), meaning further work is needed to confirm whether S[IV]-dependent prebiotic chemistries discovered in the lab could have realistically functioned in nature. [S[IV]]$\geq$ 1 μM in terrestrial waters for: (1) SO_2 outgassing $\geq$ 20$\times$ modern, (2) pond depths $<$ 10 cm, or (3) UV-attenuating agents present in early waters or the prebiotic atmosphere. Our work illustrates the synergy between planetary science, geochemistry and synthetic organic chemistry experiments in understanding the emergence and maintenance of life on early Earth.

Plain Language Summary

Sulfur cycling on early Earth is not well understood because its chemical reactions in water in the absence of biology are poorly constrained. Here, we build a new model to estimate the concentrations of a key family of sulfur molecules, S[IV] ("sulfite"), in oceans and ponds on early Earth. We build on past work by using new measurements of S[IV] reactions to calibrate our model and by including the effects of UV light. We show that S[IV] was present on early Earth, but that UV light limited its concentrations to $<$ 100 μM. This finding has significant implications for efforts to understand the origin and maintenance of early life. It means that sulfur hazes did not persist on early Earth, confirming a generally UV-rich surface environment for nascent life. It means that natural environments featured much lower S[IV] concentrations than generally considered in laboratory simulations of origin-of-life chemistry, illustrating the need to confirm whether proposed S[IV]-dependent chemical pathways can function at the lower S[IV] concentrations characteristic of realistic early Earth environments. Our work illustrates the critical role planetary science and geochemistry play in guiding and testing chemical theories of the origin and endurance of life.

1 Introduction

The abundance and speciation of sulfur in natural waters on early Earth is a key question in origin-of-life studies. Sulfur is one of the main elemental components of modern biomolecules, and sulfur-bearing molecules are critically invoked in diverse proposals for origin-of-life chemistry (Wachtershauser, 1990; G Trainer, 2013; Patel et al., 2015; Bonfio et al., 2017; Goldford et al., 2019; Li et al., 2020). Further, aqueous sulfur influence planetary habitability through regulation of atmospheric sulfur (Kasting et al., 1989; Halevy et al., 2007; Tian et al., 2010; Halevy & Head, 2014). However, direct geological constraints on the composition of terrestrial prebiotic natural waters are limited due to tectonic and hydrologic processing of the rock record (Mojzsis, 2007). In the absence of direct constraints from the rock record, understanding of sulfur speciation on early Earth is guided by theoretical modeling studies (Halevy, 2013).

Among the sulfur species, S[IV] species (SO_3^{2-}, HSO_3^-, SO_2; "sulfite"[1]) have recently emerged as being of particular importance to planetary habitability. S[IV] species are ultimately derived from the dissolution of volcanogenic SO_2 into liquid water, and are tightly linked by rapid acid/base equilibria (Kasting et al., 1989). S[IV] is important because of the key roles it has recently been demonstrated to play in synthetic organic chemistry experiments simulating potential prebiotic chemistry scenarios (J. Xu et al., 2018; Kawai et al., 2019; Liu et al., 2021), and in particular prebiotic ribonucleotide synthesis, a basic requirement for the RNA world model for the origin of life (Becker et al., 2019; J. Xu et al., 2020; Rimmer et al., 2021; Benner et al., 2019). S[IV] is also important because of the controlling role it plays in planetary sulfur cycling, and thereby on planetary climate and UV irradiation levels (Kasting et al., 1989; Tian et al., 2010; Hu et al., 2013; Halevy & Head, 2014).

Determining the concentration of S[IV] ([S[IV]]), in natural waters on prebiotic Earth is key to assessing the plausibility of S[IV]-dependent prebiotic chemistries and guiding the development of theories of the origin of life in general. On modern Earth, S[IV] is efficiently oxidized to sulfate by ambient O_2, and its concentrations are negligible in natural waters (Hegg & Hobbs, 1978; Loftus et al., 2019). However, in the anoxic atmosphere of early Earth, direct oxidation of S[IV] would have been inhibited, raising the possibility of longer lifetimes and appreciable inventories of S[IV] in some natural waters (Kasting et al., 1989; Ranjan et al., 2018).

The main uncertainty on [S[IV]] in prebiotic natural waters are the kinetics of its loss. Particularly highlighted in the literature is uncertainty regarding the rate of disproportionation of S[IV], which is proposed as the main loss mechanism (Kasting et al., 1989; Halevy, 2013). Literature estimates of the timescale of this process span > 2 orders of magnitude (Meyer et al., 1979; Guekezian et al., 1997). In addition, there are other loss mechanisms for S[IV] that are relevant to prebiotic conditions that have not been considered in estimating prebiotic S[IV] concentrations, such as photolysis (Fischer & Warneck, 1996). Finally, past modeling of S[IV] in natural waters has focused on marine waters, neglecting the diverse terrestrial waters that are invoked in numerous prebiotic chemistries.

In this work, we remediate these shortcomings. We conduct long-term experiments on S[IV] stability, constraining the kinetics of its disproportionation at room temperature. We incorporate these constraints into a simple box model, together with other loss processes like photolysis which were not previously considered for environmental S[IV]. We apply our box model to both marine and terrestrial waters, consider the prospects for the accumulation of S[IV], and explore the implications for proposed prebiotic chemistry and planetary habitability. Our analysis constitutes a significant advance over past studies because (1) we measure and leverage new chemical kinetic constraints in our model, (2) we include previously-unconsidered but important loss processes for S[IV], and (3) we consider both marine and terrestrial waters.

While we focus on the implications of our work for prebiotic chemistry on Earth, our work has broad applications for planetary habitability and sulfur cycling on rocky planets in general. In particular, it has been long debated whether the oceans on early Earth, Mars, and analogous exoplanets saturate in S[IV] with respect to the atmosphere, in which case SO_2 can accumulate in the planetary atmosphere with potential implications for planetary climate and exoplanet observables, or whether S[IV] remains sub-saturation, in which case atmospheric deposition efficiently scrubs SO_2 from the atmosphere (Kasting et al., 1989; Halevy et al., 2007; Tian et al., 2010; Hu et al., 2013; Loftus et al., 2019). We address this question as well.

[1] While sulfite formally refers only to SO_3^{2-}, it is often used as a collective shorthand for all S[IV] species (Halevy, 2013)

2 Background

2.1 Relevance of S[IV] to Prebiotic Chemistry and Planetary Habitability

S[IV] plays diverse and critical roles in synthetic organic chemical pathways for the emergence of biomolecules, and especially ribonucleotides, the monomers of RNA and a requirement for abiogenesis in the RNA world hypothesis (Higgs & Lehman, 2015). S[IV] can stabilize and concentrate simple sugars, providing the carbohydrate backbone for ribonucleotides (Pitsch et al., 2000; Kawai et al., 2019; Benner et al., 2019). Under irradiation, S[IV] releases solvated electrons, which enable high-yield syntheses of organics from CO_2 (Liu et al., 2021) as well as HCN photohomologation towards the synthesis of nucleotides, ribonucleotides and other biomolecules (J. Xu et al., 2018, 2020). Perhaps most dramatically, S[IV] underlies the only currently known pathway for the non-enzymatic synthesis of all four canonical ribonucleotides, a decades-old goal of synthetic prebiotic chemistry (Becker et al., 2019; Hud & Fialho, 2019).

S[IV] also plays an important role in planetary habitability, through regulation of atmospheric SO_2. If oceanic S[IV] is sub-saturation with respect to the atmosphere, then SO_2 efficiently deposits into the ocean by both wet and dry deposition, and atmospheric SO_2 concentrations are low (Kasting et al., 1989; Hu et al., 2013). However, if S[IV] can ever saturate the planet surface, then the depositional sink of atmospheric SO_2 is suppressed, and SO_2 can accumulate in the atmosphere with significant implications for planetary habitability. Kasting et al. (1989) showed that if early Earth featured elevated temperatures and a S[IV]-saturated surface, then an S_8 haze would have formed, blocking UV light from reaching the planetary surface. Elevated atmospheric SO_2 would also influence planetary climate, but it is uncertain exactly how. While elevated SO_2 would power an enhanced greenhouse effect, this SO_2 would also generate photochemical hazes, and it remains debated whether enhanced SO_2 would in the end be net cooling or net heating (Tian et al., 2010; Halevy & Head, 2014).

2.2 Previous Modeling of S[IV] in Natural Waters

Past consideration of S[IV] in natural waters on anoxic early Earth and similar planets has focused on marine waters. Walker and Brimblecombe (1985) muse on thermodynamic grounds that the eventual fate of S[IV] would have been oxidization to sulfate, but do not attempt estimates of its concentrations. Kasting et al. (1989) explore the possibility of an early ocean saturated in S[IV] ([S[IV]]= 1.5 mM), and show that this condition might enable a UV-blocking S_8 haze layer on early Earth. Later works extend this possibility to early Mars, exploring implications of a S[IV]-saturated ocean on planetary climate (Halevy et al., 2007; Tian et al., 2010). These works justify S[IV]-saturated oceans by the expected suppression of S[IV] disproportionation based on reaction stoichiometry. On the other hand, Loftus et al. (2019) assume sub-saturation oceanic S[IV] for anoxic Earth-like planets, and Halevy (2013) calculate sub-nanomolar marine [S[IV]] for early Earth, based on the finding of Guekezian et al. (1997) of efficient room-temperature disproportionation of S[IV]. Assumptions regarding S[IV] disproportionation kinetics control the different [S[IV]] in these works.

Consideration of S[IV] in terrestrial waters (e.g. lakes, ponds) is more limited. Recent phylogenetic evidence for ancient, exclusively sulfite-reducing metabolism operative in volcanic hot springs is consistent with the existence of sulfite-rich waters in volcanic environments on early Earth, but does not constrain the presence of S[IV] in non-volcanic environments (Colman et al., 2020; Chernyh et al., 2020). Ranjan et al. (2018) find that shallow terrestrial waters on early Earth should sustain ≥ 1 μM S[IV] concentrations, derived from dissolution of volcanogenic SO_2. However, their calculations followed previous literature in considering only thermal loss processes for S[IV], and neglected loss of S[IV] by photolysis. In this work, we remediate this omission.

2.3 Kinetics of S[IV] Disproportionation

S[IV] disproportionation is considered as the main control on S[IV] accumulation in natural waters on anoxic early Earth and similar planets in the literature, and uncertainties in its kinetics are identified as the main driver of uncertainty in model estimates of [S[IV]] (Kasting et al., 1989; Halevy et al., 2007; Halevy, 2013; Ranjan et al., 2018; Loftus et al., 2019). S[IV] disproportionates according to the reaction (Guekezian et al., 1997):

$$4SO_3^{2-} + 2H^+ \rightarrow 2SO_4^{2-} + S_2O_3^{2-} + H_2O \quad (1)$$

However, $S_2O_3^{2-}$ is itself unstable and further disproportionates. The net reaction proposed for fully equilibrated conditions is (Meyer et al., 1982):

$$3HSO_3^- \rightarrow 2SO_4^{2-} + \frac{1}{n}S_n + H^+, \ (2 < pH < 7) \quad (2)$$

$$3SO_3^{2-} + H_2O \rightarrow 2SO_4^{2-} + \frac{1}{n}S_n + 2OH^-, \ (7 < pH) \quad (3)$$

The kinetics of S[IV] disproportionation are extremely poorly constrained. High-temperature studies find S[IV] disproportionation to be autocatalytic, with activation energies of $E_A = 89$ kJ/mol ($120 - 140$°C, $\mathrm{pH}_0 = 0.6 - 1$, Ryabinina and Oshman (1972)) and $E_A = 69$ kJ/mol ($110-180$°C, pH= $2-5$, Rempel et al. (1974); T. Xu et al. (2007)) (Halevy et al., 2007; T. Xu et al., 2007). The nature and accuracy of the analytical techniques employed by Ryabinina and Oshman (1972) are not detailed, nor is it clear how rigorously O_2 was excluded, making it challenging to assess the reliability of these measurements[2]. Furthermore, Halevy et al. (2007) caution against extrapolating these measurements to cooler temperatures relevant to habitable worlds because entirely different reaction mechanisms may apply at lower temperatures, and indeed Meyer et al. (1982) report the reaction rate at 120°C to be higher than expected based on extrapolations from experiments conducted at 180°C.

If S[IV] disproportionation is poorly constrained at high temperature, it is downright contradictory at low temperatures (Table 2). Most literature studies report non-detections of S[IV] disproportionation at low temperatures, with lower limits on the room-temperature lifetime of anoxic S[IV] solutions ranging from $>$ 4 months to $\geq$ 5 years (Cohen et al., 1982; Meyer et al., 1979; Meyer et al., 1982; Petruševski et al., 2013; Halevy et al., 2007). On the other hand, Guekezian et al. (1997) reported disproportionation of room-temperature S[IV] on a timescale of 10 days. Guekezian et al. (1997) do not comment on their disagreement with prior work. A possible explanation is that Guekezian et al. (1997) worked at ultrabasic conditions (pH$>$ 12.8); perhaps these conditions facilitated S[IV] disproportionation. However, it is unclear whether high pH should facilitate S[IV] disproportionation, since from Equations 1-3, we would expect high pH to inhibit S[IV] disproportionation[3], since S[IV] disproportionation consumes H^+.

The stability of S[IV] in food storage applications (e.g., wine) is not relevant to early Earth. The stability of S[IV] in food storage is due to its stabilization by a range of organic molecules including alcohols and formaldehyde (Karchmer, 1970; de Carvalho & Schwedt, 2000). It is not known whether such organic molecules could have abiotically

[2] We were unable to locate a copy of Rempel et al. (1974), and therefore are unable to critically assess their findings. We rely on the summary of T. Xu et al. (2007) regarding the findings of Rempel et al. (1974).

[3] In a published but non-peer-reviewed annual report from Lawrence Berkeley National Laboratory, HSO_3^- is reported to be less stable than SO_3^{2-}, in accordance with stoichiometric expectation (Searcy, 1981).

accumulated in natural waters to concentrations high enough to stabilize sulfite on prebiotic Earth, and we therefore neglect this stabilization mechanism.

We conclude that the literature is highly inconsistent (> 2 orders of magnitude) regarding lifetime of S[IV] to disproportionation at temperate conditions. This conclusion motivates experiments presented in this paper, which we have conducted to provide better constraints on S[IV] disproportionation rates and lifetimes under conditions relevant for the early Earth.

2.4 S[IV] Photolysis

While past work has focused on disproportionation (Kasting et al., 1989; Halevy et al., 2007; Halevy, 2013; Loftus et al., 2019), there are other loss mechanisms for aqueous S[IV] relevant to anoxic terrestrial planets. In particular, SO_3^{2-} and HSO_3^- are efficiently photolyzed by UV-C radiation, and such radiation was abundant on early Earth and Mars(Fischer & Warneck, 1996; Cockell, 2000a). UV photolysis was earlier demonstrated to limit the accumulation of abiotic NO_X^- (nitrate, nitrite) in natural waters on early Earth and Mars (Ranjan et al., 2019; Adams et al., 2021). In this paper, we consider whether photolysis could have similarly limited the accumulation of S[IV] in natural waters on early Earth.

S[IV] photolysis is studied in the environmental science literature in the context of wastewater treatment (Yang et al., 2020; Wu et al., 2021; Cao et al., 2021). The reaction mechanism is (Fischer & Warneck, 1996):

$$SO_3^{2-} + h\nu \rightarrow SO_3^{\bullet -} + e_{aq}^- \tag{4}$$

$$HSO_3^- + h\nu \rightarrow SO_3^{\bullet -} + H^\bullet \tag{5}$$

SO_3^{2-} UV-VIS absorbance has been detected to wavelengths as long as 273 nm, but SO_3^{2-} photolyzes most efficiently at shorter wavelengths ($\leq$ 256 nm). Similarly, HSO_3^- absorption has been detected out to 320 nm, but this longwave absorption is weak and its photolysis is most efficient at $\leq$ 224 nm (Fischer & Warneck, 1996; Beyad et al., 2014). UV radiation at these wavelengths is absent on modern Earth's surface due to atmospheric oxygen and ozone, but was abundant on early Earth and early Mars (Cockell et al., 2000; Cockell, 2002; Ranjan & Sasselov, 2017; Ranjan et al., 2017).

3 Methods

We calculate the steady-state concentration of S[IV] in aqueous systems on early Earth's surface by balancing the sources ($F_{sources,S[IV]}$) and sinks ($F_{sinks,S[IV]}$) of S[IV] in a 0-D box model:

$$F_{sources,S[IV]} = F_{sinks,S[IV]} \tag{6}$$

Such box models have been extensively used to estimate solute concentrations in aqueous systems on early Earth and Mars (Kharecha et al., 2005; Halevy, 2013; Harman et al., 2013; Wong et al., 2017; Ranjan et al., 2019; Adams et al., 2021).

We consider the atmosphere as the sole source of S[IV], via wet and dry deposition of SO_2:

$$F_{sources,S[IV]} = F_{wet,S[IV]} + F_{dry,S[IV]} \tag{7}$$

We use atmospheric photochemical modeling to estimate $F_{dry,S[IV]}$ and $F_{wet,S[IV]}$ (Section 3.1). We neglect the possibility of aqueous-phase production of S[IV] due to processes like S^0 photooxidation or polythionate disproportionation, which may be relevant in specific terrestrial waters like hot springs (Johnston & McAmish, 1973; Li et al., 2020).

We consider a range of loss processes for S[IV], including disproportionation, oxidation by O_2, seepage into sediments and UV-driven photolysis:

$$F_{sinks,S[IV]} = F_{disprop,S[IV]} + F_{O_2,S[IV]} + F_{seep,S[IV]} + F_{h\nu,S[IV]} \tag{8}$$

Reports of the kinetics of room-temperature S[IV] disproportionation are contradictory in the literature; we conduct experiments to rule between the literature possibilities (Section 3.2), and incorporate them in our modeling. In addition to thermal loss processes (Section 3.3), we also consider the novel sink of direct UV photolysis of S[IV] (Section 3.4).

Combining Equations 6-8, we calculate the steady-state [S[IV]], by numerically solving:

$$F_{wet,S[IV]} + F_{dry,S[IV]} = F_{disprop,S[IV]} + F_{O_2,S[IV]} + F_{seep,S[IV]} + F_{h\nu,S[IV]} \tag{9}$$

for various terrestrial waters on prebiotic Earth, using parameters as detailed in Section 3.5. A schematic summary of our modeling approach is presented in Figure 1.

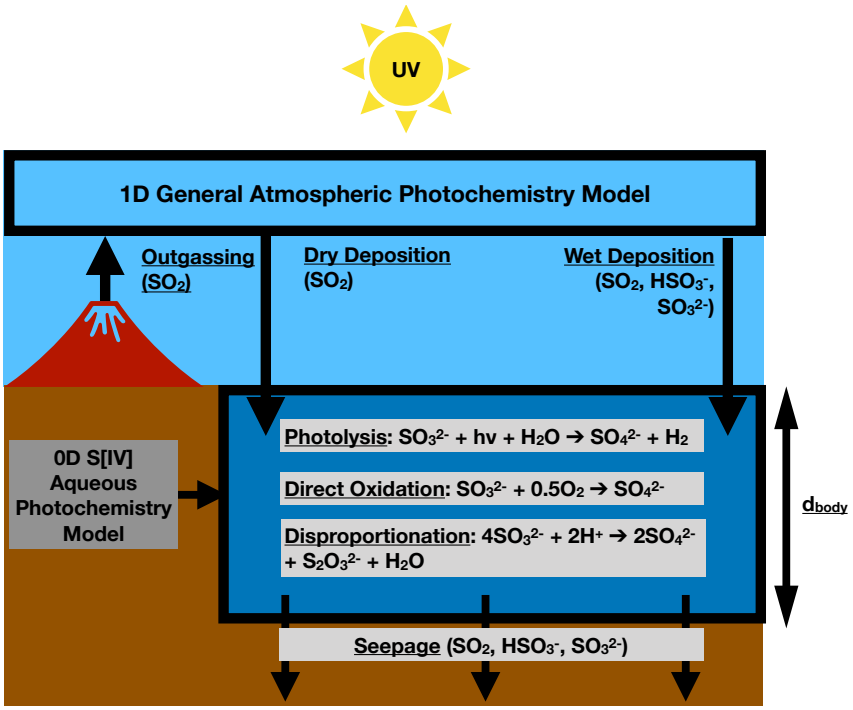

Figure 1. Schematic illustrating our model of S[IV] in natural waters on early Earth. Input of S[IV] from the atmosphere (ultimately derived from volcanic outgassing) into an aqueous body (dark blue box) via wet and dry deposition is balanced by loss of S[IV] in the aqueous body due to photolysis, direct oxidation, disproportionation, and seepage. Specification of geochemical parameters allows simulation of both marine and terrestrial waters using this modeling approach.

3.1 Atmospheric Supply of S[IV]

We model the atmosphere of early Earth and its interaction with the surface to estimate the supply of S[IV] to prebiotic natural waters ($F_{sources,S[IV]}$).

3.1.1 Photochemical Model

We use the MIT Exoplanet Atmospheric Chemistry model (MEAC) to calculate the atmospheric composition as a function of volcanic outgassing flux (Hu et al., 2012). MEAC solves the 1D continuity-transport equation to calculate the steady-state composition of a planet's atmosphere. Our version of MEAC incorporates new H_2O cross-sections and correction of errors in CO_2 cross-sections, Henry's Law estimation, and reaction rates (Ranjan et al., 2020; Hu, 2021; Ranjan, Seager, et al., 2022). Importantly, MEAC has recently been intercompared with two other models (Harman et al., 2015; G. Arney et al., 2016) for the case of prebiotic Earth-like planets, and produces consistent results as measured by pCO and O_2 false positives (Ranjan et al., 2020). MEAC encodes processes including wet and dry deposition, eddy diffusion, molecular diffusion and escape of H and H_2, formation and deposition of S_8 and H_2SO_4 aerosols, and photolysis. Shortwave radiative transfer is calculated by the δ two-stream approximation and includes gas absorption, Rayleigh scattering, and H_2SO_4 and S_8 aerosol absorption and scattering. However, MEAC does not self-consistently calculate planetary climate, meaning adjustments to the temperature-pressure profile due to photochemical effects (e.g., haze formation) must be accounted for with separate calculations.

3.1.2 Planetary Scenario

We construct our planetary scenario by modifying the abiotic CO_2-dominated benchmark atmosphere of Hu et al. (2012). SI Tables S1-S2 present the details of our planetary scenario, and we discuss the most important aspects here.

We assume bulk prebiotic atmospheric composition of 0.1 bar CO_2 and 0.9 bar N_2, which produces clement global-mean temperatures on 3.9 Ga Earth, consistent with zircon evidence interpreted as evidence of global surface oceans in this epoch (Kaltenegger et al., 2007; Rugheimer & Kaltenegger, 2018). We construct our temperature-pressure profile by assuming dry adiabatic evolution in the troposphere from a 290K surface to an isothermal 180K stratosphere (Pierrehumbert, 2010), which approximates detailed models of the prebiotic atmosphere[4] (Rugheimer & Kaltenegger, 2018). We assume an eddy diffusion profile scaled from modern Earth by atmospheric mean molecular mass (Hu et al., 2012). We estimate the TOA irradiation from the 3.9 Ga Sun from Claire et al. (2012). We include 86 CHOSN species linked by 734 reactions, excluding the higher hydrocarbon chemistry relevant to organic haze formation (Ranjan, Seager, et al., 2022). This neglect is justified because at the very low CH_4 emission rates prevalent on prebiotic Earth, higher hydrocarbon formation is negligible (DeWitt et al., 2009; G. N. Arney et al., 2017; Harman, Pavlov, et al., 2018). We include CO and NO fluxes of $3{\times}10^8$ cm^{-2} s^{-1} at the base of the atmosphere to simulate the effects of lightning (Harman, Felton, et al., 2018; Hu & Diaz, 2019).

We set volcanic outgassing fluxes by scaling modern Earth outgassing fluxes. The choice of these modern fluxes requires comment, especially the critical modern SO_2 volcanic outgassing flux ($\phi_{SO_2,0}$). Efforts to directly measure $\phi_{SO_2,0}$ yield stimates of $\phi_{SO_2,0} = 1{\times}10^9$ cm^{-2} s^{-1}, mostly emitted non-eruptively at ground level (Halmer et al., 2002; Carn et al., 2017). However, these estimates are lower bounds, because they miss the tail of weak SO_2 sources which are numerically abundant (Carn et al., 2017; Catling & Kasting, 2017). Catling and Kasting (2017) argue that $\phi_{SO_2,0} = 7 \times 10^9$ cm^{-2} s^{-1}, based on scaling CO_2 emission fluxes assuming equilibrium with modern magmas. We choose an intermediate value of $\phi_{SO_2,0} = 3 \times 10^9$ cm^{-2} s^{-1}, which has been used as a representative "Earth-like" value in the past (Hu et al., 2012). We take $\phi_{H_2S,0} = 3 \times 10^8$ cm^{-2} s^{-1}, based on the common assumption that $\frac{\phi_{H_2S,0}}{\phi_{SO_2,0}} = 0.1$ (Zahnle et al., 2006; Hu

[4] S. Rugheimer, personal communication, 10/17/2019.

et al., 2012; Claire et al., 2014). We take $\phi_{H_2,0} = 5 \times 10^9$ cm^{-2} s^{-1} and $\phi_{CO,0} = 4 \times 10^8$ cm^{-2} s^{-1} (Catling & Kasting, 2017). We assume CH_4 emission of $3{\times}10^8$ cm^{-2} s^{-1} due to serpentinization (Hu et al., 2012; Guzmán-Marmolejo et al., 2013). Serpentinization on early Earth may have been less efficient than on modern Earth (Tutolo et al., 2020); our calculations are robust to this uncertainty as CH_4 has minimal photochemical influence on SO_2.

We scale modern earth volcanic emission fluxes by $\frac{\phi}{\phi_0}$ to explore a broad range of volcanic outgassing levels. Volcanic outgassing rates on early Earth are highly uncertain (Catling & Kasting, 2017). A common assumption is for steady-state volcanic emission to have been enhanced up to an order of magnitude relative to the present day due to higher interior heat flux (Richter, 1985; Kasting et al., 1989; Sleep & Zahnle, 2001; Zahnle et al., 2006), but volcanic emission of sulfur species may also have been lower due to lower concentrations of recycled sulfur in melts due to low oceanic sulfate and sulfide (Harman, Pavlov, et al., 2018). Further, during major volcanic eruptions, volcanic outgassing may have been transiently enhanced by up to 2 orders of magnitude, though it is uncertain whether that SO_2 was released primarily from fissures (i.e., at the surface) or from cones (i.e., into the upper atmosphere where it could be processed into aerosol instead of deposited as S[IV]) (Self et al., 2006; Halevy & Head, 2014; Claire et al., 2014; Lamotte et al., 2021). We consequently consider a range of prebiotic volcanic gas emission rates relative to modern of $\frac{\phi}{\phi_0} = 0.1 - 30$, but caution that our reported pSO_2 for $\frac{\phi}{\phi_0} \gtrsim 10$ represent an upper limit because of the uncertainty regarding release altitude.

3.1.3 Dry Deposition of S[IV]

S[IV] is transferred from the atmosphere to the surface via dry[5] deposition of SO_2 (Kharecha et al., 2005). This process is the dominant removal mechanism for SO_2 for a wide range of atmospheric compositions (Hu et al., 2013; Seinfeld & Pandis, 2016). We calculate dry deposition of SO_2 via (Seinfeld & Pandis, 2016):

$$F_{dry,S[IV]} = v_{dep,SO_2} r_{SO_2}(z=0) n_{atm}(z=0) \tag{10}$$

where v_{dep,SO_2} is the dry deposition velocity of SO_2, $n_{atm}(z = 0)$ is the atmospheric number density at the surface, and $r_{SO_2}(z = 0)$ is the volume mixing ratio of SO_2 at the surface.

3.1.4 Wet Deposition of S[IV]

SO_2 can be transferred from the atmosphere to the surface by precipitation ("wet deposition"). This process is an important secondary removal mechanism for SO_2 from the modern atmosphere (Seinfeld & Pandis, 2016). We calculate atmospheric supply of S[IV] to natural waters by wet deposition of SO_2 according to the equaion:

$$F_{wet,S[IV]} = \phi_{SO_2,wet,model} \times \frac{P}{P_{model}} \tag{11}$$

where P is the precipitation rate (m year^{-1})), P_{model} is the global mean precipitation rate calculated by MEAC assuming a modern Earth-like rainout frequency, and $\phi_{SO_2,wet}$ is the global mean wet deposition rate of SO_2 calculated by MEAC (Giorgi & Chameides, 1985; Hu et al., 2012). For our temperature-pressure profile, $P_{model} = 0.9$ m year^{-1}, comparable to the modern global-mean precipitation rate of 1 m year^{-1} (Giorgi & Chameides, 1985). P is a semi-free parameter, because terrestrial waters can integrate runoff from a catchment area, which may be many times their surface area (Davies et al., 2008).

[5] This process is termed "dry" because it occurs without the mediation of rain.

Table 1. S[IV] Samples Prepared for Disproportionation Study

$[Na_2SO_3]_0^a$ (mM)	$pH_0{}^a$	λ_m (nm)	N_{samp}	Start	Solution Analytics Date	UV-Vis Through Date
100	7	260	4	10/05/21	8/20/22	8/8/22
100	13	260	4	10/05/21	8/20/22	8/8/22
100	Unadjusted	260	3[b]	10/05/21	8/20/22	8/8/22
10	Unadjusted	240	4	10/05/21	8/20/22	8/8/22

[a] At study start.
[b] 1 sample accidentally destroyed during study.

Because we are conducting steady-state modeling, we set P to balance losses due to evaporation and seepage, according to the equation:

$$P = S + E \tag{12}$$

where E is the evaporation rate and S is the seepage rate (Section 3.3.2)

3.2 Experimental Constraints on S[IV] Disproportionation Kinetics

Literature estimates of the lifetime of aqueous anoxic S[IV] near standard temperature and pressure are contradictory and fall into two time ranges: $\sim$ 10 days and $\gtrsim$ 1−5 years (Section 2.3). We conducted experiments to discriminate between these two possibilities.

We prepared solutions of sodium sulfite (Na_2SO_3) in anoxic conditions at varying concentration and pH (Table 1), and sealed them into airtight cuvettes for aging (Section 3.2.1). The reaction stoichiometry (Equations 1-3) means that S[IV] disproportionation may scale up to quartically with concentration (if the redox step is rate-limiting). Consequently, we chose a high baseline initial S[IV] concentration of 100 mM, to maximize the rate of S[IV] disproportionation and facilitate analytics. We considered solutions with unadjusted pH, and pH adjusted to 7 and 13, to explore the effect of pH. We also considered an unadjusted solution at a lower S[IV] concentration of 10 mM. We did not consider S[IV] concentrations higher than 100 mM to avoid formation of disulfite (Beyad et al., 2014). We experimented with S[IV] solutions at acidic pH and in complex solutions more representative of realistic prebiotic lakes, but our analytics failed for these cases and we are unable to report robust results (SI S2.2).

After 10.5 months, we opened the cuvettes and quantified the remaining S[IV] in the aged solutions via electropotentiomentry (Section 3.2.2) and the amount of sulfate (S[VI]) in the aged solutions via gravimetry (Section 3.2.3). We separately characterized both S[IV] and sulfate to cross-check our results for consistency (e.g. mass conservation). We also monitored the solutions with non-invasive UV-VIS spectroscopy, as additional corroboration (Section 3.2.5). Our results are described in Section 4.2, and raw data underlying both sets of measurements are presented in the SI.

3.2.1 Solution Preparation and Storage

All salts were purchased from Sigma-Aldrich (USA) at the highest available purity grade and used without further purification. All samples were dissolved anoxically in LC-MS grade freshwater (LiChrosolv, Millipore Sigma, USA). The water used to dissolved the salts was degassed for 30 minutes inside of a glove box with O_2 levels ranging from 30ppm to 200ppm.The pH was adjusted utilizing a 1 molar NaOH solution and

a 6 molar HCL solution. MQuant® pH-Indicator Strips were used to monitor the pH of the solution as it was being adjusted.

The dissolved samples were kept in sealable spectrosil quartz cuvettes (1-Q-10-GL14-C, Starna Cell's, USA) with a sample depth of 10 mm. The volume per cuvette was 4 mL. The cuvettes were cleaned solely with LS-MS grade water; we did not clean with acetone as we discovered in preliminary experiments that absorptivity due to residual acetone contaminated UV-VIS measurements. All samples were kept at 23°C. All sample cuvettes were kept in a covered box to minimize long-term exposure to light, inside a glovebox (7150000 Anaerobic Chamber, Type A, Coy Lab Products). One sample (100 mM unadjusted pH, sample #1) was accidentally dropped and destroyed during the course of the study, and consequently we do not report results for it. Another sample (10 mM unadjusted, sample #2) showed pH much smaller than the other samples in its experimental condition at the conclusion of the study, which we interpret as evidence of experimental error; we therefore do not report results for this sample, though we discuss it in SI 2.3.3 for completeness.

3.2.2 S[IV] electropotentiometry

We measured [S[IV]] via electropotentiometry, which directly measures ion concentrations by measuring the electrical potential across an ion-selective membrane (Sohail & De Marco, 2013). We fabricated a bisulfite-potentiometric Ion-Selective Electrode (ISE) (Kuratli & Pretsch, 1994). We calibrated the sensor in a neutral and alkaline background solution of $NaOH/H_2O$ to match the pH of each sample. We have used these calibration curves of the ISE to convert the measured emf (electromotive force) values to the concentrations of S[IV] in the measured samples (SI Supplemental Data).

3.2.2.1 Materials Tridodecylmethylammonium chloride (TDMACl), bis(ethylhexyl) sebacate (DOS), high molecular-weight poly(vinylchloride) (PVC), tetrahydrofuran (THF, inhibitor-free, for HPLC), hydrogen sulfite ionophore (Octadecyl 4-formylbenzoate), nitrophenyloctyl ether(NPOE, Selectophore grade) monohydrogen potassium phosphate, potassium chloride, sodium chloride, sodium hydroxide, sodium sulphate, barium chloride, sodium thiosulfate, potassium bicarbonate, barium chloride, and sodium phosphate were purchased from SigmaAldrich.

3.2.2.2 Measurements and Equipment We measured the response of the sensors using a 16-channel potentiometer (Lawson Labs) at room temperature against a free-flow double-junction AgCl/Ag reference electrode (with a movable glass sleeve junction, 1.0 M lithium acetate bridge electrolyte) purchased from Mettler Toledo. We performed the calibrations of SO_3^{2-} through performing successive dilutions of a 20 mL sample. Each 18 mL aliquot removed was replaced with the addition of 18 mL of sodium phosphate buffer (pH = 8.6), and the emf was measured for each dilution.

3.2.2.3 Fabrication of Conventional Ion-Selective Electrodes The membrane is composed of 660 mg of PVC, 1320 mg of NPOE, and 10 mg of TDMACl. We dissolved these components in 8 mL of THF, stirred the mixture until a homogenous solution was achieved, poured the solution into a petri dish and left it covered overnight; this procedure allowed the THF to evaporate and formed the membrane that provided the ISE. Circular pieces of the membrane with a diameter of ∼1.1 cm and thickness of ∼1.2 mm were cut and placed onto PVC tubing, which was wet with THF (causing the membrane to be fused to the PVC tubing).

3.2.2.4 Fabrication of bisulfite-selective electrode We prepared the ion-selective membranes following established protocols presented in the literature. The HSO_3^- sensing membrane consisted of NPOE, hydrogen sulfite ionophore (1 wt %) and TDMACl (0.20 wt. %). We dissolved these components in 8 mL THF, stirred the mixture until

a homogeneous solution was achieved, poured the solution into a petri dish and left it covered overnight; this procedure allowed the THF to evaporate and formed the membrane that provided the ion selective electrode (ISE). Circular pieces of the membrane with a diameter of 1.1 cm and thickness of 1.2 mm were cut and placed onto PVC tubing, which is wet with THF (causing the membrane to be fused to the PVC tubing). The PVC S3 tube was filled with 2 mL of an inner-filling solution consisting of 10 mM SO_3^- in phosphate buffer (pH 8.6) and 15 mM NaCl. The membrane was placed into a solution of 10 mM SO_3^{2-} for 3 hours before starting the sensor calibration, following the immersion of a Ag/AgCl wire into the inner-filling solution. This procedure allows SO_3^{2-} to replace the chloride ion associated with TDMA.

3.2.2.5 Estimation of Errors For each sample, we measured the emf three times with three different sensors. We report the concentration corresponding to the best-conditioned sensor, sensor #2, and estimate the uncertainty as the standard deviation on the three measurements collected by the three sensors. Calibration curves were obtained by serial dilution, and Nernstian response (Sohail & De Marco, 2013) was confirmed in the concentration range where samples were measured.

3.2.3 Sulfate Gravimetry with $BaCl_2$ and HCl

Sulfate is a main product of S[IV] disproportionation and is the sole product of direct S[IV] oxidation (Meyer et al., 1982; Guekezian et al., 1997). We quantified the amount of sulfate in the sample via the barium chloride gravimetric method for sulfate detection (Ferrús & Torrades, 1985). Sulfate precipitates as $BaSO_4$ using $BaCl_2$ in presence of 2 M HCl (n.b. $BaSO_3$ is soluble under these conditions).

In our study, we followed a procedure similar to Ferrús and Torrades (1985). We combined 0.8 mL of sample with 2 mL of 2 M HCl and added hot ($\sim 60°$ C) 1 M $BaCl_2$ until precipitation went to completion. We boiled the solution for 3 minutes. We gathered the precipitate with a rubber-tipped glass rod ("policeman") onto filter paper. The resulting precipitate was then washed with H_2O, filtered, dried, ignited apart from filter paper and weighed as $BaSO_4$. We took three measurements from each aged sample; we report the mean, and use the standard deviation to estimate the error. Because this technique was destructive of the sample, it was the final test we conducted.

3.2.4 Analytics Timescale

To minimize oxidation by ambient O_2, we conducted our electropotentiometry and extraction of $BaSO_4$ precipitate in $\leq$ 30 min for each sample. The drying and weighing steps of the gravimetry take a further $\sim$ 1 day to complete. Additionally, the drying and weighing steps of the gravimetry were conducted some months after the precipitate extraction, due to experimenter constraints. $BaSO_4$(s) is stable at standard conditions, so this does not affect the accuracy of our results.

3.2.5 UV-VIS Monitoring

We non-invasively tracked the evolution of the UV-VIS absorption spectra of the samples. These data are corroborative but not on their own definitive, because the potential products of S[IV] disproportionation are themselves UV absorbers (Meyer et al., 1982; Guenther et al., 2001; Beyad et al., 2014; Islam, 2018). The UV-VIS monitoring is therefore secondary to the solution-phase analytics. All absorbance spectra were recorded by a Shimadzu UV-1900 UV-VIS spectrophotometer located outside of the glovebox once a week. Before each measurement, cuvettes were blown with dry air to remove any dust from the surface. A blank water spectrum was taken with each measurement in order to correct for cuvette errors. As a control, we exposed a sample of sulfite to ambient air

Table 2. Estimates of Sulfite Disproportionation

Study	$T_{disp,0}$	$[S[IV]]_0$ (M)
Meyer et al. (1979)	> 5 year	$\sim 0.01 - 1^a$
Meyer et al. (1982)	> 1 year	$\sim 0.01 - 1^a$
Guekezian et al. (1997)	10 days	0.09
Petruševski et al. (2013)	> 7 months	3.4

[a] $[S[IV]]_0$ not stated. Lower limit based on limits of analytics (Meyer, Ospina, & Peter, 1980). Upper limit based on associated Lawrence Berkeley National Laboratory annual reports (Shirley, 1980; Searcy, 1981).

overnight and verified loss of UV opacity as expected due to the rapid oxidation of UV-absorbing sulfite to UV-transparent sulfate (Beyad et al., 2014; Birkmann et al., 2018).

3.3 Thermal S[IV] Loss Processes

3.3.1 S[IV] Disproportionation

The extreme uncertainties in the kinetics of S[IV] disproportionation (Section 2.3) motivate a simplistic, cautious implementation in our model. Past implementations of S[IV] disproportionation have modeled it as first order (Halevy, 2013). However, because disproportionation requires multiple S[IV] molecules, it is possible that the reaction is higher-order. Indeed, based on the stoichiometry the naive assumption would be that the reaction would be fourth-order, and thereby highly suppressed at low concentrations. We therefore implement a generalized rate law for S[IV] disproportionation. Assuming S[IV] disproportionation to be order n:

$$\frac{dS[IV]}{dt} = k_{disp,n}[S[IV]]^n \tag{13}$$

where $k_{disp,n}$ is the rate constant for S[IV] disproportionation (M^{1-n} s^{-1}).

From literature reports and our own experiments, we obtain $T_{disp,0}$, the S[IV] lifetime to disproportionation for a sample with initial S[IV] concentration $[S[IV]]_0$. We use $T_{disp,0}$ to estimate k_{disp}:

$$T_{disp,0}\frac{dS[IV]}{dt}(t=0) + [S[IV]]_0 = 0 \tag{14}$$

$$\Rightarrow k_{disp,n} = T_{disp,0}^{-1}[S[IV]]_0^{1-n} \tag{15}$$

We summarize literature values for $T_{disp,0}$ and $[S[IV]]_0$ in Table 2. Values for $T_{disp,0}$ in the literature range fall into two broad ranges: $T_{disp,0} \gtrsim$ years, and $T_{disp,0} = 10$ days. We conduct experiments to discriminate between these two possibilities, and use the results in our model (Section 4.2). Finally, we compute the flux of S[IV] loss by disproportionation integrated through the full water column:

$$F_{disprop,S[IV]} = \int_0^{d_{body}} dy(k_{disp,n}[S[IV]]^n) = d_{body}(k_{disp,n}[S[IV]]^n) \tag{16}$$

where d_{body} is the depth of the water column (cm).

3.3.2 Seepage Loss

If the base of an aqueous body is not saturated with water, then water will seep out of this body, carrying with it S[IV]. Seepage can limit the concentration of solutes in lakes (Wood & Sanford, 1990; Rosen, 1994; Pearce et al., 2017). We calculate the rate of this process according to the equation (Pearce et al., 2017):

$$F_{seepage,S[IV]} = [S[IV]]S \tag{17}$$

where S is the seepage rate (m year^{-1}). A wide range of S is possible depending on permeability and hydraulic gradient, and we explore the range $S = 0 - 2$ m/year. The lower limit for S is motivated by closed-basin lakes with impermeable bottoms. These systems are characterized by no surface outflow and water loss dominated by evaporation, resulting in concentration of solutes (Toner & Catling, 2019). Modeling of salinity and water budgets for some lakes excludes seepage altogether (Langbein, 1961; van der Kamp et al., 2008; Yapiyev et al., 2017). Estimates of seepage for Lake Titicaca range from $\sim 0-10\%$ of evaporation, or $\sim 0-0.15$ m year^{-1} (Roche et al., 1992; Carmouze et al., 1992; Delclaux et al., 2007; Yapiyev et al., 2017). Modeling of oxygen isotopes in Lakes Scanlon and Castor reveals outseepage of $0.5 \pm 0.3\%$ and $1.5 \pm 0.3\%$ of the lake volume per month, respectively, corresponding to seepage rates of $0.4 - 0.5$ m year$^{-}1$ and 2 m year$^{-}1$, respectively (Steinman et al., 2010). A value of 2 m year^{-1} also corresponds to the average seepage rate in fishponds near Auburn, Alabama; this rate is higher than the seepage seen in many natural ponds (Boyd, 1982; Pearce et al., 2017), and we adopt it as the upper bound of the range we explore.

3.3.3 Direct Oxidation of S[IV]

For completeness, we consider direct oxidation of S[IV] by trace photochemical O_2 present on early Earth. We follow Halevy (2013) in using the rate law of Zhang and Millero (1991) for the rate of oxidation of sulfite by O_2:

$$SO_3^{2-} + \frac{1}{2}O_2 \rightarrow SO_4^{2-} \tag{18}$$

$$\frac{dS[IV]}{dt} = -k[S[IV]]^2[O_2]^{0.5} = -k"[HSO_3^-][SO_3^{2-}][O_2]^{0.5} \tag{19}$$

where k (M$^{-1.5}$ min^{-1}) and k" (M$^{-1.5}$ min^{-1}) are rate constants. For modern seawater at pH=8.2, Zhang and Millero (1991) report

$$\log_{10}(\frac{k}{1\text{M}^{-1.5}\ \text{min}^{-1}}) = 19.54 - 5069.47T^{-1} + 14.74I^{0.5} - 2.93I - 2877.0I^{0.5}T^{-1} \tag{20}$$

where T is temperature, I is molal ionic strength, and this relation is valid for $T = 288-318$K and $I = 0-0.72$ (salinity $S_A = 0-35$). We use this expression for k to estimate k", according to the equation (Zhang & Millero, 1991):

$$k" = \frac{k}{\alpha_{SO_3^{2-},seawater}\alpha_{HSO_3^-,seawater}} \tag{21}$$

where $\alpha_{SO_3^{2-},seawater}$ is the mol fraction of S[IV] in SO_3^{2-} and $\alpha_{HSO_3^-,seawater}$ is the mol fraction of S[IV] in HSO_3^- in seawater at $S_A = 35$ and $T = 298$K. We estimate $\alpha_{SO_3^{2-}}$ and $\alpha_{HSO_3^-}$ according to the equations (Millero et al., 1989; Zhang & Millero, 1991):

$$I = \frac{0.0199 S_A}{1 - 10^{-3} S_A} \tag{22}$$

$$pKa_1^* = 1.87 - 0.50 I^{0.5} + 0.31 I (T = 298K) \tag{23}$$

$$pKa_2^* = 7.12 - 1.052 I^{0.5} + 0.36 I \tag{24}$$

$$\alpha_{HSO_3^-} = (\frac{[H^+]}{K_1^*} + \frac{K_2^*}{[H^+]} + 1)^{-1} \tag{25}$$

$$\alpha_{SO_3^{2-}} = (\frac{[H^+]^2}{K_1^* K_2^*} + \frac{[H^+]}{K_2^*} + 1)^{-1} \tag{26}$$

Where Ka_1^* and Ka_2^* correspond to the first and second dissociation constants for SO_2, and $pKa = -\log_{10}(Ka)$ as usual. These expressions assume the main forms of S[IV] to be SO_2, HSO_3^-, and SO_3^{2-}. They are invalid at high [S[IV]], where sulfite dimers form (Beyad et al., 2014). We do not deploy our models in this regime.

With this formalism, we are able to reproduce the k" measured at pH=8.2 to within 0.11 log units[6] (Figure 7 of Zhang and Millero (1991)). Note that for solutions with relative solute concentrations corresponding to seawater, there is additional pH dependence not fully captured by this formalism; Zhang and Millero (1991) attribute this to pH-dependent complex formation in seawater. These uncertainties do not affect our conclusions because direct oxidation is not a significant loss mechanism for S[IV] in the anoxic conditions prevalent on prebiotic Earth.

With the rate law in hand, we compute the flux of S[IV] loss due to direct oxidation integrated through the full water column:

$$F_{O_2,S[IV]} = \int_0^{d_{body}} dy (k"[HSO_3^-][SO_3^{2-}][O_2]^{0.5}) = d_{body} (k"[HSO_3^-][SO_3^{2-}][O_2]^{0.5}) \tag{27}$$

We estimate $[O_2]$ using Henry's Law, i.e.:

$$[O_2] = H_{O_2} pO_2 (z = 0) \tag{28}$$

where H_{O_2} is the Henry's Law constant for O_2 and pO_2 is the partial pressure of O_2. Photochemical models predict abiotic O_2 volume mixing ratios to be sub-parts per billion (ppb) (Kasting & Walker, 1981; Ranjan et al., 2020), while the upper limit on O_2 mixing ratio derived from model interpretation of the sulfur mass-independent fractionation signal (S-MIF) is 2×10^{-7} (Zahnle et al., 2006). We adopt pO_2 from our photochemical model calculations. We take $H_{O_2} = 1.3 \times 10^{-3}$ M/bar (Sander et al., 2011; Sander, 2015), which is valid for 298 K and 0 salinity. Increased salinity would decrease H_{O_2} and hence $[O_2]$, suppressing direct oxidation even more than calculated here.

3.4 Photolytic S[IV] Loss

Measured S[IV] photolysis rates in natural waters on modern Earth are unavailable, because S[IV] is absent from natural waters on modern Earth due to the oxic atmosphere (Loftus et al., 2019). However, S[IV] photolysis has been well-studied in laboratory settings, both for its fundamental photophysics, as well as for its applications to wastewater treatment (Fischer & Warneck, 1996; Sauer, Crowell, & Shkrob, 2004; Wu et al., 2021). We utilize these laboratory measurements to estimate the S[IV] photolysis rates in natural waters on prebiotic Earth.

[6] Note that Zhang and Millero (1991) feature a persistent typo: the values they quote in-text for k" are really for $\log_{10}(k")$. This can be seen by comparing the quoted values to Figure 7 of their paper, and by attempting to calculate k" directly from k.

3.4.1 Calculation of Photolysis Rate

We calculate the photolysis rate coefficient for loss of species X, $J_X(d)$ (s^{-1}), at depth d according to the equation:

$$J_{SO_3^{2-}}(d) = \int d\lambda \Phi_{SO_3^{2-}}(\lambda)\sigma_{SO_3^{2-}}(\lambda)\dot{E}(\lambda, d) \tag{29}$$

$$J_{HSO_3^-}(d) = \int d\lambda \Phi_{HSO_3^-}(\lambda)\sigma_{HSO_3^-}(\lambda)\dot{E}(\lambda, d) \tag{30}$$

where $\Phi_{SO_3^{2-}}$ is the quantum efficiency of net loss of SO_3^{2-} due to photolysis, $\Phi_{HSO_3^-}$ is the quantum efficiency of net loss of HSO_3^- due to photolysis, $\sigma_{SO_3^{2-}}$ (cm^2) is the absorption cross-section of $SO_{3,aq}^{2-}$, $\sigma_{HSO_3^-}$ (cm^2) is the absorption cross-section of $HSO_{3,aq}^-$, $\dot{E}(\lambda, d)$ (cm^{-2} s^{-1} nm^{-1}) is the scalar irradiance as a function of wavelength (λ) and depth (d).

3.4.1.1 S[IV] Absorption Cross-Sections We compute the absorption cross-section σ from the linear decadic absorption coefficient ϵ (M^{-1} cm^{-1}), which is more commonly reported for aqueous absorbers, according to the equation (Lakowicz, 2010):

$$\sigma = \frac{10^3 \ln(10)}{N_A}\epsilon \tag{31}$$

where N_A is Avogadro's number, and σ and ϵ are in units of cm^2 and M^{-1} cm^{-1} respectively . We take ϵ for HSO_3^- and SO_3^{2-} from Fischer and Warneck (1996) and Beyad et al. (2014), as synthesized by Ranjan, Kufner, et al. (2022). We neglect corrections to absorptivity and quantum yield due to high ionic strength (Sauer, Shkrob, et al., 2004).

3.4.1.2 S[IV] Photolysis Quantum Yields We synthesize estimates for $\Phi_{HSO_3^-}(\lambda)$ and $\Phi_{SO_3^{2-}}(\lambda)$ based on laboratory measurements. These laboratory measurements are summarized in Table 3 and fall into two types. Many of these studies sought to quantify the quantum yields of primary photolysis, i.e. production of H for HSO_3^- photolysis and production of e_{aq}^- for SO_3^{2-} photolysis. However, this is not necessarily the same as the quantum yield of net loss of the photolyzed molecules, because H and e_{aq}^- can subsequently undergo back-reactions to regenerate HSO_3^- and SO_3^{2-}, respectively (Sauer, Crowell, & Shkrob, 2004; Lian et al., 2006; Li et al., 2012, 2014). The efficacy of the back-reaction depends on the composition of the solution: if scavengers for the photoproduced radicals are present, the back-reaction is inefficient and the net loss to photolysis is higher (Fischer & Warneck, 1996).

In this study, we assume the quantum yield of sulfite and bisulfite photolysis to be equal to the quantum yield of net loss of sulfite and bisulfite due to photolysis. Our choice is motivated by the more abundant data available for direct photolysis, as well as by the belief that in natural waters scavengers for radicals like H and e_{aq}^- would likely have been present that would have inhibited the back-reaction. This is the case for NO_X^-, which is regenerated after photolysis in pure water but not in natural waters (Zafiriou & True, 1979b, 1979b; Mack & Bolton, 1999). The difference in quantum yield is $< 1.6\times$ (Fischer & Warneck, 1996); our conclusions are robust to such uncertainty.

We approximate the quantum yield of sulfite photolysis as a piecewise linear function (Figure S15). Where available, we adopt the terminal quantum yields, as opposed to the prompt quantum yields; the terminal quantum yields account for germinate recombination immediately after photolysis. Our function is anchored by (λ, $\Phi_{SO_3^{2-}}$) of (193 nm, 0.39) (Sauer, Crowell, & Shkrob, 2004), (200 nm, 0.23) (Lian et al., 2006), (248 nm, 0.11) (Sauer, Crowell, & Shkrob, 2004) and (253.7 nm, 0.116) (Li et al., 2012). These

Table 3. Laboratory Measurements of Quantum Yields Relevant to Aqueous S[IV] Photolysis

Study	Species	λ nm	Photoprocess	Quantum Yield
Fischer and Warneck (1996)	HSO_3^-	213.9	HSO_3^{2-} photolysis	$\Phi_{HSO_3^-} = 0.19 \pm 0.03$
Fischer and Warneck (1996)	HSO_3^-	213.9	Net photolytic HSO_3^- loss in anoxic H_2O	$\Phi_{C,HSO_3^-} = 0.12 \pm 0.03$ [b]
Sauer, Crowell, and Shkrob (2004)	SO_3^{2-}	193	SO_3^{2-} Photolysis	$\Phi_{SO_3^{2-}} = 0.391 \pm 0.011$
Lian et al. (2006)	SO_3^{2-}	200	SO_3^{2-} Photolysis	$\Phi_{SO_3^{2-}} = 0.231 \pm 0.023$[a]
Sauer, Crowell, and Shkrob (2004)	SO_3^{2-}	248	SO_3^{2-} Photolysis	$\Phi_{SO_3^{2-}} = 0.108 \pm 0.001$
Fischer and Warneck (1996)	SO_3^{2-}	253.7	SO_3^{2-} Photolysis	$\Phi_{SO_3^{2-}} = 0.39 \pm 0.04$
Fischer and Warneck (1996)	SO_3^{2-}	253.7	Net photolytic SO_3^{2-} loss in anoxic H_2O	$\Phi_{C,SO_3^{2-}} = 0.25 \pm 0.02$ [b]
Li et al. (2012)	SO_3^-	253.7	SO_3^{2-} Photolysis	$\Phi_{SO_3^{2-}} = 0.116 \pm 0.002$

[a] Uncertainty not explicitly stated in source publication; assumed to be 10%, as for OH^- and I^-.
[b] Subscript C emphasizes that this photoprocess is not the same as direct photolysis.

quantum yields we choose conform to the expectation from theory that quantum yield of photolysis should increase as wavelength decreases (Wu et al., 2021), and are generally consistent with most other measurements of sulfite photolysis. (Sauer, Crowell, & Shkrob, 2004) argue that measurements based on actinometry and scavenger studies overestimate Φ, and that quantum yields reported by such studies must be interpreted as upper limits. Based on their argument, we do not utilize the quantum yield at 254 nm measured by (Fischer & Warneck, 1996), which is indeed higher ($\sim 4\times$) than follow-up studies which are otherwise consistent. We are not aware of constraints on $\Phi_{SO_3^{2-}}$ at wavelengths > 253.7 nm. To bracket the possibilities, we explore $\Phi_{SO_3^{2-}}(> 253.7 \text{ nm}) = 0$ and $\Phi_{SO_3^{2-}}(> 253.7 \text{ nm}) = \Phi_{SO_3^{2-}}(253.7 \text{ nm})$ (Figure S15).

Measurements of the quantum yield of bisulfite photolysis are extremely scarce. The sole measurement we found is that of Fischer and Warneck (1996) at 214 nm, but that measurement must be interpreted as an upper limit (Sauer, Crowell, & Shkrob, 2004). We convert the upper limit of Fischer and Warneck (1996), $\Phi^{UL}_{HSO_3^-}$, to an estimate of $\Phi_{HSO_3^-}$ by assuming that $\Phi^{UL}_{HSO_3^-}$ is enhanced proportionately to $\Phi_{HSO_3^-}$ as their estimate of $\Phi^{UL}_{SO_3^{2-}}$ is enhanced relative to $\Phi_{SO_3^{2-}}$:

$$\Phi_{HSO_3^-}(214 \text{ nm}) = \frac{\Phi_{SO_3^{2-}}(253.7 \text{ nm})}{\Phi^{UL}_{SO_3^{2-}}(253.7 \text{ nm})} \times \Phi^{UL}_{HSO_3^-}(213.9 \text{ nm}) \tag{32}$$

implying that $\Phi_{HSO_3^-}(213.9nm) = \frac{0.116}{0.39} \times 0.19 = 0.057$. This still leaves the question of how to treat photolysis at other wavelengths. In the absence of guiding data, we assume bisulfite photolysis quantum yields to be proportional to sulfite quantum yields, i.e.:

$$\Phi_{HSO_3^-} = \frac{\Phi_{HSO_3^-}(213.9 \text{ nm})}{\Phi_{SO_3^{2-}}(213.9 \text{ nm})} \Phi_{SO_3^{2-}} \tag{33}$$

We sensitivity-test our conclusions to the possibility that $\Phi_{HSO_3^-} = 0$ and find our overall conclusions to be unaffected, justifying this treatment, but advocate for better constraints on this quantity to improve our calculations (Section 5.3).

3.4.1.3 Estimation of Scalar Irradiance We estimate the scalar irradiance $\dot{E}(\lambda, d)$ by adapting the treatment of Morel (1991), which was originally developed to treat photosynthetically active radiation in the modern ocean. We begin by estimating the downwelling (planar) irradiance (flux) $E_d(\lambda, d)$ (Morel, 1991; Mobley et al., 2009):

$$E_d(\lambda, d) = E_d(\lambda, 0^-) \exp\left(-\int_0^d dx K_d(\lambda, x)\right) \tag{34}$$

Here, $E_d(\lambda, 0^-)$ is the downwelling irradiance just below the surface and K_d is the apparent vertical Naperian downwelling attenuation coefficient.

We estimate $E_d(\lambda, 0^-)$ from the downwelling flux just above the surface, $E_d(\lambda, 0^+)$, according to the equation (Morel, 1991; Sakshaug et al., 1997):

$$E_d(\lambda, 0^-) = r_{sky} E_{d,sky}(\lambda, 0^+) + r_{sun} E_{d,sun}(\lambda, 0^+) \tag{35}$$

Where $E_{sky}(\lambda, 0^+)$ is the diffuse irradiance just above the surface, r_{sky} is the reflectance of the diffuse irradiance, $E_{sun}(\lambda, 0^+)$ is the direct (solar) irradiance just above the surface, r_{sun} is the reflectance of the direct irradiance (altitude-dependent), and $E_d(\lambda, 0^+) = E_{sky}(\lambda, 0^+) + E_{sun}(\lambda, 0^+)$. We take $E_{sun}(\lambda, 0^+)$ and $E_{sky}(\lambda, 0^+)$ from Ranjan and Sasselov (2017), assuming a prebiotic Earth atmospheric composition from Rugheimer et al. (2015), a solar zenith angle $\theta_{sun} = 60°$, and a surface albedo $A = 0.2$ (A and θ_{sun} chosen for consistency with Rugheimer et al. (2015)). We take $r_{sky} = 0.066$ (Morel, 1991; Cockell, 2000b). We compute r_{sun} as a function of solar zenith angle via the Fresnel equations assuming unpolarized light incident on a flat water surface and a ratio of aqueous and aerial indices of refraction of $\frac{n_{aq}}{n_{air}} = 1.33$ (Kirk, 1994), following Cockell (2000b). Reflectance losses are small for $\theta_{sun} < 70°$ (Kirk, 1984), meaning that our sensitivity to these assumptions is minimal.

The heart of the aqueous radiative transfer calculation is computation of K_d. Precisely calculating K_d requires a full solution of the aqueous radiative transfer equations as a function of Naperian absorption coefficient $a(\lambda, d)$, Naperian scattering coefficient $b(\lambda, d)$, the volume scattering function for the water in question, and the radiance distribution above the surface (Kirk, 1984; Morel, 1991). Given these complexities, K_d is in practice generally empirically constrained or estimated (Thomas & Stamnes, 2002). We follow Morel (1991) in estimating K_d according to the equation (Kirk, 1984):

$$K_d = \frac{a}{\mu_0}[1 + (0.425\mu_0 - 0.19)\frac{b}{a}]^{0.5} \tag{36}$$

where μ_0 is the average cosine for downwelling radiation. This expression is valid for waters with volume scattering function corresponding to the waters of modern San Diego Harbor (Kirk, 1984). We estimate μ_0 according to the equation (Morel, 1991):

$$\mu_0(\lambda) = \frac{1}{E_d(\lambda, 0^-)}[\mu_{sun,aq} E_{d,sun}(\lambda, 0^-) + \mu_{sky,aq} E_{d,sky}(\lambda, 0^-)] \tag{37}$$

Here, $E_{d,sun}(\lambda, 0^-)$ is the component of $E_d(\lambda, 0^-)$ due to the direct solar irradiance, $E_{d,sky}(\lambda, 0^-)$ is the component of E_d due to the sky (diffuse) irradiance, $\mu_{sun,aq}$ is the cosine of the solar zenith angle after refraction, and $\mu_{sky,aq} = 0.86$ is the consine of the sky zenith angle after refraction.

The above formalism to estimate K_d is complex. To determine the sensitivity of our results to the estimation of K_d, we consider two simpler approximations for K_d. First, we estimate $K_d = \frac{1.0395}{\mu_0}(a+b_b)$, where b_b is the backscattering coefficient; this expression is known valid for diverse marine waters (Morel et al., 2007). Second, we estimate $K_d = \frac{a}{\cos(\theta_{sun,aq})}$, ignoring scattering entirely. Our conclusions were unaffected, indicating that they are robust to choice of K_d calculation technique.

We take values for a from Ranjan, Kufner, et al. (2022), converting their linear decadic absorption coefficients ϵ to linear naperian absorption coefficients via $a = \epsilon \ln(10)$ (Kirk, 1994). We adopt b from the tabulation of Smith and Baker (1981) for modern freshwater and seawater. We use modern freshwater b for prebiotic freshwater lakes, and the Smith and Baker (1981) seawater b for the prebiotic ocean and prebiotic carbonate lakes. We approximate $b_b = 0.5b$ (Smith & Baker, 1981). This approximation is valid for waters with low particulate scattering, which is reasonable for early Earth since prebiotic waters should have been less scattering than modern waters due to the absence of biogenic organics (Cockell, 2000b; Morel et al., 2007).

So far, we have computed the downwelling plane irradiance E_d, which calculates the net flow of energy across a plane, but the quantity required to estimate photolysis rates is $\dot{E}$, the scalar irradiance. We estimate $\dot{E}$ according to (Morel, 1991; Mobley et al., 2009):

$$\dot{E}(\lambda, d) \approx \frac{K_d(\lambda, d)}{a(\lambda, d)} E_d(\lambda, d) \tag{38}$$

This formalism is valid for waters which are absorption-dominated, as is the case for most natural waters on modern Earth (Morel, 1991; Sakshaug et al., 1997; Cockell, 2000b). However, it is possible that some natural waters may be scattering-dominated on early Earth, in which case the above expression would dramatically overestimate $\dot{E}$. We impose an ad-hoc correction for this case by imposing a ceiling on $\dot{E}$, $\dot{E}_{max} = 2.5\frac{E_d}{\mu_0}$. This ad-hoc correction is based on the finding of Kirk (1994) that for extremely highly scattering waters, $\frac{\dot{E}}{E_d} = 2.0 - 2.5$ for vertically incident light ($\mu_0 = 1$), and adding a correction for $\mu_0 \neq 1$.

3.4.1.4 Calculation of Column-Integrated S[IV] Photolysis Rate We calculate the column-integrated photolysis flux of S[IV] by integrating and adding the depth-dependent photolysis rate of bisulfite and sulfite:

$$F_{h\nu,S[IV]} = \int dy J_{SO_3^{2-}}(y) C_{SO_3^{2-}}(y) + \int dy J_{HSO_3^-}(y) C_{HSO_3^-}(y) \tag{39}$$

where C_X is the concentration of species X, assumed to be well-mixed (constant with depth) in our 0D box model.

3.5 Geological Scenario and Parameter Choices

The geochemical properties of the prebiotic ocean are uncertain. To reflect this uncertainty in our estimations of prebiotic S[IV], we construct S[IV] maximizing and minimizing endmember scenarios based on estimates of relevant geochemical parameters in the literature (Table 4). We consider a pH range of 6.25-9 (Krissansen-Totton et al., 2018; Kadoya et al., 2020; Sahai et al., 2022), with higher pH corresponding to less S[IV] because of speciation as SO_3^{2-}, which is more vulnerable to photolysis. We consider background marine UV linear decadic absorption coefficients corresponding to the low-absorption and high-absorption endmember scenarios from Ranjan, Kufner, et al. (2022), with S[IV] removed. Low absorption minimizes S[IV] due to more efficient photolysis. Higher I corresponds to less S[IV] due to more efficient direct oxidation; we would like to consider an ionic strength range of $I = 0.3 - 1.2$ (Knauth, 2005; Marty et al., 2018), but are

forced to impose a ceiling of 0.72 on I because of limitations of the formalism we use to estimate direct oxidation rates of S[IV] (Zhang & Millero, 1991); this does not affect our conclusions because direct oxidation is a minor loss process for S[IV] (Figure 3). This approach is purely parametric, and not self-consistent (i.e. we are merely choosing extreme values from the literature, not conducting self-consistent modeling of a specific scenario).

Table 4. Extremal geochemical parameters assumed in estimating [S[IV]] in marine waters on early Earth. Parameters are categorized by whether they maximize or minimize [S[IV]], thus enabling a measure of the uncertainty. Note that this approach is purely parametric, and is not self-consistent. In simulating marine waters, we set $S = 0$ m year^{-1} and $P = P_{model}$, and take $d = 3.8 \times 10^5$ cm, corresponding to the modern ocean (Rumble, 2017).

Parameter	[S[IV]]-minimizing	[S[IV]]-maximizing	Comment
pH	9.0	6.25	(Krissansen-Totton et al., 2018; Kadoya et al., 2020)
$a(\lambda)$ (cm^{-1})	Ocean, low-a endmember	Ocean, high-a endmember	(Ranjan, Kufner, et al., 2022) (S[IV] removed)
I (M)	0.72	0.3	(Knauth, 2005; Marty et al., 2018)

In calculating terrestrial [S[IV]], we focus on shallow closed-basin waters, which are particularly invoked in proposed prebiotic chemistry because of their potential for wet-dry cycling, their propensity to accumulate key prebiotic reagents, and their favorable physicochemical conditions (Patel et al., 2015; Becker et al., 2018; Ranjan et al., 2019; Sahai et al., 2022; Benner, 2023). We specifically focus on on freshwater (Damer & Deamer, 2020) and carbonate lakes (Toner & Catling, 2020; Sahai et al., 2022). While we simulate only these two types of terrestrial water in detail, our methods and open-source code can be readily adapted to other natural waters. Further, we expect our basic results to generalize to diverse closed-basin terrestrial waters (e.g., Sahai et al. (2022)) because the same basic supply and loss processes apply.

As with marine waters, we explore a wide range of parameter space to construct extremal endmember S[IV]-maximizing and -minimizing scenarios (Table 5). For carbonate lakes, we draw pH and ionic strength estimates from (Toner & Catling, 2020). We are forced to impose a ceiling of 0.72 on I because of limitations of the formalism we use to estimate direct oxidation rates of S[IV]; this does not affect our conclusions because direct oxidation is a minor loss process for S[IV] (Figure 4). For freshwater lakes, we draw pH and ionic strength estimates from (Hao et al., 2017). For both lakes, we draw estimates of background UV absorptivity from Ranjan, Kufner, et al. (2022), with S[IV] species removed. As in the marine case, the higher pH, higher I, and less absorptive waters minimize S[IV]. We consider $S = 0 - 2$ m year^{-1} (Section 3.3.2). As in the marine case, our approach is purely parametric, and is not self-consistent.

4 Results

4.1 Atmospheric Processing and Surface Deposition of SO_2

Our photochemical modeling predicts SO_2 surface concentrations on early Earth that are comparable to past work (Figure 2). Our predicted pSO_2 is much lower than that calculated by Kasting et al. (1989) for early Earth; this is because Kasting et al.

Table 5. Extremal geochemical parameters assumed in estimating [S[IV]] in closed-basin terrestrial waters on early Earth. Parameters are categorized by whether they maximize or minimize [S[IV]], thus enabling a measure of the uncertainty. Note that this approach is purely parametric, and is not self-consistent. We simulate lakes with $d = 1$ m.

Parameter	[S[IV]]-minimizing	[S[IV]]-maximizing	Comment
		Carbonate Lake	
pH	9.0	6.5	(Toner & Catling, 2020)
I (M)	0.72	0.1	(Toner & Catling, 2020)
$a(\lambda)$ (cm^{-1})	Carb. Lake, low-a end-member	Carb. Lake, high-a end-member	(Ranjan, Kufner, et al., 2022) (S[IV] removed)
S (m yr^{-1})	0	2	
		Freshwater Lake	
pH	6.34	6.34	(Hao et al., 2017)
I (M)	0.001	0.001	(Lerman et al., 1995; Hao et al., 2017)
$a(\lambda)$ (cm^{-1})	Fresh. Lake, low-a end-member	Fresh. Lake, high-a end-member	(Ranjan, Kufner, et al., 2022) (S[IV] removed)
S (m yr^{-1})	0	2	

(1989) considered the limiting case of no surface deposition of SO_2. We include surface deposition of SO_2, which suppresses pSO_2. Our predicted pSO_2 is slightly higher than that calculated by Claire et al. (2014) for high ϕ_{SO_2}. We attribute this to the assumption of Claire et al. (2014) that SO_2 is substantially explosively outgassed, which injects SO_2 into the stratosphere where it is photochemically processed into aerosols, reducing pSO_2 relative to our calculation.

Our modeling predicts that most outgassed SO_2 is returned to the surface via wet and dry deposition. This reflects our assumption of low-altitude outgassing of SO_2, where it is most vulnerable to surface deposition (Hu et al., 2013). If SO_2 is instead released explosively at high altitudes, then at elevated $\phi_{SO_2} \sim 0.5$ of the SO_2 can be photochemically processed into sulfate and elemental sulfur aerosols (Claire et al., 2014). This means that our calculation may overestimate SO_2 deposition by up to $\sim 2\times$ at elevated ϕ_{SO_2}.

4.2 S[IV] Disproportionation Experiments & Implications for Modeling

Our experimental results are consistent with a long lifetime (≥ 1 year) of anoxic S[IV] solutions (Table 6). This finding is valid at pH≥ 7, near standard temperature and pressure, and in the absence of catalysts and UV light. Our electropotentiometric measurements of S[IV] and gravimetric measurements of sulfate are consistent in every sample, and the long lifetimes inferred from the solution-phase analytics are consistent with the slow rate of change of UV absorbance measured by the UV-VIS tracking. The largest degree of S[IV] loss is seen in the 10 mM solutions, which show loss of 60-70% of S[IV] over 10.5 months (electropotentiometry). This corresponds to a S[IV] lifetime to disproportionation of $T_{disp,0} \geq 1$ year.

However, 1 year may significantly underestimate $T_{disp,0}$. The 100 mM S[IV] solutions uniformly show lower fractional loss than the 10 mM solution, corresponding to $T_{disp,0} = 4{-}5$ years. We are unaware of any rationale for higher concentrations of S[IV] to show

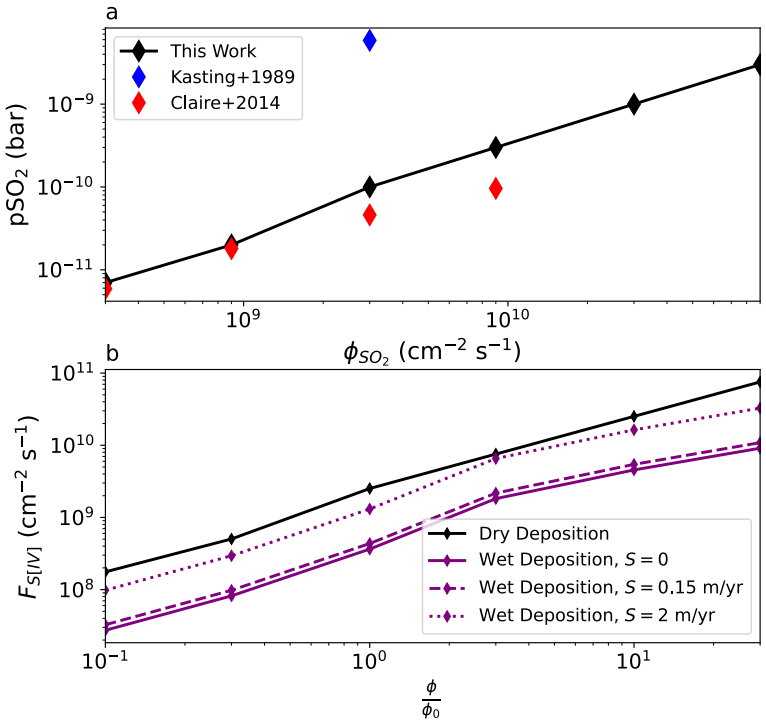

Figure 2. Photochemical processing of SO_2 in the atmosphere of prebiotic Earth. (a) Top: partial pressure of SO_2 as a function of surficial SO_2 emission rate. Shown for comparison are similar estimates from Kasting et al. (1989) and Claire et al. (2014), Figure 6. (b) Bottom: wet and dry deposition fluxes of S[IV] species from the atmosphere to the surface. Wet deposition fluxes are given for various seepage rates, which for the steady-state modeling we conduct here dictate the implied precipitation rate.

slower disproportionation rates; indeed, the opposite is the naive expectation given the reaction stoichiometry (Equation 1). A possible explanation is given by the sulfate concentrations we measure. The sulfate concentrations we measure are in 14/15 cases consistent within 5σ of the amount of S[IV] lost, which means that we cannot firmly rule out the possibility that the S[IV] lost from our samples was stoichiometrically converted to sulfate, as is expected due to direct oxidation. One possibility is that the bulk of S[IV] loss in our samples is due to slow leakage of O_2 into our cuvettes over the multi-month course of the experiments. Though we took care to minimize O_2 leakage by utilizing air-tight cuvettes and storing the cuvettes in an anaerobic glove box, complete exclusion of O_2 was not possible in our setup. Our anaerobic glove box still maintained 30−200 ppm O_2, and the frictive seals of our nominally gas-tight cuvettes may still admit some degree of gas interchange on the long timescales of our experiment. In support of this hypothesis is the observation that the absolute concentration of sulfates in the aged 10 mM and 100 mM samples are similar to within $\leq 3\times$. Similar sulfate concentrations are consistent with a significant contribution of direct oxidation (which should be controlled by the rate of O_2 leakage and insensitive to S[IV] concentration), but not an origin from S[IV] disproportionation (which should be sensitive to sulfite concentration). Our samples may therefore reflect contributions from direct oxidation, and our results must therefore be considered lower bounds on $T_{disp,0}$.

Table 6. Analytics of Aged S[IV] Samples

$[Na_2SO_3]_0^{\dagger}$ (mM)	$pH_0^{\dagger}$	Sample	$[SO_3^{2-}]_{f,tot}^{\ddagger,a}$ (mM)	$[SO_4^{2-}]_f^{\ddagger,b}$ (mM)	λ_m nm	$\frac{A_{\lambda_m,f}}{A_{\lambda_m,0}}$ ★
100	7	1	85 ± 4	8.4 ± 0.2	260	0.87 ± 0.13
100	7	2	83 ± 5	9.1 ± 0.1	260	0.91 ± 0.14
100	7	3	84 ± 3	9.5 ± 0.2	260	0.91 ± 0.14
100	7	4	83 ± 4	12.1 ± 0.1	260	0.89 ± 0.13
100	Unadjusted	2♦	84 ± 3	9.5 ± 0.3	260	0.85 ± 0.13
100	Unadjusted	3	86 ± 4	10.5 ± 0.5	260	0.90 ± 0.13
100	Unadjusted	4	81 ± 2	10.6 ± 0.3	260	0.87 ± 0.13
100	13	1	83 ± 3	9.7 ± 0.4	260	0.87 ± 0.13
100	13	2	84 ± 2	11.7 ± 0.5	260	0.84 ± 0.13
100	13	3	83 ± 3	11.0 ± 0.5	260	0.89 ± 0.13
100	13	4	81 ± 3	12.6 ± 0.5	260	0.89 ± 0.13
10	Unadjusted	1	3.7 ± 0.3	4.9 ± 0.2	240	0.35 ± 0.05
10	Unadjusted	3▲	3.1 ± 0.3	5.7 ± 0.2	240	0.33 ± 0.05
10	Unadjusted	4	3.8 ± 0.3	4.2 ± 0.2	240	0.24 ± 0.04

†Sample preparation (10/5/2021)
‡Cuvettes opened 8/20/2022
^{a}Electropotentiometry
^{b}Gravimetry
★UV-VIS last day 8/8/2022
♦ Sample #1 was accidentally destroyed during course of experiment
▲ Sample #2 appears to reflect experimenter error and is not reported (Section 3.2.1, SI 2.3.3)

We cannot claim a definitive constraint on S[IV] disproportionation lifetime. For one, as discussed above, it is possible that the loss of S[IV] from our samples includes substantial contributions from non-disproportionation loss processes such as direct oxidation. More significantly, we are unable to explain why Guekezian et al. (1997) find such a short lifetime for S[IV]. The experiments of Guekezian et al. (1997) were conducted at ultrabasic pH (pH> 12.8), and we hypothesized that perhaps basic conditions somehow contributed to faster S[IV] disproportionation. However, the samples of S[IV] that we adjusted to pH=13 showed *slower* decay than the unadjusted S[IV] (Table 6), contradicting this hypothesis. S[IV] disproportionation is sensitive to a wide range of catalysts and inhibitors (Meyer, Mulliken, & Weeks, 1980b, 1980a; Meyer et al., 1982; Petruševski et al., 2013)[7], and it is possible that a catalyst for S[IV] disproportionation was unknowningly present in the Guekezian et al. (1997) measurements. Efforts to contact the authors of Guekezian et al. (1997) to explore this possibility were unsuccessful, and it therefore remains mere speculation. These caveats mean that our data do not fully stand on their own as definitive estimates of $T_{disp,0}$.

However, our data do clearly favor one family of literature reports of anoxic S[IV] lifetime over the other, contradictory literature report. Specifically, even the fastest-decaying of our S[IV] samples shows S[IV] lifetimes ≥ 1 year, favoring the literature reports indicating long S[IV] lifetimes (Meyer et al., 1979; Meyer et al., 1982; Petruševski et al., 2013; Cohen et al., 1982; Halevy et al., 2007) over the literature report indicating short (~ 10 days) S[IV] lifetimes (Guekezian et al., 1997). In our modeling, we therefore do

[7] Meyer (1980) and Searcy (1981) indicate even further reaction sensitivity, including to multivalent transition metal ions; however, these reports are not peer-reviewed.

not adopt the lifetime measure of Guekezian et al. (1997). We instead consider $T_{disp,0} \geq 1 - 5$ years (Meyer et al., 1979; Meyer et al., 1982), a range consistent with our work and that of others (Cohen et al., 1982; Halevy et al., 2007; Petruševski et al., 2013). The bracketing range of key chemical parameters we consider to account for uncertainties in disproportionation kinetics and photolysis quantum yields is summarized in Table 7.

Table 7. Ranges of chemical parameters considered in estimating [S[IV]] in natural waters on early Earth. Parameters are categorized by whether they maximize or minimize [S[IV]], thus enabling a measure of the uncertainty on this quantity. These ranges reflect intrinsic uncertainty regarding the chemical processes controlling [S[IV]] in temperate anoxic environments.

Parameter	[S[IV]]-minimizing	[S[IV]]-maximizing	Comment
$T_{disp,0}$ (years)	1[a]	5[a]	(Meyer et al., 1979; Meyer et al., 1982)
$[S[IV]]_0$ (M)	1	1	(Meyer et al., 1979; Meyer et al., 1982; Searcy, 1981)
n	1	4	Halevy (2013); reaction stoichiometry
$\Phi(> 253.7$ nm)	$\Phi(253.7$ nm)	0	

[a] Lower bounds

4.3 Prebiotic Marine Waters

A wide range of chemical (Table 7) and planetary (Table 4) uncertainties affect estimates of [S[IV]] in marine waters on early Earth. We explore this range. We find that chemical uncertainties dominate the uncertainty in prebiotic marine [S[IV]], with geological uncertainties playing a secondary role that is only relevant in the limit of inefficient chemical loss of S[IV] (Figure 3). The main source of chemical uncertainty is the reaction order of S[IV] disproportionation n. If $n = 1$, then prebiotic marine S[IV] concentrations are suppressed to sub-micromolar concentrations, and possibly sub-nanomolar concentrations, in concordance with Halevy (2013). On the other hand, if $n = 4$, then S[IV] disproportionation is kinetically inhibited and S[IV] is able to accumulate to higher concentrations, as recognized by Kasting et al. (1989). An upper limit on [S[IV]] is imposed by photolysis even in the limit of $n > 1$ and even if S[IV] photolysis is inefficient ($\Phi_{HSO_3^-}(> 254$ nm$) = \Phi_{SO_3^{2-}}(> 254$ nm$) = 0$). This upper limit keeps S[IV] subsaturation with respect to atmospheric SO_2, meaning that surface deposition of SO_2 remains efficient, consistent with the assumptions in our photochemical modeling. Efficient deposition of SO_2 means that a UV-attenuating S_8 layer did not persist on early Earth (Kasting et al., 1989).

4.4 Prebiotic Terrestrial Waters

Terrestrial waters embrace hydrological and chemical diversity far exceeding marine waters (Lerman et al., 1995), and it is impractical to explore their full diversity. Nevertheless, we can gain some sense of [S[IV]] in terrestrial waters on prebiotic Earth by considering a few representative end-member scenarios, motivated by proposed origin-of-life theories. We specifically consider 1 m-deep freshwater and closed-basin carbonate lakes, with inorganic ion composition and corresponding absorbances following Ranjan, Kufner, et al. (2022) (Table 5).

We find that the choice of geological scenario dominates chemical uncertainties in controlling [S[IV]] (Figure 4). Thermal loss processes are less important than the pho-

tochemical loss processes, because they are integrated over a shallower column compared to the marine scenario. Photolysis is the main control on S[IV] in most terrestrial scenarios. In most scenarios, photolysis regulates S[IV] to sub-micromolar concentrations for $\frac{\phi}{\phi_0} \leq 10$. S[IV] exceeds micromolar concentrations for enhanced volcanic outgassing rates relative to modern Earth ($\frac{\phi}{\phi_0} > 10$). As in the marine case, the uncertainty in disproportionation rates is dominated by the order of reaction of sulfite disproportionation, but the influence of this uncertainty on S[IV] is muted by the decreased importance of disproportionation relative to photolysis. Photolysis is minimized in non-basic waters where less-absorptive HSO_3^- is the main form of S[IV]. Photolysis may also be reduced in UV-opaque waters, though in this case radical generation from absorption of UV by environmental reagents may yet lead to S[IV] loss (e.g., Li et al. (2020)). In this scenario, S[IV] may exceed micromolar concentrations at modern Earth-like outgassing fluxes, and disproportionation and seepage may be sinks of comparable importance to photolysis (Figure 4).

5 Discussion

5.1 [S[IV]] in Prebiotic Natural Waters

S[IV] was a prebiotic reagent, but its steady-state global-mean concentrations were modest at best due to photolysis. The rate of disproportionation of S[IV] at temperate conditions, previously proposed as the main sink of prebiotic S[IV], is slow even at high concentrations, and may be even slower at prebiotically-relevant [S[IV]]. However, UV photolysis places a strong upper limit on prebiotic [S[IV]], which was neglected by previous studies (Kasting et al., 1989; Halevy, 2013; Ranjan et al., 2018; Loftus et al., 2019). HSO_3^- and SO_3^{2-}, the main forms of S[IV] at concentrations and pH relative to prebiotic natural waters, are strong UV chromophores. Absorption of prebiotically-abundant UV radiation by HSO_3^- and SO_3^{2-} ultimately leads to oxidation to sulfate. This phenomenon has been characterized in the laboratory, and is used in environmental applications to remove aqueous pollutants (Fischer & Warneck, 1996; Huang et al., 2010; Cao et al., 2021; Wu et al., 2021).

Photolysis confines S[IV] to submicromolar concentrations in the prebiotic ocean across most of parameter space. For S[IV] to exceed micromolar concentrations, the kinetics of chemical loss of S[IV] need to be near the efficiency limit allowed by experiments ($\Phi(\lambda > 254 \text{ nm}) = 0$, $n \geq 2$). Additionally, volcanic outgassing on early Earth must exceed volcanic outgassing on modern Earth by an order of magnitude or more ($\frac{\phi}{\phi_0} \geq 10$), and the pH must be acidic (maximizing the amount of sulfite in less-photolytic HSO_3^-). However, the pH likely cannot be too acidic, due to tentative indications that disproportionation is more efficient at low pH (SI 2.3.1; Searcy (1981)). We may wonder whether it is possible for enhanced concentrations of S[IV] to build up in the deep ocean, where it is protected from photolysis. If the sole source of S[IV] is the atmosphere and assuming diffusion to be the sole mechanism transporting S[IV] from the surface where it is injected down to depth, then this scenario is not possible, because it would require diffusion to create a gradient. However, local sources of SO_2 at depth (e.g., hydrothermal systems; (Butterfield et al., 2011; Peters et al., 2021; Barge & Price, 2022)) could generate locally enhanced [S[IV]] at depth. Similarly, non-diffusive transport processes might be able to generate enhanced marine [S[IV]] at depth. Models incorporating 3D transport are required to probe these possibilities and resolve the degree of enhancement possible.

Higher concentrations of S[IV] are possible in atmospherically-supplied terrestrial waters relative to marine waters, because the supply rate remains the same while loss processes have a shallower column over which to operate. Even so, photolysis rigorously limits accumulation of S[IV]. Achieving higher [S[IV]] in terrestrial waters at modern Earth-like volcanic outgassing requires a geologically favorable environment, of which the most

important factors are the background UV absorptivity and the depth. Shallower waters can accumulate higher [S[IV]] because fewer total UV photons are absorbed (Figure 5). In other words, as depth decreases, a larger fraction of incident photons are absorbed by the base of the water body or scattered back out of the surface, as opposed to photolyzing S[IV]. Similarly, if UV-absorbing compounds are present in the water, then these compounds can absorb UV photons that would otherwise photolyze S[IV], which may permit S[IV] accumulation (Figure 6). We say *may* because absorption of UV photons by background absorbers may yet lead to sulfite loss. For example, absorption of UV radiation by UV-attenuating halogen salts leads to radical production (Jortner et al., 1964), and such radicals may react with and destroy S[IV] (Yu et al., 2018). On the other hand, Fe^{2+} appears to inhibit S[IV] photolysis by attenuation of UV (Li et al., 2014), as does humic acid (Yang et al., 2020). Detailed studies on a case-by-case basis of specific natural waters are required to confirm the effect of background absorbers on S[IV] accumulation (Yang et al., 2020; Cao et al., 2021).

The volcanic outgassing rate, especially of SO_2, is a key uncertainty on [S[IV]]. If steady-state volcanic outgassing were elevated relative to modern ($\frac{\phi}{\phi_0} \geq 20$), then steady-state [S[IV]] should have exceeded micromolar [S[IV]] in even geologically unfavorable terrestrial waters. On the other hand, if steady-state volcanic outgassing were suppressed relative to modern ($\frac{\phi}{\phi_0} \leq 0.1$), then micromolar [S[IV]] is not accessible in even geologically favorable terrestrial waters. ϕ_{SO_2} is highly uncertain. Scalings based on plate tectonics suggest volcanic outgassing was enhanced on early Earth 4−9× (Richter, 1985; Sleep & Zahnle, 2001). However, early Earth may have featured less SO_2 outgassing due to lower concentrations of recycled oceanic sulfate (Harman, Pavlov, et al., 2018), or due to higher magmatic degassing pressures (Gaillard et al., 2011), though this is debated (Brounce et al., 2017; Korenaga, 2021). Measurements of sulfur mass-independent fractionation (S-MIF) may ultimately directly constrain early sulfur outgassing fluxes, and indeed attempts to match S-MIF measurements with photochemical models hint at enhanced SO_2 column densities (Endo et al., 2016). However, all photochemical models ultimately fail to accurately reproduce the S-MIF signal to the accuracy required to infer ϕ_{SO_2} (Ono et al., 2003; Claire et al., 2014; Harman, Felton, et al., 2018; Endo et al., 2019). We advocate for detailed modeling of early Earth SO_2 outgassing, as well as the improved laboratory measurements and photochemical modeling required to directly constrain SO_2 emission rates from S-MIF measurements, to constrain this key uncertainty.

5.2 Implications for Prebiotic Chemistry and Early Habitability

S[IV] was suppressed in prebiotic terrestrial waters by photolysis. [S[IV]]$< 100\ \mu$M for terrestrial waters in almost all of the parameter space relevant to early Earth, and [S[IV]] could have been in the nM range for transparent global-mean 1-m deep ponds and lakes if volcanic outgassing were suppressed relative to modern ($\frac{\phi}{\phi_0} = 0.1$). For comparison, [S[IV]] used in laboratory studies of prebiotic chemistry ranges from 10 mM (Kawai et al., 2019; Rimmer et al., 2021; Liu et al., 2021) to 3 M (Becker et al., 2019). That these concentrations are unrealistically high is well-understood, and justified on the grounds that reaction mechanisms discovered at elevated concentrations which render their kinetics accessible to laboratory study will still apply at lower, more prebiotically relevant concentrations. There is evidence to support this view; for example, HCN homologation via photoredox cycling of cyanocuprate was first demonstrated with 10 mM Cu[I] but also functions at 63 μM Cu[I] (Ritson & Sutherland, 2012; Todd et al., 2018), sugar sequestration via sulfonate formation was demonstrated at 10 mM S[IV] but is thought to function at micromolar S[IV] as well (Kawai et al., 2019; Benner et al., 2019), and CO_2 photoreduction by S[IV] *improves* in yield with 10 mM S[IV] compared to 100 mM S[IV] (Liu et al., 2021). However, it is also possible that there is a critical [S[IV]] below which a given S[IV]-dependent prebiotic chemistry will not function, just as there are critical UV flux levels below which UV-dependent prebiotic chemistries fail to function (Rimmer et al., 2018; Rimmer et al., 2021). To confirm that a S[IV]-dependent prebiotic chem-

istry demonstrated in the laboratory could have occurred in nature, it is necessary to characterize the minimum [S[IV]] required for the chemistry to function, and to compare this threshold [S[IV]] to the [S[IV]] available in the natural waters invoked by the prebiotic chemical scenario (Benner et al., 2010, 2019; Sasselov et al., 2020; Walton et al., 2022). We advocate for such studies.

While steady-state global-mean [S[IV]] was low, [S[IV]] was transiently elevated after stochastic events like large volcanic eruptions and perhaps also after large impacts which generate a UV-attenuating haze layer. During major volcanic eruptions on Earth, $\frac{\phi}{\phi_0} = 20 - 200$ for a period of $10 - 1$ years (Self et al., 2006; Halevy & Head, 2014), which would permit $\geq 1\mu$M S[IV] in shallow closed-basin lakes during the eruption (Figure 4). Origins-of-life chemistry invoking this scenario would need to be shown to function with transient, relatively short-lived elevated S[IV]. Similarly, early Earth is proposed to have experienced epochs with very low surface UV irradiation due to formation of UV-attenuating atmospheric hazes in the aftermaths of large impacts (Benner et al., 2020; Zahnle et al., 2020; Citron & Stewart, 2022; Itcovitz et al., 2022). In the absence of UV light, the sink on S[IV] due to photolysis would have been absent, permitting accumulation of S[IV] until limited by disproportionation, seepage, or outgassing. This scenario would work for prebiotic chemistry which does not require UV light (e.g., Benner et al. (2019); Becker et al. (2019)). However, prebiotic chemistry that invokes S[IV] in conjunction with UV light would not be able to exploit this case (e.g., J. Xu et al. (2018); Liu et al. (2021); Green et al. (2021)).

Steady-state S[IV] could also have been enhanced in specific geophysical contexts. Most obviously, [S[IV]] would have been high in hydrothermal systems such as hot springs. Terrestrial hot springs have been proposed as compelling venues for origins-of-life chemistry, due to favorable ionic composition for lipid membrane assembly, presence of key reagents for prebiotic syntheses, and propensity for wet-dry cycles towards oligomerization and compartmentalization (Mulkidjanian et al., 2012; Rimmer & Shorttle, 2019; Damer & Deamer, 2020; Omran & Pasek, 2020). Such hot springs could have featured enhanced [S[IV]] due to continuous hydrothermal supply from below; for example, hot springs in Yellowstone National Park feature [S[IV]]$= 0.4{-}5\mu$M (Kamyshny et al., 2014). In support of this hypothesis is phylogenetic evidence suggesting ancient sulfite reducing metabolism in hot spring-dwelling microbes, which implies the existence of hot springs with elevated sulfite concentrations early in Earth's history (Colman et al., 2020). Hot springs would have been a particularly favorable environment for prebiotic chemistry which also invokes sulfide (e.g., J. Xu et al. (2020)), which is not generally available beyond hydrothermal systems (Ranjan et al., 2018). [S[IV]] is also enhanced in extremely shallow waters, due to a reduced column over which loss processes can operate while the atmospheric delivery flux remains unchanged (Figure 5). Notably, waters undergoing wet-dry cycles pass through shallow phases during which [S[IV]] would have been enhanced; the timescale for a 1-cm layer of water to accumulate 1 μM of S[IV] from dry deposition under an early Earth atmosphere under exposure to modern Earth-like outgassing rates is 3 days. This means that a pond experiencing slow seasonal wet-dry cycling as invoked by some prebiotic chemistries (Deamer & Damer, 2017; Pearce et al., 2017; Becker et al., 2018; Campbell et al., 2019) would inevitably have passed through S[IV]-rich phases. Finally, waters which contain a UV-shielding compound (one which absorbs UV light at concentrations accessible in natural waters on early Earth without generating S[IV]-destroying products) would have accumulated higher [S[IV]]. Fe^{2+} is a potential UV shield based on its broad UV absorption (Fontana et al., 2007; Ranjan, Kufner, et al., 2022), which inhibits S[IV] photolysis at 2 mg L^{-1} (36 μM) in industrial applications (Li et al., 2014). However, the abundance of Fe^{2+} in prebiotic natural waters remains unclear, with dependence on pCO_2, pH_2S, and assumptions regarding photoredox cycling, among other parameters (Braterman et al., 1983; Konhauser et al., 2017; Hao et al., 2017; Sahai et al., 2022). Our consideration of potential UV absorbers is by no means exhaustive; a number of further candidates remain to be evaluated, including silicate and basaltic dust and

meteoritic or atmospheric organics (B. Pearce, personal communication, 2019). Finally, prebiotic chemistry may itself generate UV-attenuating organic surface layers (Cleaves & Miller, 1998; Yang et al., 2020; Todd et al., 2021). We encourage the experimental and modeling work required to self-consistently explore these potential UV-shielded prebiotic scenarios.

Marine S[IV] levels were even lower than terrestrial S[IV]. Global mean marine S[IV] could only have exceeded micromolar concentrations if volcanic outgassing were significantly enhanced relative to modern ($\frac{\phi}{\phi_0} \geq 10$), oceanic geologic parameters (especially pH) favorable for S[IV] accumulation, and the kinetics of prebiotic S[IV] near the inefficiency limit currently allowed by measurements (subject to the caveats in Section 5.3). However, most marine abiogenesis scenarios invoke specific marine sub-environments, especially hydrothermal vents (Martin et al., 2008; Barge & Price, 2022). Submarine volcanic and hydrothermal settings can feature enhanced [S[IV]] even on modern Earth (Butterfield et al., 2011; Peters et al., 2021), and might have furnished enhanced [S[IV]] on early Earth as well. Such environments are promising venues for S[IV]-dependent chemistry in marine environments.

Our findings imply that UV-attenuating sulfur hazes did not form on prebiotic Earth, because photochemical loss of S[IV] in the prebiotic oceans was sufficient to keep the oceans sub-saturation in S[IV] and atmospheric deposition of SO_2 efficient, despite the considerable uncertainties regarding S[IV] disproportionation kinetics (Kasting et al., 1989; Hu et al., 2013). This means that UV remained a dominant feature of the steady-state prebiotic environment, though transient hazy epochs in the aftermath of large impacts or volcanic explosions may have occurred (Ranjan et al., 2018; Benner et al., 2020; Zahnle et al., 2020).

5.3 Validity and Effect of Simplifying Assumptions

Our modeling is steady-state, and therefore does not resolve time-dependent effects relevant to terrestrial waters. In particular, our modeling ignores the fact that terrestrial waters are likely to vary in depth and therefore [S[IV]] as a function of time, e.g. due to seasonal variations in precipitation and evaporation rate. Time-dependent modeling (e.g., Pearce et al. (2017)) is required to resolve this effect. Similarly, our modeling is global-mean, and does not resolve the heterogeneity of early Earth environments. For example, photolysis rates will be lower in polar regions and higher in equatorial regions relative to the global-mean conditions we model here. Further, SO_2 may not be well-mixed in early Earth's atmosphere, but should have been more abundant near volcanic SO_2 source regions and less abundant far from them, proportionately affecting surface deposition rates; 3D atmospheric modeling is required to capture this affect (Warneck, n.d.; Chin et al., 2000). These limitations mean that our modeling is accurate only to the order-of-magnitude level, which is relevant when interpreting its results.

In calculating wet deposition with MEAC, we have implicitly assumed raindrop pH= 5, as on modern Earth (Giorgi & Chameides, 1985; Hu et al., 2012). However, on early Earth with elevated pCO_2, raindrops would have been more acidic (Halevy et al., 2007; Sahai et al., 2022). More acidic pH would have reduced S[IV] concentrations in raindrops due to less favorable acid dissociation, meaning that this assumption overestimates wet deposition of SO_2. Our conclusions are insensitive to this simplification because for the closed-basin waters we model here, S[IV] supply is dominated by dry deposition, not wet deposition. Furthermore, decreased efficiency of wet deposition is partially compensated by increased efficiency of dry deposition, since less efficient wet deposition of atmospheric SO_2 increases pSO_2. However, raindrop pH may have more significant implications for open basin systems, which can be modeled as weathered rainwater (Hao et al., 2017; Sahai et al., 2022).

When calculating scalar irradiance in aqueous solution, we have employed formalisms primarily derived from marine waters. These formalisms may not be accurate for terrestrial waters. In particular, for marine waters we may assume that the radiation field vanishes at depth, but the radiation field might not vanish at depth for terrestrial waters. By analogy with atmospheric UV transmission (Ranjan & Sasselov, 2017), photolysis rates may be enhanced up to 4× for the worst-case scenario of shallow, low-absorptivity waters underlain by a surface with high-UV reflectivity. However, this worst-case scenario is unlikely to be realized, because most natural surfaces, including the basalts proposed to have constituted the first land (Bada & Korenaga, 2018; Rosas & Korenaga, 2021; Korenaga, 2021), have low reflectivity in the UV (Dollfus et al., 1980; Turner & Parisi, 2018), meaning that the radiation field should vanish at depth.

The S[IV] photochemical kinetic parameters employed at this work were typically derived at [S[IV]] much higher than available in realistic prebiotic environments. It is possible that the value of some of these parameters is a function of [S[IV]]. For example, studies of photolysis of 2-aminooxazole and photodegradation of ferrocyanide suggest concentration-dependent effective loss rates, perhaps explained by more efficient geminate recombination (i.e. back-reactions which reform the photolyzate) at high photolyzate concentrations (Todd et al., 2021; Todd et al., 2022). We have attempted to control for this effect by selecting terminal quantum yields when available for our model, which account for prompt geminate recombination (Lian et al., 2006). Nevertheless, we advocate for characterization of S[IV] photochemical kinetics at lower, more prebiotically relevant [S[IV]] to confirm the validity of our approach.

In our calculations, we have followed our underlying sources and past work in quantifying chemical kinetics using chemical concentrations, not activities (Zhang & Millero, 1991; Halevy, 2013). That is, we have implicitly assumed activity coefficients of unity, neglecting the potentially decreased reactivity of chemical species like S[IV] in solutions with high ionic strength. Formally, this means that our calculations may underestimate S[IV] in solutions with high ionic strength. This does not directly affect our conclusions, as the upper limits on [S[IV]] are set by photolysis. However, increased ionic strength can suppress the efficacy of photolysis, with SO_3^{2-} photolysis quantum yields decreasing by 6-12% per 1M ionic strength (Sauer, Shkrob, et al., 2004). This means that our calculation may underestimate [S[IV]] by $\leq$14% in the prebiotic ocean and $\leq 2\times$ of closed-basin carbonate lakes; our conclusions are robust to uncertainties of this magnitude.

We have modeled the transformations of S[IV] in isolation in this work, as is common in assessing potential prebiotic reagents on early Earth (e.g., Harman et al. (2013); Wong et al. (2017); Adams et al. (2021)). In reality, S[IV] would have existed in conjunction with diverse other chemical species on early Earth, and those chemical species could have interacted with S[IV]. Significantly, NO_3^- was likely also atmospherically synthesized on early Earth, and might have reacted with S[IV] (Littlejohn et al., 1986; Mancinelli & McKay, 1988; Summers & Khare, 2007). This means that our calculation may omit other relevant sinks of S[IV], and hence may overestimate [S[IV]]. We advocate coupled modeling/laboratory simulation of the interaction of S[IV] with other prebiotic reagents to remediate this caveat.

The quantum yield of HSO_3^- photolysis, $\Phi_{HSO_3^-}(\lambda)$ is extremely poorly constrained, and may be overestimated in our model. We are aware of only one constraint on $\Phi_{HSO_3^-}(\lambda)$, at 213.9 nm, and this measurement must be interpreted as an upper bound (Fischer & Warneck, 1996; Sauer, Crowell, & Shkrob, 2004). We have implemented HSO_3^- photolysis in our model under the assumption that $\Phi_{HSO_3^-}$(213.9 nm) corresponds to its upper bound, and estimated its value at other wavelengths on the basis of scaling the quantum yield of SO_3^- photolysis. While this scaling reproduces the observation that solutions with S[IV] primarily present as HSO_3^- photolyze less efficiently than solutions with S[IV] primarily present as SO_3^{2-} (Li et al., 2012, 2014; Wu et al., 2021), this is an easy

constraint to satisfy and our estimate of $\Phi_{HSO_3^-}(\lambda)$ remains a major assumption with minimal physical justification. In particular, our implementation leaves open the possibility that we are overestimating the efficiency of $\Phi_{HSO_3^-}(\lambda)$. For example, studies of the effect of pH on S[IV] photolysis-driven photodegradation are able to reproduce measurements while neglecting HSO_3^- photolysis altogether (solely considering SO_3^{2-} photolysis), even at pH regimes where HSO_3^- is dominant (Li et al., 2012, 2014). Sensitivity tests with $\Phi_{HSO_3^-} = 0$ indicate that we may underestimate [S[IV]] by up to a factor of a few at slightly acidic pH (pH= 6.25); the underestimate may be worse at more acidic pH due to increased speciation as HSO_3^-, but our current modeling is not able to probe this regime because we lack robust constraints on $T_{disp,0}$ at acidic pH. We advocate better constraints on $\Phi_{HSO_3^-}(\lambda)$ to remediate this caveat.

5.4 Prospects for Empirical Test

The calculations in this paper constitute theoretical predictions of [S[IV]] on early Earth; here we consider possibilities for testing these predictions. Direct geological constraints on early [S[IV]] would be ideal, but such constraints are so far nonexistent because of the generally high solubility of S[IV] minerals which inhibits their preservation through geological time on Earth. However, three pathways are emerging which may permit empirical constraints on early [S[IV]]. First, phylogenetic studies have begun to elucidate the origin of sulfur reducing metabolism, including whether it was sulfite or sulfate that was first reduced, and in which environments (Colman et al., 2020; Chernyh et al., 2020). Since the existence of sulfite reduction implies the existence of sulfite, such studies may eventually probe [S[IV]] in early natural waters. Second, nitrate and nitrite minerals face similar preservation challenges as S[IV] minerals, but isotopic studies of ancient kerogens have constrained differential NO_X^- abundances in marine and lacustrine waters on 3.2 Ga Earth by probing for signatures of NO_X^--reducing metabolism (Homann et al., 2018). If similar techniques can be developed for S[IV], they may permit similar constraints on early [S[IV]] in natural waters. Finally, plate tectonics and hydrology on Earth render ancient rocks rare, but these processes have been inoperative on Mars for billions of years, and much of the Martian surface is ancient (Sasselov et al., 2020). Measurements from the Curiosity rover are consistent with the presence of trace Fe sulfate or Ca sulfite minerals on Mars (McAdam et al., 2014; Franz et al., 2017; Franz et al., 2019). If Martian chemical analyses can be refined to discriminate between these two progenitor possibilities, then they will enable direct tests of models like the one developed in this paper, though secondary alteration processes will need to be controlled for (Marion et al., 2013).

6 Conclusions

S[IV] plays key roles in proposed prebiotic chemistries and in controlling planetary climate and UV irradiation. Here, we have developed a novel 0D aqueous photochemical model calibrated with new laboratory measurements of S[IV] disproportionation kinetics and 1D atmospheric photochemical modeling to estimate [S[IV]] in marine and closed-basin terrestrial waters on early Earth. We show that S[IV] disproportionation was inhibited at pH$>$ 7 ($T_{disp,0} \geq 1$ year), meaning that S[IV] was a prebiotic reagent on early Earth. Nevertheless, we also show that photolysis imposed a firm upper limit on [S[IV]] (< 100 μM). Marine [S[IV]] was sub-saturation with respect to atmospheric SO_2, meaning atmospheric deposition of SO_2 was efficient on early Earth and climate-altering, UV-attenuating sulfur hazes suggested as possibilities for early Earth and similar worlds did not form (Kasting et al., 1989). Terrestrial [S[IV]]≥ 1 μM on a steady-state global-mean basis if volcanic outgassing of SO_2 was enhanced relative to modern ($\frac{\phi}{\phi_0} \geq 20$). Terrestrial [S[IV]]$\geq 1$ μM on a transient global-mean basis after major volcanic eruptions and after large, haze-generating impacts. Terrestrial [S[IV]]≥ 1 μM on a steady-state local basis in waters proximate to SO_2 supply (e.g, hydrothermal systems),

in shallow waters ($d < 10$ cm), or in UV-opaque waters. Terrestrial [S[IV]]≥ 1 μM on a transient local basis for waters undergoing wet-dry cycling, as has been invoked by diverse prebiotic chemistries. Our predictions may eventually be empirically tested by phylogenetic studies, terrestrial geochemical measurements, or measurements from Martian rocks may directly constrain early S[IV]. We encourage such investigations.

Our work is a first step in understanding prebiotic [S[IV]]. The substantial uncertainties on our estimates of prebiotic S[IV] can be reduced by an improved understanding of S[IV] photochemical kinetics and the early geochemical environment. The main planetary uncertainties are the SO_2 outgassing rate (ϕ_{SO_2}) and the absorptivity of prebiotic natural waters. Outgassing modeling and/or interpretation of the S-MIF record can constrain the former; self-consistent investigation of potential UV absorbers (e.g., Fe^{2+}) and their abundances in prebiotic natural waters can constrain the latter. For terrestrial waters, it is most important to measure $\Phi_{HSO_3^-}(\lambda)$ ($\lambda = 200{-}320$ nm), $\Phi_{SO_3^{2-}}(\lambda)$ for $\lambda = 254 - 280$ nm, the order of S[IV] disproportionation n at standard conditions and at prebiotically-relevant concentrations ($< 100\mu$M), and $T_{disp,0}$ at standard conditions, in that order. For marine waters, it is most important to measure n, $\Phi_{HSO_3^-}(\lambda = 200 - 320$ nm), $\Phi_{SO_3^{2-}}(\lambda = 254 - 280$ nm) and $T_{disp,0}$ at standard conditions, in that order. Finally, we advocate for experimental characterization of the sensitivity of S[IV]-dependent prebiotic chemistries to [S[IV]], to confirm whether organic synthetic chemical pathways that work under laboratory conditions ([S[IV]]≥ 10 mM) could also have functioned in natural prebiotic environments ([S[IV]]< 100 μM). Such work is being done for UV irradiation (Rimmer et al., 2018; Rimmer et al., 2021); we argue for similar work for S[IV] (Benner et al., 2019).

7 Open Research

The code implementing the S[IV] aqueous box model, the UV-VIS raw data and processing scripts, and the atmospheric photochemistry simulation outputs employed in this work are available on GitHub (`https://github.com/sukritranjan/sulfite-kinetics-release`). The solution-phase analytics raw data and processing is available in Supplemental Information Data Set 1. The atmospheric photochemistry model used to generate the atmospheric photochemistry simulation outputs, MEAC, is not publicly available, but its simulation outputs used in this paper are available in the GitHub repository, (`https://github.com/sukritranjan/sulfite-kinetics-release`), and MEAC's input files are available by request.

Acknowledgments

This work was supported in part by grants from the Simons Foundation (SCOL Award# 495062 to S.R.; 390360 to D. D. S.). Z.R.T. acknowledges support for this work from NASA through the NASA Hubble Fellowship grant # HST:HF2-51471 awarded by the Space Telescope Science Institute, which is operated by the Association of Universities for Research in Astronomy, Incorporated, under NASA contract NAS5-26555. N.S. acknowledges support from NSF EAR 1829695, NASA Award 80NSSC18K1139 subaward RK558-G2 and generous private gift funds from Ed. Weil. S. R. thanks Northwestern University for support via the CIERA Postdoctoral Fellowship. This research has made use of NASA's Astrophysics Data System.

We thank Rebecca Rapf and Alec Kroll for discussions regarding sulfite in raindrops; Furktan Ozturk for assistance with the electropotentiometry setup; Ruibo Hu for investigations of solid formation in some of our failed experiments; Itay Halevy for sharing a poster (Mirzoyan & Halevy, 2014); David Catling for answers to questions (Toner & Catling, 2020); and Furkan Ozturk, Itay Halevy, Kaitlyn Loftus, Sarah Crucilla, Paul Rimmer, Steven Benner, William Bains, and John Sutherland for valuable discussions.

We thank the Simons Collaboration on the Origin of Life and the Harvard Origins of Life Initiative for nurturing many fruitful conversations related to this paper.

Author Contribution Statement:

S.R. conceived research; K. A. developed solution analytics; K.A. and C.Y.Z. executed solution analytics; G. L. and C. K. developed and carried out preparation of solutions and UV-VIS spectroscopy; S. M. and S. R. carried out atmospheric photochemical modelling; S. R. developed and executed aqueous photochemistry modeling; N.S. critiqued aqueous modeling; S. R., Z. R. T., and D. D. S. explored implications for prebiotic chemistry; S. R. drafted manuscript. All authors reviewed and commented on the manuscript.

Conflict of Interest

The authors declare no conflicts of interest relevant to this study.

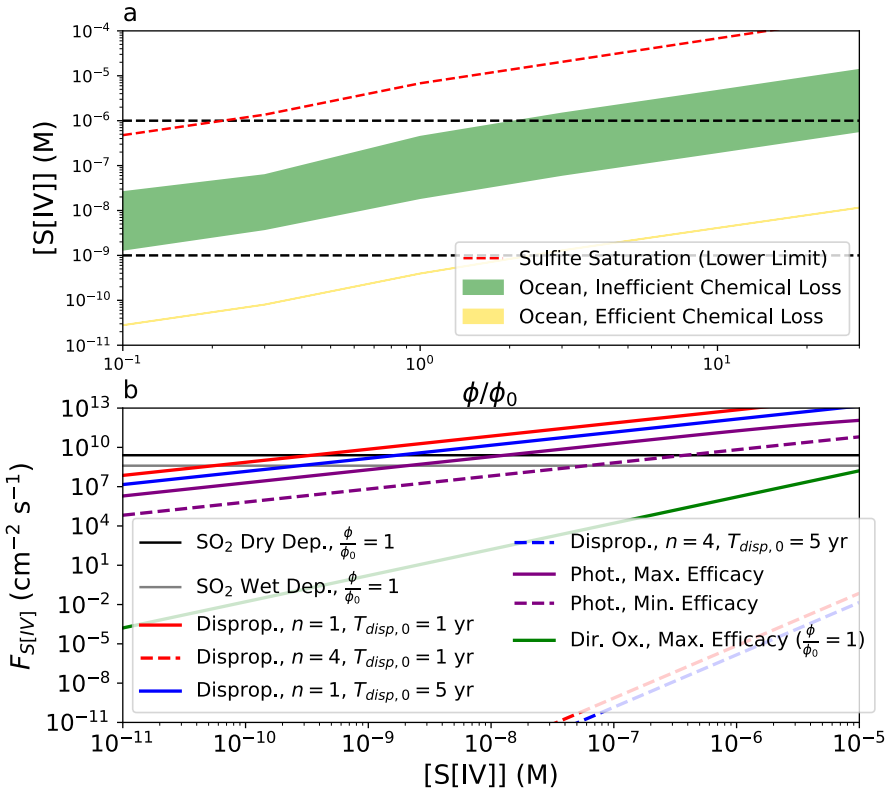

Figure 3. (a) Top: Range of S[IV] concentrations in the prebiotic ocean as a function of volcanic outgassing. Uncertainty in prebiotic marine [S[IV]] is dominated by uncertainties in the chemical parameters, with uncertainty in the geological parameters playing a secondary role. Regardless, the oceans do not saturate in S[IV] (red dashed line). S[IV] saturation threshold calculated assuming Henry equilibrium with the atmosphere, including the first and second dissociations of SO_2, and for an acidic ocean pH= 6.25 which favors saturation (Millero et al., 1989; Burkholder et al., 2015; Ranjan et al., 2018; Krissansen-Totton et al., 2018). (b) Bottom: Major S[IV] supply and loss processes in the prebiotic ocean. Each line represents the rate of S[IV] supply/loss as a function of [S[IV]]. pO_2 adopted in estimating oxidation rate corresponds to $\frac{\phi}{\phi_0}=1$; pO_2 decreases as $\frac{\phi}{\phi_0}$ increases because of the increased reductant flux. The main chemical uncertainty is the order of the disproportionation reaction; if disproportionation is high-order, then sulfite disproportionation is kinetically inhibited (Kasting et al., 1989). Regardless, photolysis imposes an upper bound on [S[IV]] that keeps the oceans sub-saturation.

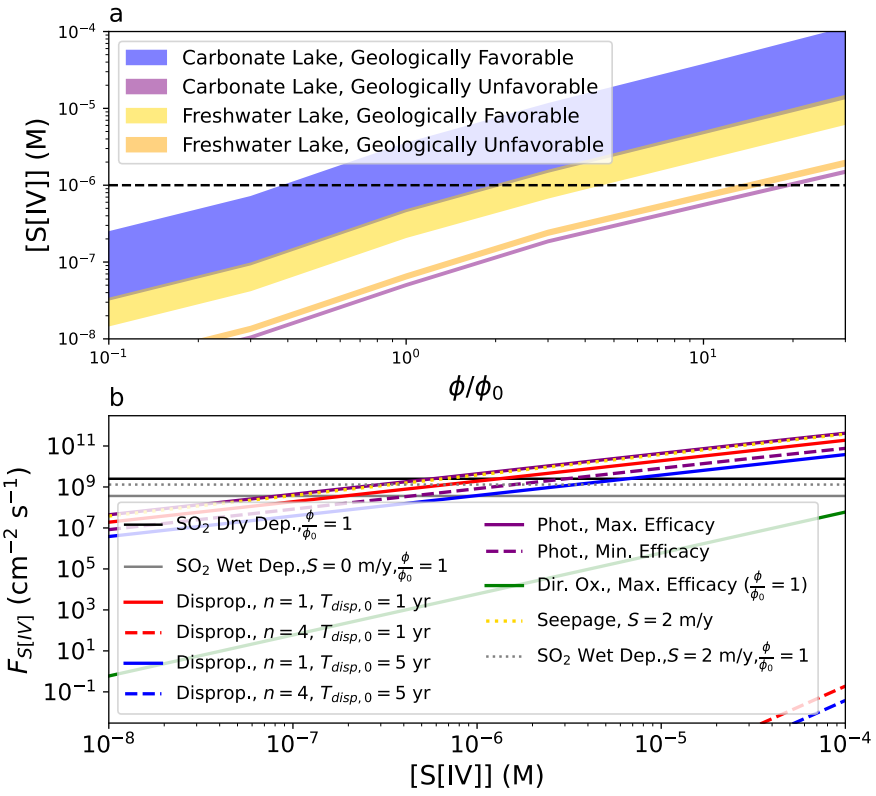

Figure 4. (a) Top: Range of S[IV] concentrations in the prebiotic ocean as a function of volcanic outgassing. Range of [S[IV]] is dominated by geological scenario. (b) Bottom: Major S[IV] supply and loss processes for the geologically-favorable carbonate lake scenario from (a). Each line represents the rate of S[IV] supply/loss as a function of [S[IV]]. pO_2 adopted in estimating oxidation rate corresponds to $\frac{\phi}{\phi_0} = 1$; pO_2 decreases as $\frac{\phi}{\phi_0}$ increases because of the increased reductant flux. To illustrate the potential impact of seepage, the dotted lines show the sink due to seepage if $S = 2$ m/yr, as well as the implicit enhancement in P (Equation 12) in the steady-state lake we assume. Such high seepage rates correspond to a more porous lake bottom.

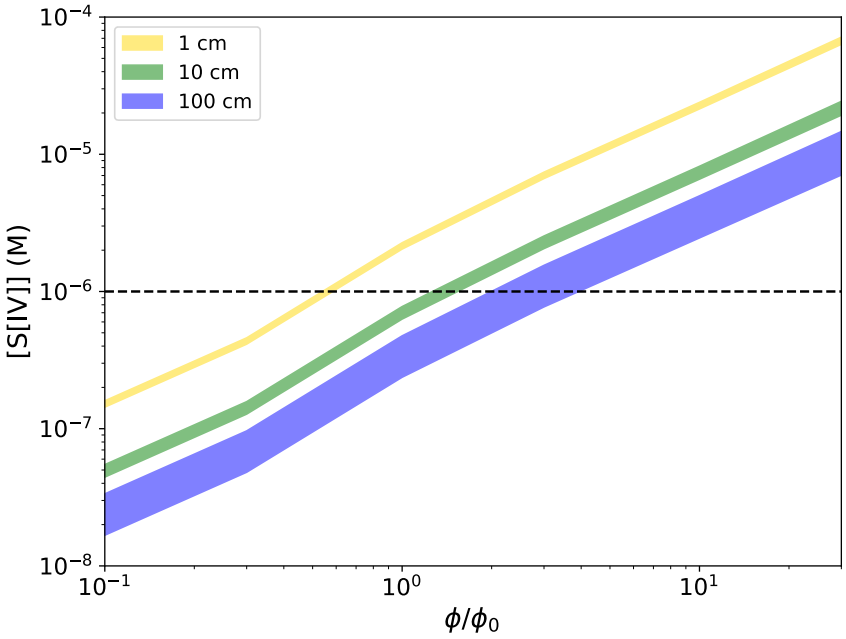

Figure 5. [S[IV]] in lakes as a function of volcanic outgassing, for lakes of depth 1 cm, 10, cm, and 100 cm. Shallow lakes favor S[IV] accumulation because of a shorter column for loss processes to operate over. Scenario corresponds to a prebiotic freshwater lake with geologically favorable parameters for S[IV] accumulation (Table 5). Spread for each scenario is due to uncertainties in chemical kinetics.

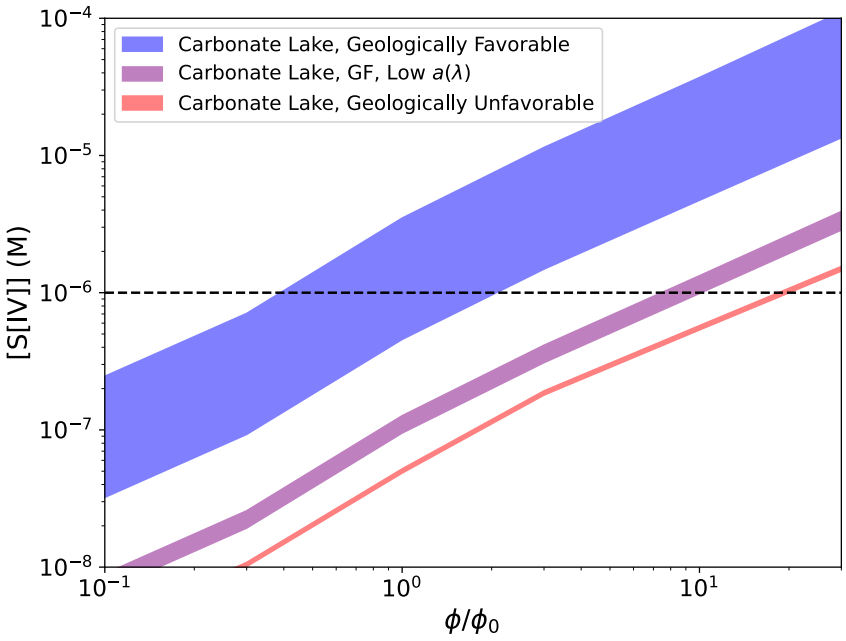

Figure 6. [S[IV]] in prebiotic carbonate lakes for geologically favorable and geologically unfavorable scenarios for S[IV] accumulation (Table 5). The main difference between the favorable and unfavorable scenarios is the background absorptivity of the lake ($a(\lambda)$), as illustrated by the purple curve, which corresponds to the favorable scenario with the sole modification that $a(\lambda)$ is taken to correspond to the low-absorptivity endmember. The purple curve is closer to the red curve than the blue, illustrating the controlling role of $a(\lambda)$) and the need to understand the UV absorptivity of prebiotic natural waters (Ranjan, Kufner, et al., 2022). Spread for each scenario is due to uncertainties in chemical kinetics.

References

Adams, D., Luo, Y., Wong, M. L., Dunn, P., Christensen, M., Dong, C., ... Yung, Y. (2021, August). Nitrogen Fixation at Early Mars. *Astrobiology*, *21*(8), 968-980. doi: 10.1089/ast.2020.2273

Anbar, A. D., & Holland, H. D. (1992, July). The photochemistry of manganese and the origin of banded iron formations. *Geochimica et Cosmochimica Acta*, *56*(7), 2595-2603. doi: 10.1016/0016-7037(92)90346-K

Arney, G., Domagal-Goldman, S. D., Meadows, V. S., Wolf, E. T., Schwieterman, E., Charnay, B., ... Trainer, M. G. (2016, Nov). The Pale Orange Dot: The Spectrum and Habitability of Hazy Archean Earth. *Astrobiology*, *16*(11), 873-899. doi: 10.1089/ast.2015.1422

Arney, G. N., Meadows, V. S., Domagal-Goldman, S. D., Deming, D., Robinson, T. D., Tovar, G., ... Schwieterman, E. (2017, February). Pale Orange Dots: The Impact of Organic Haze on the Habitability and Detectability of Earthlike Exoplanets. *Astrophysical Journal*, *836*(1), 49. doi: 10.3847/1538-4357/836/1/49

Bada, J. L., & Korenaga, J. (2018). Exposed areas above sea level on earth¿ 3.5 gyr ago: Implications for prebiotic and primitive biotic chemistry. *Life*, *8*(4), 55.

Barge, L. M., & Price, R. E. (2022, December). Diverse geochemical conditions for prebiotic chemistry in shallow-sea alkaline hydrothermal vents. *Nature Geoscience*, *15*(12), 976-981. doi: 10.1038/s41561-022-01067-1

Becker, S., Feldmann, J., Wiedemann, S., Okamura, H., Schneider, C., Iwan, K., ... Carell, T. (2019). Unified prebiotically plausible synthesis of pyrimidine and purine rna ribonucleotides. *Science*, *366*(6461), 76–82.

Becker, S., Schneider, C., Okamura, H., Crisp, A., Amatov, T., Dejmek, M., & Carell, T. (2018). Wet-dry cycles enable the parallel origin of canonical and non-canonical nucleosides by continuous synthesis. *Nature communications*, *9*(1), 163.

Benner, S. A. (2023). Rethinking nucleic acids from their origins to their applications. *Philosophical Transactions of the Royal Society B*, *378*(1871), 20220027.

Benner, S. A., Bell, E. A., Biondi, E., Brasser, R., Carell, T., Kim, H.-J., ... Trail, D. (2020). When did life likely emerge on earth in an rna-first process? *ChemSystemsChem*, *2*(2), e1900035.

Benner, S. A., Kim, H.-J., & Biondi, E. (2019). Prebiotic chemistry that could not not have happened. *Life*, *9*(4), 84.

Benner, S. A., Kim, H.-J., Kim, M.-J., & Ricardo, A. (2010). Planetary organic chemistry and the origins of biomolecules. *Cold Spring Harbor perspectives in biology*, *2*(7), a003467.

Beyad, Y., Burns, R., Puxty, G., & Maeder, M. (2014). A speciation study of sulfur (iv) in aqueous solution. *Dalton Transactions*, *43*(5), 2147–2152.

Birkmann, J., Pasel, C., Luckas, M., & Bathen, D. (2018). Uv spectroscopic properties of principal inorganic ionic species in natural waters. *Water Practice & Technology*, *13*(4), 879–892.

Bonfio, C., Valer, L., Scintilla, S., Shah, S., Evans, D. J., Jin, L., ... Mansy, S. S. (2017). Uv-light-driven prebiotic synthesis of iron–sulfur clusters. *Nature Chemistry*.

Boyd, C. E. (1982). Hydrology of small experimental fish ponds at auburn, alabama. *Transactions of the American Fisheries Society*, *111*(5), 638–644.

Braterman, P. S., Cairns-Smith, A. G., & Sloper, R. W. (1983). Photo-oxidation of hydrated fe2+—significance for banded iron formations. *Nature*, *303*(5913), 163–164.

Brounce, M., Stolper, E., & Eiler, J. (2017, August). Redox variations in Mauna Kea lavas, the oxygen fugacity of the Hawaiian plume, and the role of volcanic

gases in Earth's oxygenation. *Proceedings of the National Academy of Science*, *114*(34), 8997-9002. doi: 10.1073/pnas.1619527114

Burkholder, J., Abbatt, J., Huie, R., Kolb, C., Orkin, V., Wine, P., ... Wilmouth, D. (2015). *Chemical kinetics and photochemical data for use in atmospheric studies: Evaluation number 18* (Tech. Rep.). NASA Jet Propulsion Laboratory.

Butterfield, D. A., Nakamura, K.-i., Takano, B., Lilley, M. D., Lupton, J. E., Resing, J. A., & Roe, K. K. (2011). High so2 flux, sulfur accumulation, and gas fractionation at an erupting submarine volcano. *Geology*, *39*(9), 803–806.

Campbell, T. D., Febrian, R., McCarthy, J. T., Kleinschmidt, H. E., Forsythe, J. G., & Bracher, P. J. (2019, October). Prebiotic condensation through wet-dry cycling regulated by deliquescence. *Nature Communications*, *10*, 4508. doi: 10.1038/s41467-019-11834-1

Cao, Y., Qiu, W., Li, J., Jiang, J., & Pang, S. (2021). Review on uv/sulfite process for water and wastewater treatments in the presence or absence of o2. *Science of The Total Environment*, *765*, 142762.

Carmouze, J.-P., Arze, C., & Quintanilla, J. (1992). Lake titicaca: A synthesis of limnological knowledge. In C. Dejoux & E. A. Iltis (Eds.), (Vol. 68, chap. Hydrochemical regulation of the lake and water chemistry of its inflow rivers). Dordrecht: Kluwer Academic.

Carn, S. A., Fioletov, V. E., McLinden, C. A., Li, C., & Krotkov, N. A. (2017, March). A decade of global volcanic SO_2 emissions measured from space. *Scientific Reports*, *7*, 44095. doi: 10.1038/srep44095

Catling, D. C., & Kasting, J. F. (2017). *Atmospheric evolution on inhabited and lifeless worlds*. Cambridge University Press.

Chernyh, N. A., Neukirchen, S., Frolov, E. N., Sousa, F. L., Miroshnichenko, M. L., Merkel, A. Y., ... others (2020). Dissimilatory sulfate reduction in the archaeon 'candidatus vulcanisaeta moutnovskia'sheds light on the evolution of sulfur metabolism. *Nature Microbiology*, *5*(11), 1428–1438.

Chin, M., Rood, R. B., Lin, S.-J., Müller, J.-F., & Thompson, A. M. (2000, October). Atmospheric sulfur cycle simulated in the global model GOCART: Model description and global properties. *Journal of Geophysical Research*, *105*(D20), 24,671-24,687. doi: 10.1029/2000JD900384

Citron, R. I., & Stewart, S. T. (2022, May). Large Impacts onto the Early Earth: Planetary Sterilization and Iron Delivery. *Planetary Science Journal*, *3*(5), 116. doi: 10.3847/PSJ/ac66e8

Claire, M. W., Kasting, J. F., Domagal-Goldman, S. D., Stüeken, E. E., Buick, R., & Meadows, V. S. (2014, September). Modeling the signature of sulfur mass-independent fractionation produced in the Archean atmosphere. *Geochimica Cosmochimica Acta*, *141*, 365-380. doi: 10.1016/j.gca.2014.06.032

Claire, M. W., Sheets, J., Cohen, M., Ribas, I., Meadows, V. S., & Catling, D. C. (2012, September). The Evolution of Solar Flux from 0.1 nm to 160 μm: Quantitative Estimates for Planetary Studies. *Astrophysical Journal*, *757*, 95. doi: 10.1088/0004-637X/757/1/95

Cleaves, H. J., & Miller, S. L. (1998, June). Oceanic Protection of Prebiotic Organic Compounds from UV Radiation. *Proceedings of the National Academy of Science*, *95*, 7260-7263. doi: 10.1073/pnas.95.13.7260

Cockell, C. S. (2000a, February). The ultraviolet history of the terrestrial planets - implications for biological evolution. *Planetary and Space Science*, *48*, 203-214. doi: 10.1016/S0032-0633(99)00087-2

Cockell, C. S. (2000b, October). Ultraviolet Radiation and the Photobiology of Earth's Early Oceans. *Origins of Life and Evolution of the Biosphere*, *30*, 467-500.

Cockell, C. S. (2002, January). Photobiological uncertainties in the Archaean and post-Archaean world. *International Journal of Astrobiology*, *1*, 31-38. doi: 10

.1017/S1473550402001003

Cockell, C. S., Catling, D. C., Davis, W. L., Snook, K., Kepner, R. L., Lee, P., & McKay, C. P. (2000, August). The Ultraviolet Environment of Mars: Biological Implications Past, Present, and Future. *Icarus*, *146*(2), 343-359. doi: 10.1006/icar.2000.6393

Cohen, A., Zangen, M., Koenigsbuch, M., & Goldschmidt, J. (1982). Studies on alkaline earth sulfites—iii [1]. transient solubilities and phase changes of calcium sulfite in seawater. *Desalination*, *41*(2), 215–232.

Colman, D. R., Lindsay, M. R., Amenabar, M. J., Fernandes-Martins, M. C., Roden, E. R., & Boyd, E. S. (2020). Phylogenomic analysis of novel diaforarchaea is consistent with sulfite but not sulfate reduction in volcanic environments on early earth. *The ISME journal*, *14*(5), 1316–1331.

Damer, B., & Deamer, D. (2020, April). The Hot Spring Hypothesis for an Origin of Life. *Astrobiology*, *20*(4), 429-452. doi: 10.1089/ast.2019.2045

Davies, B., Biggs, J., Williams, P., Lee, J., & Thompson, S. (2008). A comparison of the catchment sizes of rivers, streams, ponds, ditches and lakes: implications for protecting aquatic biodiversity in an agricultural landscape. *Hydrobiologia*, *597*(1), 7–17.

Deamer, D., & Damer, B. (2017). Can life begin on enceladus? a perspective from hydrothermal chemistry. *Astrobiology*.

de Carvalho, L. M., & Schwedt, G. (2000). Sulfur speciation by capillary zone electrophoresis: conditions for sulfite stabilization and determination in the presence of sulfate, thiosulfate and peroxodisulfate. *Fresenius' journal of analytical chemistry*, *368*(2), 208–213.

Delclaux, F., Coudrain, A., & Condom, T. (2007). Evaporation estimation on lake titicaca: a synthesis review and modelling. *Hydrological Processes: An International Journal*, *21*(13), 1664–1677.

DeWitt, H. L., Trainer, M. G., Pavlov, A. A., Hasenkopf, C. A., Aiken, A. C., Jimenez, J. L., ... Tolbert, M. A. (2009, June). Reduction in Haze Formation Rate on Prebiotic Earth in the Presence of Hydrogen. *Astrobiology*, *9*, 447-453. doi: 10.1089/ast.2008.0289

Dollfus, A., Cailleux, A., Cervelle, B., Hua, C. T., & Mandeville, J. C. (1980, September). Reflectance spectrophotometry extended to u.v. for terrestrial, lunar and meteoritic samples. *Geochimica et Cosmochimica Acta*, *44*(9), 1293,1299-1297,1310. doi: 10.1016/0016-7037(80)90090-3

Endo, Y., Danielache, S. O., & Ueno, Y. (2019, January). Total Pressure Dependence of Sulfur Mass-Independent Fractionation by SO_2 Photolysis. *Geophysical Research Letters*, *46*(1), 483-491. doi: 10.1029/2018GL080730

Endo, Y., Ueno, Y., Aoyama, S., & Danielache, S. O. (2016, November). Sulfur isotope fractionation by broadband UV radiation to optically thin SO_2 under reducing atmosphere. *Earth and Planetary Science Letters*, *453*, 9-22. doi: 10.1016/j.epsl.2016.07.057

Ferrús, R., & Torrades, F. (1985). Limit of detection in barium sulphate gravimetry for water analysis. *Analyst*, *110*(4), 403–406.

Fischer, M., & Warneck, P. (1996). Photodecomposition and photooxidation of hydrogen sulfite in aqueous solution. *The Journal of Physical Chemistry*, *100*(37), 15111–15117.

Fontana, I., Lauria, A., & Spinolo, G. (2007). Optical absorption spectra of fe2+ and fe3+ in aqueous solutions and hydrated crystals. *Physica status solidi (b)*, *244*(12), 4669–4677.

Franz, H. B., King, P. L., & Gaillard, F. (2019). Sulfur on mars from the atmosphere to the core. In *Volatiles in the martian crust* (pp. 119–183). Elsevier.

Franz, H. B., McAdam, A. C., Ming, D. W., Freissinet, C., Mahaffy, P. R., Eldridge, D. L., ... Sutter, B. (2017, September). Large sulfur isotope fractionations in Martian sediments at Gale crater. *Nature Geoscience*, *10*(9), 658-662. doi:

10.1038/ngeo3002

Gaillard, F., Scaillet, B., & Arndt, N. T. (2011, October). Atmospheric oxygenation caused by a change in volcanic degassing pressure. *Nature*, *478*(7368), 229-232. doi: 10.1038/nature10460

Giorgi, F., & Chameides, W. (1985). The rainout parameterization in a photochemical model. *Journal of Geophysical Research: Atmospheres*, *90*(D5), 7872–7880.

Goldford, J. E., Hartman, H., Marsland, R., & Segrè, D. (2019). Environmental boundary conditions for the origin of life converge to an organo-sulfur metabolism. *Nature ecology & evolution*, *3*(12), 1715–1724.

Green, N. J., Xu, J., & Sutherland, J. D. (2021). Illuminating life's origins: Uv photochemistry in abiotic synthesis of biomolecules. *Journal of the American Chemical Society*, *143*(19), 7219–7236.

G Trainer, M. (2013). Atmospheric prebiotic chemistry and organic hazes. *Current organic chemistry*, *17*(16), 1710–1723.

Guekezian, M., Coichev, N., Suárez-Iha, M. E. V., & Neves, E. d. A. (1997). Stability of sulfur (iv) solutions in the presence of amines and the tendency of sulfite ions to disproportionate in stock solutions. *Analytical letters*, *30*(7), 1423–1436.

Guenther, E. A., Johnson, K. S., & Coale, K. H. (2001). Direct ultraviolet spectrophotometric determination of total sulfide and iodide in natural waters. *Analytical Chemistry*, *73*(14), 3481–3487.

Guzmán-Marmolejo, A., Segura, A., & Escobar-Briones, E. (2013, June). Abiotic Production of Methane in Terrestrial Planets full access. *Astrobiology*, *13*, 550-559. doi: 10.1089/ast.2012.0817

Halevy, I. (2013, October). Production, preservation, and biological processing of mass-independent sulfur isotope fractionation in the Archean surface environment. *Proceedings of the National Academy of Science*, *110*(44), 17644-17649. doi: 10.1073/pnas.1213148110

Halevy, I., & Head, J. W., III. (2014, December). Episodic warming of early Mars by punctuated volcanism. *Nature Geoscience*, *7*, 865-868. doi: 10.1038/ngeo2293

Halevy, I., Zuber, M. T., & Schrag, D. P. (2007, December). A Sulfur Dioxide Climate Feedback on Early Mars. *Science*, *318*, 1903-. doi: 10.1126/science.1147039

Halmer, M. M., Schmincke, H.-U., & Graf, H.-F. (2002, June). The annual volcanic gas input into the atmosphere, in particular into the stratosphere: a global data set for the past 100 years. *Journal of Volcanology and Geothermal Research*, *115*, 511-528. doi: 10.1016/S0377-0273(01)00318-3

Hao, J., Sverjensky, D. A., & Hazen, R. M. (2017, January). A model for late Archean chemical weathering and world average river water. *Earth and Planetary Science Letters*, *457*, 191-203. doi: 10.1016/j.epsl.2016.10.021

Harman, C. E., Felton, R., Hu, R., Domagal-Goldman, S. D., Segura, A., Tian, F., & Kasting, J. F. (2018, Oct). Abiotic O_2 Levels on Planets around F, G, K, and M Stars: Effects of Lightning-produced Catalysts in Eliminating Oxygen False Positives. *Astrophysical Journal*, *866*(1), 56. doi: 10.3847/1538-4357/aadd9b

Harman, C. E., Kasting, J. F., & Wolf, E. T. (2013). Atmospheric production of glycolaldehyde under hazy prebiotic conditions. *Origins of Life and Evolution of Biospheres*, *43*(2), 77–98.

Harman, C. E., Pavlov, A. A., Babikov, D., & Kasting, J. F. (2018, August). Chain formation as a mechanism for mass-independent fractionation of sulfur isotopes in the Archean atmosphere. *Earth and Planetary Science Letters*, *496*, 238-247. doi: 10.1016/j.epsl.2018.05.041

Harman, C. E., Schwieterman, E. W., Schottelkotte, J. C., & Kasting, J. F. (2015,

October). Abiotic O_2 Levels on Planets around F, G, K, and M Stars: Possible False Positives for Life? *Astrophysical Journal*, *812*, 137. doi: 10.1088/0004-637X/812/2/137

Hegg, D. A., & Hobbs, P. V. (1978). Oxidation of sulfur dioxide in aqueous systems with particular reference to the atmosphere. In *Sulfur in the atmosphere* (pp. 241–253). Elsevier.

Higgs, P. G., & Lehman, N. (2015). The rna world: molecular cooperation at the origins of life. *Nature Reviews Genetics*, *16*(1), 7–17.

Homann, M., Sansjofre, P., Van Zuilen, M., Heubeck, C., Gong, J., Killingsworth, B., ... Lalonde, S. V. (2018, July). Microbial life and biogeochemical cycling on land 3,220 million years ago. *Nature Geoscience*, *11*(9), 665-671. doi: 10.1038/s41561-018-0190-9

Hu, R. (2021, November). Photochemistry and Spectral Characterization of Temperate and Gas-rich Exoplanets. *Astrophysical Journal*, *921*(1), 27. doi: 10.3847/1538-4357/ac1789

Hu, R., & Diaz, H. D. (2019). Stability of nitrogen in planetary atmospheres in contact with liquid water. *The Astrophysical Journal*, *886*(2), 126.

Hu, R., Seager, S., & Bains, W. (2012, December). Photochemistry in Terrestrial Exoplanet Atmospheres. I. Photochemistry Model and Benchmark Cases. *Astrophysical Journal*, *761*, 166. doi: 10.1088/0004-637X/761/2/166

Hu, R., Seager, S., & Bains, W. (2013, May). Photochemistry in Terrestrial Exoplanet Atmospheres. II. H_2S and SO_2 Photochemistry in Anoxic Atmospheres. *Astrophysical Journal*, *769*, 6. doi: 10.1088/0004-637X/769/1/6

Huang, C., Linkous, C. A., Adebiyi, O., & T-Raissi, A. (2010). Hydrogen production via photolytic oxidation of aqueous sodium sulfite solutions. *Environmental science & technology*, *44*(13), 5283–5288.

Hud, N. V., & Fialho, D. M. (2019). Rna nucleosides built in one prebiotic pot. *Science*, *366*(6461), 32–33.

Islam, M. A. (2018). *Competitive sorption of metal ions and humic acid onto manganese oxides and boehmite* (Unpublished doctoral dissertation). La Trobe University, Australia.

Itcovitz, J. P., Rae, A. S. P., Citron, R. I., Stewart, S. T., Sinclair, C. A., Rimmer, P. B., & Shorttle, O. (2022, May). Reduced Atmospheres of Post-impact Worlds: The Early Earth. *Planetary Science Journal*, *3*(5), 115. doi: 10.3847/PSJ/ac67a9

Johnston, F., & McAmish, L. (1973). A study of the rates of sulfur production in acid thiosulfate solutions using s-35. *Journal of Colloid and Interface Science*, *42*(1), 112–119.

Jortner, J., Ottolenghi, M., & Stein, G. (1964). On the photochemistry of aqueous solutions of chloride, bromide, and iodide ions. *The Journal of Physical Chemistry*, *68*(2), 247–255.

Kadoya, S., Krissansen-Totton, J., & Catling, D. C. (2020, January). Probable Cold and Alkaline Surface Environment of the Hadean Earth Caused by Impact Ejecta Weathering. *Geochemistry, Geophysics, Geosystems*, *21*(1), e08734. doi: 10.1029/2019GC008734

Kaltenegger, L., Traub, W. A., & Jucks, K. W. (2007, March). Spectral Evolution of an Earth-like Planet. *Astrophysical Journal*, *658*, 598-616. doi: 10.1086/510996

Kamyshny, A., Druschel, G., Mansaray, Z. F., & Farquhar, J. (2014). Multiple sulfur isotopes fractionations associated with abiotic sulfur transformations in yellowstone national park geothermal springs. *Geochemical Transactions*, *15*(1), 1–22.

Karchmer, J. H. (1970). *Analytical chemistry of sulfur and its compounds*. Wiley-Interscience.

Kasting, J. F., & Walker, J. C. (1981). Limits on oxygen concentration in the pre-

biological atmosphere and the rate of abiotic fixation of nitrogen. *Journal of Geophysical Research: Oceans*, *86*(C2), 1147–1158.

Kasting, J. F., Zahnle, K. J., Pinto, J. P., & Young, A. T. (1989, March). Sulfur, ultraviolet radiation, and the early evolution of life. *Origins of Life and Evolution of the Biosphere*, *19*, 95-108. doi: 10.1007/BF01808144

Kawai, J., McLendon, D. C., Kim, H. J., & Benner, S. A. (2019, April). Hydroxymethanesulfonate from Volcanic Sulfur Dioxide: A "Mineral" Reservoir for Formaldehyde and Other Simple Carbohydrates in Prebiotic Chemistry. *Astrobiology*, *19*(4), 506-516. doi: 10.1089/ast.2017.1800

Kharecha, P., Kasting, J., & Siefert, J. (2005). A coupled atmosphere–ecosystem model of the early archean earth. *Geobiology*, *3*(2), 53–76.

Kirk, J. T. O. (1984). Dependence of relationship between inherent and apparent optical properties of water on solar altitude. *Limnology and Oceanography*, *29*(2), 350–356.

Kirk, J. T. O. (1994). *Light and photosynthesis in aquatic ecosystems*. Cambridge university press.

Knauth, L. P. (2005). Temperature and salinity history of the precambrian ocean: implications for the course of microbial evolution. *Palaeogeography, Palaeoclimatology, Palaeoecology*, *219*(1), 53–69.

Konhauser, K. O., Planavsky, N. J., Hardisty, D. S., Robbins, L. J., Warchola, T. J., Haugaard, R., ... others (2017). Iron formations: A global record of neoarchaean to palaeoproterozoic environmental history. *Earth-Science Reviews*, *172*, 140–177.

Korenaga, J. (2021). Was there land on the early earth? *Life*, *11*(11), 1142.

Krissansen-Totton, J., Arney, G. N., & Catling, D. C. (2018). Constraining the climate and ocean ph of the early earth with a geological carbon cycle model. *Proceedings of the National Academy of Sciences*, 201721296.

Kuratli, M., & Pretsch, E. (1994). Sulfur dioxide-selective optodes. *Analytical Chemistry*, *66*(1), 85–91.

Lakowicz, J. R. (2010). *Principles of fluorescence spectroscopy*. Springer.

Lamotte, C., Guth, J., Marécal, V., Cussac, M., Hamer, P. D., Theys, N., & Schneider, P. (2021, July). Modeling study of the impact of SO_2 volcanic passive emissions on the tropospheric sulfur budget. *Atmospheric Chemistry & Physics*, *21*(14), 11379-11404. doi: 10.5194/acp-21-11379-2021

Langbein, W. B. (1961). *Salinity and hydrology of closed lakes: A study of the long-term balance between input and loss of salts in closed lakes* (Vol. 412). US Government Printing Office.

Lerman, A., Imboden, D., & Gat, J. (Eds.). (1995). *Physics and chemistry of lakes, second edition*. Springer-Verlag.

Li, X., Fang, J., Liu, G., Zhang, S., Pan, B., & Ma, J. (2014). Kinetics and efficiency of the hydrated electron-induced dehalogenation by the sulfite/uv process. *Water research*, *62*, 220–228.

Li, X., Ma, J., Liu, G., Fang, J., Yue, S., Guan, Y., ... Liu, X. (2012). Efficient reductive dechlorination of monochloroacetic acid by sulfite/uv process. *Environmental science & technology*, *46*(13), 7342–7349.

Li, Y., Li, Y., Liu, Y., Wu, Y., Wu, J., Wang, B., ... Lu, A. (2020, November). Photoreduction of inorganic carbon(+IV) by elemental sulfur: Implications for prebiotic synthesis in terrestrial hot springs. *Science Advances*, *6*(47), eabc3687. doi: 10.1126/sciadv.abc3687

Lian, R., Oulianov, D. A., Crowell, R. A., Shkrob, I. A., Chen, X., & Bradforth, S. E. (2006). Electron photodetachment from aqueous anions. 3. dynamics of geminate pairs derived from photoexcitation of mono-vs polyatomic anions. *The Journal of Physical Chemistry A*, *110*(29), 9071–9078.

Littlejohn, D., Hu, K., & Chang, S. (1986). Kinetics of the reaction of nitric oxide with sulfite and bisulfite ions in aqueous solution. *Inorganic Chemistry*,

25(18), 3131–3135.

Liu, Z., Wu, L.-F., Kufner, C., Sasselov, D. D., Fischer, W., & Sutherland, J. (2021). Prebiotic photoredox synthesis from carbon dioxide and sulfite. *ChemRxiv*. Retrieved from `https://chemrxiv.org/articles/preprint/Prebiotic_Photoredox_Synthesis_from_Carbon_Dioxide_and_Sulfite/13692772/1` (Accepted to XXX)

Loftus, K., Wordsworth, R. D., & Morley, C. V. (2019, December). Sulfate Aerosol Hazes and SO_2 Gas as Constraints on Rocky Exoplanets' Surface Liquid Water. *Astrophysical Journal*, *887*(2), 231. doi: 10.3847/1538-4357/ab58cc

Mack, J., & Bolton, J. R. (1999). Photochemistry of nitrite and nitrate in aqueous solution: a review. *Journal of Photochemistry and Photobiology A: Chemistry*, *128*(1-3), 1–13.

Mancinelli, R. L., & McKay, C. P. (1988, December). The evolution of nitrogen cycling. *Origins of Life*, *18*, 311-325. doi: 10.1007/BF01808213

Marion, G. M., Kargel, J. S., Crowley, J. K., & Catling, D. C. (2013, July). Sulfite-sulfide-sulfate-carbonate equilibria with applications to Mars. *Icarus*, *225*(1), 342-351. doi: 10.1016/j.icarus.2013.02.035

Martin, W., Baross, J., Kelley, D., & Russell, M. J. (2008). Hydrothermal vents and the origin of life. *Nature Reviews Microbiology*, *6*(11), 805–814.

Marty, B., Avice, G., Bekaert, D. V., & Broadley, M. W. (2018). Salinity of the archaean oceans from analysis of fluid inclusions in quartz. *Comptes Rendus Geoscience*, *350*(4), 154–163.

McAdam, A. C., Franz, H. B., Sutter, B., Archer, P. D., Freissinet, C., Eigenbrode, J. L., ... Wray, J. J. (2014, February). Sulfur-bearing phases detected by evolved gas analysis of the Rocknest aeolian deposit, Gale Crater, Mars. *Journal of Geophysical Research (Planets)*, *119*(2), 373-393. doi: 10.1002/2013JE004518

Meyer, B. (1980). Aqueous sulfur chemistry. In *Workshop on sulfur chemistry in flue gas desulfurization* (p. 39-46).

Meyer, B., Mulliken, B., & Weeks, H. (1980a). The reactions of ammonia with excess sulfur dioxide. *Phosphorus and Sulfur and the Related Elements*, *8*(3), 291–299.

Meyer, B., Mulliken, B., & Weeks, H. (1980b). The reactions of sulfur dioxide with excess ammonia. *Phosphorus and Sulfur and the Related Elements*, *8*(3), 281–290.

Meyer, B., Ospina, M., & Peter, L. (1980). Raman spectrometric determination of oxysulfur anions in aqueous systems. *Analytica Chimica Acta*, *117*, 301–311.

Meyer, B., Peter, L., & Ospina, M. (1979, September). Geochemical and cosmochemical cycles involving sulfur, sulfide, sulfite and sulfate. *Geochimica et Cosmochimica Acta*, *43*(9), 1579-1582. doi: 10.1016/0016-7037(79)90152-2

Meyer, B., Rigdon, M., Burner, T., Ospina, M., Ward, K., & Koshlap, K. (1982). Thermal decomposition of sulfite, bisulfite, and disulfite solutions. In *Flue gas desulfurization* (Vol. 188, pp. 113–125). American Chemical Society Washington. doi: 10.1021/bk-1982-0188.ch006

Millero, F. J., Hershey, J. P., Johnson, G., & Zhang, J.-Z. (1989). The solubility of so2 and the dissociation of h2so3 in nacl solutions. *Journal of atmospheric chemistry*, *8*(4), 377–389.

Mirzoyan, N., & Halevy, I. (2014). Kinetics of sulfite disproportionation and thiosulfate acid dissociation [abstract 1701]. In *Goldschmidt conference abstracts.*

Mobley, C., Sundman, L., Bissett, W., & Cahill, B. (2009). Fast and accurate irradiance calculations for ecosystem models. *Biogeosciences Discussions*, *6*(6), 10625–10662.

Mojzsis, S. J. (2007). Sulphur on the early earth. *Developments in Precambrian Geology*, *15*, 923–970.

Morel, A. (1991). Light and marine photosynthesis: a spectral model with geochemical and climatological implications. *Progress in oceanography*, *26*(3), 263–306.

Morel, A., Gentili, B., Claustre, H., Babin, M., Bricaud, A., Ras, J., & Tieche, F. (2007). Optical properties of the "clearest" natural waters. *Limnology and oceanography*, *52*(1), 217–229.

Mulkidjanian, A. Y., Bychkov, A. Y., Dibrova, D. V., Galperin, M. Y., & Koonin, E. V. (2012, April). PNAS Plus: Origin of first cells at terrestrial, anoxic geothermal fields. *Proceedings of the National Academy of Science*, *109*, E821-E830. doi: 10.1073/pnas.1117774109

Omran, A., & Pasek, M. (2020). A constructive way to think about different hydrothermal environments for the origins of life. *Life*, *10*(4), 36.

Ono, S., Eigenbrode, J. L., Pavlov, A. A., Kharecha, P., Rumble, D., Kasting, J. F., & Freeman, K. H. (2003, August). New insights into Archean sulfur cycle from mass-independent sulfur isotope records from the Hamersley Basin, Australia. *Earth and Planetary Science Letters*, *213*(1-2), 15-30. doi: 10.1016/S0012-821X(03)00295-4

Patel, B. H., Percivalle, C., Ritson, D. J., Duffy, C. D., & Sutherland, J. D. (2015, April). Common origins of RNA, protein and lipid precursors in a cyanosulfidic protometabolism. *Nature Chemistry*, *7*, 301-307. doi: 10.1038/nchem.2202

Pearce, B. K. D., Pudritz, R. E., Semenov, D. A., & Henning, T. K. (2017, October). Origin of the RNA world: The fate of nucleobases in warm little ponds. *Proceedings of the National Academy of Science*, *114*(43), 11327-11332. doi: 10.1073/pnas.1710339114

Peters, C., Strauss, H., Haase, K., Bach, W., de Ronde, C. E., Kleint, C., ... Diehl, A. (2021). So2 disproportionation impacting hydrothermal sulfur cycling: Insights from multiple sulfur isotopes for hydrothermal fluids from the tonga-kermadec intraoceanic arc and the ne lau basin. *Chemical Geology*, *586*, 120586.

Petruševski, V. M., Bukleski, M., & Stojanovska, M. (2013). On the catalyzed disproportionation of so 2 in aqueous solution of ki: A marathon classroom demonstration. *J. Lab. Chem. Educ*, *1*, 1–4.

Pierrehumbert, R. T. (2010). *Principles of planetary climate*. Cambridge University Press.

Pitsch, S., Krishnamurthy, R., & Arrhenius, G. (2000). Concentration of simple aldehydes by sulfite-containing double-layer hydroxide minerals: Implications for biopoesis. *Helvetica chimica acta*, *83*(9), 2398–2411.

Ranjan, S., Kufner, C. L., Lozano, G. G., Todd, Z. R., Haseki, A., & Sasselov, D. D. (2022, March). UV Transmission in Natural Waters on Prebiotic Earth. *Astrobiology*, *22*(3), 242-262. doi: 10.1089/ast.2020.2422

Ranjan, S., & Sasselov, D. D. (2017, March). Constraints on the Early Terrestrial Surface UV Environment Relevant to Prebiotic Chemistry. *Astrobiology*, *17*, 169-204. doi: 10.1089/ast.2016.1519

Ranjan, S., Schwieterman, E. W., Harman, C., Fateev, A., Sousa-Silva, C., Seager, S., & Hu, R. (2020, June). Photochemistry of Anoxic Abiotic Habitable Planet Atmospheres: Impact of New H_2O Cross Sections. *Astrophysical Journal*, *896*(2), 148. doi: 10.3847/1538-4357/ab9363

Ranjan, S., Seager, S., Zhan, Z., Koll, D. D. B., Bains, W., Petkowski, J. J., ... Lin, Z. (2022, May). Photochemical Runaway in Exoplanet Atmospheres: Implications for Biosignatures. *Astrophysical Journal*, *930*(2), 131. doi: 10.3847/1538-4357/ac5749

Ranjan, S., Todd, Z. R., Rimmer, P. B., Sasselov, D. D., & Babbin, A. R. (2019). Nitrogen oxide concentrations in natural waters on early earth. *Geochemistry, Geophysics, Geosystems*, *20*(4), 2021–2039.

Ranjan, S., Todd, Z. R., Sutherland, J. D., & Sasselov, D. D. (2018). Sulfidic anion concentrations on early earth for surficial origins-of-life chemistry. *Astrobi-*

ology.

Ranjan, S., Wordsworth, R., & Sasselov, D. D. (2017, August). Atmospheric Constraints on the Surface UV Environment of Mars at 3.9 Ga Relevant to Prebiotic Chemistry. *Astrobiology*, *17*, 687-708. doi: 10.1089/ast.2016.1596

Rempel, S., Ryabinina, A., & Oshman, V. (1974). Kinetics and mechanism of the thermal decomposition of solutions of sulfur dioxide and bisulfites. *Ural. Lesotekh. Inst., Sverdovsk. Deposited document*.

Richter, F. M. (1985, May). Models for the Archean thermal regime. *Earth and Planetary Science Letters*, *73*, 350-360. doi: 10.1016/0012-821X(85)90083-4

Rimmer, P. B., & Shorttle, O. (2019). Origin of life's building blocks in carbon-and nitrogen-rich surface hydrothermal vents. *Life*, *9*(1), 12.

Rimmer, P. B., Thompson, S. J., Xu, J., Russell, D. A., Green, N. J., Ritson, D. J., ... Queloz, D. P. (2021). Timescales for prebiotic photochemistry under realistic surface ultraviolet conditions. *Astrobiology*. Retrieved from `http://doi.org/10.1089/ast.2020.2335`

Rimmer, P. B., Xu, J., Thompson, S. J., Gillen, E., Sutherland, J. D., & Queloz, D. (2018, August). The origin of RNA precursors on exoplanets. *Science Advances*, *4*(8), eaar3302. doi: 10.1126/sciadv.aar3302

Ritson, D., & Sutherland, J. D. (2012, November). Prebiotic synthesis of simple sugars by photoredox systems chemistry. *Nature Chemistry*, *4*, 895-899. doi: 10.1038/nchem.1467

Roche, M. A., Bourges, J., Cortes, J., & Mattos, R. (1992). Lake titicaca: A synthesis of limnological knowledge. In C. Dejoux & E. A. Iltis (Eds.), (Vol. 68, chap. Climatology and hydrology of the Lake Titicaca basin). Dordrecht: Kluwer Academic.

Rosas, J. C., & Korenaga, J. (2021, January). Archaean seafloors shallowed with age due to radiogenic heating in the mantle. *Nature Geoscience*, *14*(1), 51-56. doi: 10.1038/s41561-020-00673-1

Rosen, M. R. (1994, 01). The importance of groundwater in playas: A review of playa classifications and the sedimentology and hydrology of playas. In *Paleoclimate and Basin Evolution of Playa Systems*. Geological Society of America. Retrieved from `https://doi.org/10.1130/SPE289-p1` doi: 10.1130/SPE289-p1

Rugheimer, S., & Kaltenegger, L. (2018). Spectra of earth-like planets through geological evolution around fgkm stars. *The Astrophysical Journal*, *854*(1), 19.

Rugheimer, S., Segura, A., Kaltenegger, L., & Sasselov, D. (2015, June). UV Surface Environment of Earth-like Planets Orbiting FGKM Stars through Geological Evolution. *Astrophysical Journal*, *806*, 137. doi: 10.1088/0004-637X/806/1/137

Rumble, J. R. (Ed.). (2017). *Crc handbook of chemistry and physics* (98th ed.). Boca Raton, FL: CRC Press.

Ryabinina, A., & Oshman, V. (1972). Thermal decomposition of aqueous sulfur dioxide solutions. *Tr Ural Lesotekh Inst*, *28*, 182–189.

Sahai, N., Adebayo, S., & Schoonen, M. A. (2022, June). Freshwater and Evaporite Brine Compositions on Hadean Earth: Priming the Origins of Life. *Astrobiology*, *22*(6), 641-671. doi: 10.1089/ast.2020.2396

Sakshaug, E., Bricaud, A., Dandonneau, Y., Falkowski, P. G., Kiefer, D. A., Legendre, L., ... Takahashi, M. (1997). Parameters of photosynthesis: definitions, theory and interpretation of results. *Journal of Plankton Research*, *19*(11), 1637–1670.

Sander, R. (2015, April). Compilation of Henry's law constants (version 4.0) for water as solvent. *Atmospheric Chemistry & Physics*, *15*, 4399-4981. doi: 10.5194/acp-15-4399-2015

Sander, S. P., Friedl, R. R., Barker, J. R., Golden, D. M., Kurylo, M. J., Wine, P. H., ... Orkin, V. L. (2011). *Chemical Kinetics and Photochemical*

Data for Use in Atmospheric Studies Evaluation Number 17 (Vol. JPL Pub 10-6; Tech. Rep. No. 17). NASA JPL. Retrieved from `http://jpldataeval.jpl.nasa.gov/`

Sasselov, D. D., Grotzinger, J. P., & Sutherland, J. D. (2020). The origin of life as a planetary phenomenon. *Science Advances*, *6*(6). Retrieved from `https://advances.sciencemag.org/content/6/6/eaax3419` doi: 10.1126/sciadv.aax3419

Sauer, M. C., Crowell, R. A., & Shkrob, I. A. (2004). Electron photodetachment from aqueous anions. 1. quantum yields for generation of hydrated electron by 193 and 248 nm laser photoexcitation of miscellaneous inorganic anions. *The Journal of Physical Chemistry A*, *108*(25), 5490–5502.

Sauer, M. C., Shkrob, I. A., Lian, R., Crowell, R. A., Bartels, D. M., Chen, X., ... Bradforth, S. E. (2004). Electron photodetachment from aqueous anions. 2. ionic strength effect on geminate recombination dynamics and quantum yield for hydrated electron. *The Journal of Physical Chemistry A*, *108*(47), 10414–10425.

Searcy, A. W. (1981). *Materials and molecular research division. annual report 1980* (Tech. Rep.). Lawrence Berkeley National Laboratory. Retrieved from `https://escholarship.org/uc/item/71d1h52c`

Seinfeld, J. H., & Pandis, S. N. (2016). *Atmospheric chemistry and physics: from air pollution to climate change*. John Wiley & Sons.

Self, S., Widdowson, M., Thordarson, T., & Jay, A. E. (2006, August). Volatile fluxes during flood basalt eruptions and potential effects on the global environment: A Deccan perspective. *Earth and Planetary Science Letters*, *248*, 518-532. doi: 10.1016/j.epsl.2006.05.041

Shirley, D. A. (1980). *Materials and molecular research division. annual report 1980* (Tech. Rep.). Lawrence Berkeley National Laboratory. Retrieved from `https://escholarship.org/uc/item/8w27h6rr`

Sleep, N. H., & Zahnle, K. (2001, January). Carbon dioxide cycling and implications for climate on ancient Earth. *Journal of Geophysics Research*, *106*, 1373-1400. doi: 10.1029/2000JE001247

Smith, R. C., & Baker, K. S. (1981). Optical properties of the clearest natural waters (200–800 nm). *Applied optics*, *20*(2), 177–184.

Sohail, M., & De Marco, R. (2013). Electrodes— ion-selective electrodes. *Reference Module in Chemistry, Molecular Sciences and Chemical Engineering*, 1–12.

Steinman, B. A., Rosenmeier, M. F., Abbott, M. B., & Bain, D. J. (2010). The isotopic and hydrologic response of small, closed-basin lakes to climate forcing from predictive models: Application to paleoclimate studies in the upper columbia river basin. *Limnology and Oceanography*, *55*(6), 2231–2245.

Summers, D. P., & Khare, B. (2007, May). Nitrogen Fixation on Early Mars and Other Terrestrial Planets: Experimental Demonstration of Abiotic Fixation Reactions to Nitrite and Nitrate. *Astrobiology*, *7*, 333-341. doi: 10.1089/ast.2006.0032

Thomas, G. E., & Stamnes, K. (2002). *Radiative transfer in the atmosphere and ocean*. Cambridge University Press.

Tian, F., Claire, M. W., Haqq-Misra, J. D., Smith, M., Crisp, D. C., Catling, D., ... Kasting, J. F. (2010, July). Photochemical and climate consequences of sulfur outgassing on early Mars. *Earth and Planetary Science Letters*, *295*, 412-418. doi: 10.1016/j.epsl.2010.04.016

Todd, Z. R., Fahrenbach, A. C., Magnani, C. J., Ranjan, S., Björkbom, A., Szostak, J. W., & Sasselov, D. D. (2018). Solvated-electron production using cyanocuprates is compatible with the uv-environment on a hadean–archaean earth. *Chemical Communications*.

Todd, Z. R., Lozano, G. G., Kufner, C. L., Sasselov, D. D., & Catling, D. C. (2022). Ferrocyanide survival under near ultraviolet (300–400 nm) irradiation on early

earth. *Geochimica et Cosmochimica Acta*, *335*, 1–10.

Todd, Z. R., Szostak, J. W., & Sasselov, D. D. (2021, February). Shielding from UV Photodamage: Implications for Surficial Origins of Life Chemistry on the Early Earth. *ACS Earth and Space Chemistry*, *5*(2), 239-246. doi: 10.1021/acsearthspacechem.0c00270

Toner, J. D., & Catling, D. C. (2019). Alkaline lake settings for concentrated prebiotic cyanide and the origin of life. *Geochimica et Cosmochimica Acta*, *260*, 124–132.

Toner, J. D., & Catling, D. C. (2020). A carbonate-rich lake solution to the phosphate problem of the origin of life. *Proceedings of the National Academy of Sciences*, *117*(2), 883–888.

Turner, J., & Parisi, A. V. (2018). Ultraviolet radiation albedo and reflectance in review: the influence to ultraviolet exposure in occupational settings. *International Journal of Environmental Research and Public Health*, *15*(7), 1507.

Tutolo, B. M., Seyfried, W. E., & Tosca, N. J. (2020, June). A seawater throttle on H_2 production in Precambrian serpentinizing systems. *Proceedings of the National Academy of Science*, *117*(26), 14756-14763. doi: 10.1073/pnas.1921042117

van der Kamp, G., Keir, D., & Evans, M. S. (2008). Long-term water level changes in closed-basin lakes of the canadian prairies. *Canadian Water Resources Journal*, *33*(1), 23–38.

Vincent, L., Colón-Santos, S., Cleaves, H. J., Baum, D. A., & Maurer, S. E. (2021). The prebiotic kitchen: A guide to composing prebiotic soup recipes to test origins of life hypotheses. *Life*, *11*(11), 1221.

Wachtershauser, G. (1990, January). Evolution of the First Metabolic Cycles. *Proceedings of the National Academy of Science*, *87*(1), 200-204. doi: 10.1073/pnas.87.1.200

Walker, J. C., & Brimblecombe, P. (1985). Iron and sulfur in the pre-biologic ocean. *Precambrian Research*, *28*(3-4), 205–222.

Walton, C. R., Rimmer, P., & Shorttle, O. (2022, December). Can prebiotic systems survive in the wild? An interference chemistry approach. *Frontiers in Earth Science*, *10*, 1011717. doi: 10.3389/feart.2022.1011717

Warneck, P. (n.d.). Chemistry of the natural atmosphere. In (chap. Sulfur Compounds in the Atmosphere). Academic Press Inc., year=1998, address=San Diego, pages=484–542.

Wong, M. L., Charnay, B. D., Gao, P., Yung, Y. L., & Russell, M. J. (2017, October). Nitrogen Oxides in Early Earth's Atmosphere as Electron Acceptors for Life's Emergence. *Astrobiology*, *17*, 975-983. doi: 10.1089/ast.2016.1473

Wood, W. W., & Sanford, W. E. (1990). Ground-water control of evaporite deposition. *Economic Geology*, *85*(6), 1226–1235.

Wu, S., Shen, L., Lin, Y., Yin, K., & Yang, C. (2021). Sulfite-based advanced oxidation and reduction processes for water treatment. *Chemical Engineering Journal*, *414*, 128872.

Xu, J., Chmela, V., Green, N. J., Russell, D. A., Janicki, M. J., Góra, R. W., ... Sutherland, J. D. (2020). Selective prebiotic formation of rna pyrimidine and dna purine nucleosides. *Nature*, *582*(7810), 60–66.

Xu, J., Ritson, D. J., Ranjan, S., Todd, Z. R., Sasselov, D. D., & Sutherland, J. D. (2018). Photochemical reductive homologation of hydrogen cyanide using sulfite and ferrocyanide. *Chemical Communications*.

Xu, T., Apps, J. A., Pruess, K., & Yamamoto, H. (2007). Numerical modeling of injection and mineral trapping of co2 with h2s and so2 in a sandstone formation. *Chemical Geology*, *242*(3-4), 319–346.

Yang, L., He, L., Xue, J., Ma, Y., Shi, Y., Wu, L., & Zhang, Z. (2020). Uv/so32-based advanced reduction processes of aqueous contaminants: Current status and prospects. *Chemical Engineering Journal*, *397*, 125412.

Yapiyev, V., Sagintayev, Z., Inglezakis, V. J., Samarkhanov, K., & Verhoef, A. (2017). Essentials of endorheic basins and lakes: A review in the context of current and future water resource management and mitigation activities in central asia. *Water*, *9*(10), 798.

Yu, K., Li, X., Chen, L., Fang, J., Chen, H., Li, Q., ... Ma, J. (2018). Mechanism and efficiency of contaminant reduction by hydrated electron in the sulfite/iodide/uv process. *Water research*, *129*, 357–364.

Zafiriou, O. C., & True, M. B. (1979a). Nitrate photolysis in seawater by sunlight. *Marine Chemistry*, *8*(1), 33–42.

Zafiriou, O. C., & True, M. B. (1979b). Nitrite photolysis in seawater by sunlight. *Marine Chemistry*, *8*(1), 9–32.

Zahnle, K., Claire, M., & Catling, D. (2006). The loss of mass-independent fractionation in sulfur due to a palaeoproterozoic collapse of atmospheric methane. *Geobiology*, *4*(4), 271–283.

Zahnle, K. J., Lupu, R., Catling, D. C., & Wogan, N. (2020, June). Creation and Evolution of Impact-generated Reduced Atmospheres of Early Earth. *Planetary Science Journal*, *1*(1), 11. doi: 10.3847/PSJ/ab7e2c

Zhang, J.-Z., & Millero, F. J. (1991, March). The rate of sulfite oxidation in seawater. *Geochimica et Cosmochimica Acta*, *55*(3), 677-685. doi: 10.1016/0016-7037(91)90333-Z

Supplementary Information: Geochemical and Photochemical Constraints on S[IV] Concentrations in Natural Waters on Prebiotic Earth

Sukrit Ranjan[1,2,3,4,5], Khaled Abdelazim[6], Gabriella G. Lozano[7], Sangita Mandal[8], Cindy Y. Zhou[9], Corinna L. Kufner[7], Zoe R. Todd[10], Nita Sahai[11], Dimitar D. Sasselov[7]

[1]Lunar & Planetary Laboratory/Department of Planetary Sciences, University of Arizona, Tucson, AZ 85721, USA

[2]Blue Marble Space Institute of Science, Seattle, WA 98104, USA

[3]School of Earth and Planetary Sciences, National Institute of Science Education and Research, HBNI, Jatni 752050, Odisha, India

[4]Department of Physics and Astronomy & Center for Interdisciplinary Exploration and Research in Astrophysics, Northwestern University, Evanston, IL 60201, USA

[5]Department of Earth, Atmospheric and Planetary Sciences, Massachusetts Institute of Technology, Cambridge, MA 02139, USA

[6]Department of Chemistry and Chemical Biology, Harvard University, Cambridge, MA 02138, USA

[7]Harvard-Smithsonian Center for Astrophysics, Cambridge, MA 02138, USA

[8]School of Chemical Sciences, National Institute of Science Education and Research, HBNI, Jatni 752050, Odisha, India

[9]Department of Biochemistry and Molecular Biology, Boston University, Boston, MA 02215, USA

[10]Department of Earth and Space Sciences, University of Washington, Seattle, WA 98195, USA

[11]Department of Geosciences; Department of Biology; and Integrated Bioscience Program, School of Polymer Science and Polymer Engineering, University of Akron, Akron, OH 44325, USA

Corresponding author: S. Ranjan, Lunar & Planetary Laboratory/Department of Planetary Sciences, University of Arizona, Tucson, AZ 85721, USA. (sukrit@arizona.edu)

March 16, 2023, 3:30pm

Contents of this file

1. Text S1 to S4
2. Figures S1 to S15
3. Tables S1 to S6

Additional Supporting Information (Files uploaded separately)

1. Caption for Data Set S1 (Excel file sulfite_solution_phase_raw_processed_data_v5.xlsx)

Introduction

In this Supporting Information, we give further details on our work. These details are ancillary to the main thrust of our work, but are potentially of interest to specialists or individuals seeking to reproduce or validate our work. Specifically, in Section S1, we give further details of the atmospheric photochemical modeling, including species-by-species chemical boundary conditions; in Section S2, we give further details of the experimental study of aged S[IV] solutions, including the solution-phase sulfite electropotentiometry, corroborative UV-VIS tracking, and information regarding failed experiments; in Section S3, we present explicitly the details of our aqueous photochemical modeling, including our validation of our photolysis calculation against nitrate, and graphical presentation of key input data; in Section S4, we demonstrate that we can recover the main results of our detailed modeling with a simplistic order-of-magnitude calculation, increasing our confidence in the conclusions. In Data Set S1, we give the raw data from the solution-phase analytics, and show the processing applied to it to extract the measurements shown in Table 7 of the main text.

S1. Further Details on Atmospheric Photochemistry Simulation

S1.1. Further Details on Methods

In Table S1, we present the simulation parameters of our photochemical model. In Table S2, we present the detailed boundary species-by-species conditions associated with our photochemical model.

S1.2. Further Details on Simulation Outputs

In Table S3, we present the SO_2 mixing ratios and wet deposition rates predicted by our photochemical modeling. The SO_2 mixing ratios correspond to Figure 1 from the main text.

S2. Further Details on S[IV] Lifetime Experiments

S2.1. Further Details on Sulfite Electropotentiometry

S2.1.1. Effect of pH

The influence of pH on the potentiometric response of the ISE sensors to sulfite anion was studied by making calibration curves at pH values close to both neutral pH range (6.0–9.0), acidic pH range (3.5–4.5) and alkaline pH range (12.0–13.0) by using few drops of 6M HCl and NaOH as shown in Data Set S1. The reason behind studying the pH effect at different values is the presence of two electrically ionizable groups within the sulfite anion structure with pKa values of 1.9 and 7.2 (Beyad et al., 2014).

For this reason, the results showed that a significant differences in the corresponding calibration Nernstian slopes in acidic rather than neutral and alkaline conditions. At acidic conditions pH range (3.5–4.5), the sulfite anion is singly charged (monovalent ion, HSO_3^-) when it was sensed by the ISE, and hence a Nernstian slope of almost 47.2 ± 5

mV/concentration decade was obtained. While at neutral conditions (at pH 7.6), the sulfite anion is mostly sensed as divalent ion and the corresponding Nernstian slope of about 30.0 ± 3.0 mV/concentration decade was obtained. At alkaline conditions (pH$\sim$13.0), the sulfite anion is fully doubly charged, and therefore it was sensed as divalent ion and the corresponding Nernstian slope of about 27.0 ± 2.0 mV/concentration decade was obtained in the first day of measurements. However, one of the main challenges that was practically observed when considering sulfite measurements in extremely alkaline solution is the remarkable decrease in the slope in the following day of measurements, (especially upon longer exposure to an alkaline solution background as a storage solution between measurements), which may possibly be attributed to interference of hydroxyl group (Hutchins et al., 1994).

S2.1.2. Dynamic Response Time

Dynamic response time is an important factor for analytical applications of ISEs. In this study, practical response time was recorded by diluting the initial sulfite anion concentration (100 mM) up to 1000-fold. The required time for the sensors to reach values within ± 2 mV of the final equilibrium potential was $\sim$ 40 s for the three sensors. The time traces of the calibration curve of the sensors are presented in Data Set S1.

S2.1.3. Repeatability of the Measurements

Repeatability of the potential reading for each sensor was examined by subsequent measurement in the range of 100 mM to 10 μM of sulfite anion solution immediately after measuring the first set of samples. The electrode potential for three replicate measurements exhibit a standard deviation of 1.31, 1.42 and 1.21, respectively. While the corresponding values in samples solution of pH 13 showed a standard deviation of 1.59,

1.05 and 1.85, respectively. This indicates an acceptable repeatability of the potential response of the three proposed electrodes.

S2.1.4. Performance characteristics of the sulfite ISE

The potentiometric response characteristics of the designed sensors (n=3) were checked by plotting the potential readings against the logarithmic concentrations as presented in Data Set S1. Results of performance characteristics showed that the linear dynamic range of our sulfite ISE (100 mM to 10 μM) was comparable to that of another previously reported electrode (500 mM to 5 μM; Hutchins et al. (1994)). The response times in samples with concentration higher than 10 mM were of the order of seconds ($\sim$20 s), whereas in more diluted samples the time required to reach a stable potential was considerably longer, around 45 s for the three sensors.

The lifetime of the proposed sensors was evaluated by constructing calibration graph on different days over a period of three weeks. The prepared ISEs exhibited life span of 14 days; during this time the slope of calibration curves remained constant with no significant change in slopes of the calibration curves. After this period, a remarkable decrease in the slope was practically observed which might be attributed to the ionophore leaching from the sensing membrane as previously reported (Hutchins et al., 1994).

After 3 weeks of dry storage, the ISE is still sensitive to sulfite; it showed a close to Nernstian response (24.4$\pm$1 mV/decade) in the linear range from 100 mM to 0.1 mM. The improvement in the electrode lifetime may be attributed to the leaching of the ionophore from the electrode matrix due to the lack of external storage solution and inner filling solutions. Therefore, the potentiometric sulfite-ISEs can be stored in dry conditions for relatively prolonged periods with no significant loss of performance characteristics.

S2.2. Further Details of UV-VIS Tracking

Figures S3, S4, S5, and S6 present the detailed UV/VIS measurements summarized in main text Table 6.

S2.3. Failed Experiments

We initially sought to explore a broader range of experimental conditions than discussed in the main text. Specifically, we sought to explore acidic solutions (pH=4), as well as solutions enriched in inorganic ions with compositions representative of carbonate lakes (Toner & Catling, 2020). We successfully prepared these solutions and tracked them with UV/VIS spectroscopy. However, our solution-phase analytics failed for these additional solutions. We consequently do not report them in the main text, but for the sake of completeness we discuss them here. We also discuss here sample #2 of the 10 mM [S[IV]] unadjusted pH experimental condition, which we discarded because we suspected experimentor error in its preparation or storage.

S2.3.1. Acidic S[IV] Solution

We prepared and aged solutions of 100 mM S[IV] adjusted to acidic pH=4 as the other samples. However, we were unable to measure [S[IV]] in the aged solution via electropotentiometry, because we were unable to construct stable calibration curves via serial dilution. We attribute this instability to significant speciation of S[IV] as SO_2 at this pH, which then exsolves, altering [S[IV]] over time. Indeed, in attempting to calibrate the ISE at pH=4 we observed strong sulfur smells from our calibration solutions, consistent with exsolution. We therefore do not report results for this regime.

However, we did conduct UV/VIS tracking of these samples (Figure S7), which reveals behaviour very different from the non-acidic samples. Specifically, the acidic samples

are characterized by an absorbance *increase* with time (as opposed to decrease with the non-acidic samples), and the rate of change of absorbance is much higher than in the non-acidic samples. We hypothesize that these observations can be explained by disproportionation. This hypothesis explains the increase in absorbance with time, because the sulfite is turning into reduced forms of sulfur like thiosulfate or sulfide, which are more absorptive than sulfite. This hypothesis explains the faster rate of change in the acidic solutions relative to the non-acidic solutions, because we expect faster disproportionation at lower pH based on the overall reaction stoichiometry (main text Equations 2-3). Faster disproportionation at low pH was mentioned in a non-peer-reviewed LBL technical report, which is consistent with this scenario (Searcy, 1981). These observations are suggestive (but not definitive) that S[IV] concentrations in very acidic waters should be lower than S[IV] concentrations in non-acidic waters due to enhanced efficiency of disproportionation.

S2.3.2. "Carbonate Lake" Solutions

Our experimental study focuses on S[IV] in pure water, but other solutes were likely present in natural waters on prebiotic Earth which may have catalyzed or inhibited S[IV] loss (Vincent et al., 2021; Walton et al., 2022; Ranjan, Kufner, et al., 2022). For example, formaldehyde and alcohols stabilize sulfite, while ammonia and elemental sulfur catalyze sulfite disproportionation (Karchmer, 1970; de Carvalho & Schwedt, 2000; Meyer et al., 1979; Meyer et al., 1980b, 1980a). As a sensitivity test, we aged 100 mM sulfite in a background solution containing inorganic ions at concentrations motivated by closed-basin carbonate lakes (Toner & Catling, 2020). We constructed two sample waters, with compositions approximately motivated by a closed-basin carbonate lake with 10^{-2} mol kg^{-1} P. We constructed dilute (low ionic strength) and concentrated (high ionic strength) end-

members to approximately bracket the range of compositions expected for such a lake, drawing primarily on Toner and Catling (2020) (especially their Figure S1), augmented by Ranjan, Kufner, et al. (2022) (their Table 2). For the dilute and concentrated end-members, we adjusted the solution to pHs of 9 and 7 respectively, reflecting the assumed [HCO_3] and [CO_3] (Ranjan, Kufner, et al., 2022). Given the high carbonate concentration in the concentrated scenario, we omitted Mg^{2+} and chose a lower Ca^{2+}, to minimize removal of carbonate by precipitation. Tables S5 and S6 summarize our preparation of these background waters.

As in the acidic case, our solution-phase analytics failed for the "carbonate lake" solutions. We were unable to confirm that the background ions present in the solution did not interfere with the ISE, and therefore were unable to robustly measure [S[IV]]. Consequently, we do not report results from this sensitivity test. However, as with the acidic case, we were able to conduct UV/VIS tracking of these samples. The UV/VIS evolution of these 100 mM sulfite-doped "carbonate lake" samples (Figure S8, S9) was very similar to the UV/VIS evolution of the 100 mM sulfite-doped non-acidic pure water samples (Figure S4, S3, S5). This leads us to speculate that the ions in this sensitivity test did not radically accelerate or inhibit S[IV] loss.

S2.3.3. Discarded Sample

One sample (10 mM S[IV], unadjusted pH, Sample #2) showed significantly lower pH (7.2 vs 8.3) compared to other samples in its experimental condition upon opening for solution-phase analytics. We have no explanation for why this particular sample showed lower pH than its peers, interpret this anomaly as evidence of experimenter error in the preparation or storage of this sample which somehow influenced its pH, and consequently

do not report results from this sample in the main text. However, for completeness, we report its results here (Table S4). The lower UV/VIS absorptivity of this sample can be attributed to its lower pH, which would lead to greater speciation of S[IV] as less-absorptive HSO_3^- ($pK_a = 7 - 7.2$; Millero, Hershey, Johnson, and Zhang (1989); Neta and Huie (1985)). The $T_{disp,0}$ inferred from this sample is $T_{disp,0} = 1.3$ years (electropotentiometry), which remains consistent with the $T_{disp,0} > 1$ year reported in the main text.

S3. Further Details of Aqueous Photochemistry Model

S3.1. Photolysis Calculation Validation With Nitrate

We validate our photolysis calculation method by using it to estimate the photolysis of nitrate in modern ocean water and comparing it to the estimates of Zafiriou and True (1979). We use nitrate absorption cross-sections from Ranjan, Kufner, et al. (2022), nitrate photolysis quantum yields from Mack and Bolton (1999) (their Table 2), UV surface flux from Ranjan and Sasselov (2017) (their modern Earth validation case), and oceanic attenuation coefficients from Smith and Baker (1981) (corresponding to the clearest modern ocean waters). We find that our method estimates a surface photolysis rate for nitrate which fits within the range of surface photolysis rates measured by Zafiriou and True (1979) (our estimate: 5×10^{-8} s^{-1}, Zafiriou and True (1979): $8 \times 10^{-9} - 7 \times 10^{-8}$ s^{-1}, median 2×10^{-8} s^{-1}). Consistency with this measurement is an important check on our methodology.

We compare our estimate of column-integrated photolysis rate to the simplified calculation of Zafiriou and True (1979). In estimating the column-integrated photolysis rate, we explicitly integrate over depth and include wavelength-dependent attenuation via clear

ocean water (Smith & Baker, 1981), while Zafiriou and True (1979) follow a simplified procedure, assuming step-function photolysis down to the 310 nm photic depth of ocean water. We estimate a column-integrated photolysis rate 8× that of Zafiriou and True (1979). Of this, a factor of 2× is attributable to our higher surface photolysis rate compared to the median; a factor of 3.0× is attributable to our explicit integration over depth; and a factor of 1.2× is attributable to our consideration of wavelength-dependent attenuation. This calculation demonstrates the necessity of explicit integration over depth in calculating photolysis rates.

We conclude that the validation case of nitrate photolysis in the modern ocean suggests that our procedure is capable of estimating column-integrated photolysis rate to within an order of magnitude but may overestimate photolysis rate by a factor of a few, possibly due to neglect of back-reactions which reform the photolyzed substrate.

S3.2. Graphical Representations of Key Inputs.

In Section 3.4 of the main text, we described key inputs into our aqueous photochemistry model. Here, we provide graphical representations of these inputs, for easy evaluation by readers. Specifically, Figure S10 presents the surface UV flux at the base of the atmosphere, from Ranjan and Sasselov (2017); it can be compared to similar[1] estimates (Cockell, 2002; Rugheimer et al., 2015). Figures S11, S12, and S13 present the high- and low-absorbance endmembers considered for the prebiotic oceans, freshwater lakes, and carbonate lakes, modified from Ranjan, Kufner, et al. (2022) by removing S[IV] species; the ocean case can be compared to Anbar and Holland (1992). Figure S14 presents $\sigma_{HSO_3^-}(\lambda)$ and $\sigma_{SO_3^{2-}}(\lambda)$, based on underlying data from Fischer and Warneck (1996) and Beyad et al. (2014) and synthesized by Ranjan, Kufner, et al. (2022). Figure S15

presents $\Phi_{HSO_3^-}(\lambda)$ and $\Phi_{SO_3^{2-}}(\lambda)$, estimated as described in Section 3.4.1.1, along with the literature measurements at specific wavelengths on which the estimate is based.

S4. Simplified Order-of-Magnitude Calculation

The model calculation we have described in this paper is complex, raising the risk that it contains an implementation error that might invalidate its results. In this section, we carry out a simplified order-of-magnitude analytic calculation and demonstrate recovery of our main finding that sulfite was a trace prebiotic reagent, with higher concentrations in terrestrial waters compared to marine waters. The agreement of this highly simplified calculation with our full model increases our confidence in our conclusions.

We seek to solve Equation 6:

$$F_{sources,S[IV]} = F_{sinks,S[IV]}$$

The primary fate of atmospheric SO_2 is deposition back to the surface. So, we can approximate $F_{sources,S[IV]} \approx \phi_{SO_2}$, taking a drainage ratio of 1. The main sink of of aqueous S[IV] is photolysis. So we can take $F_{sinks,S[IV]} \approx F_{h\nu,S[IV]} = [S[IV]] \int d\lambda \phi_{S[IV]}(\lambda)\sigma_{S[IV]}(\lambda)\dot{E}(\lambda, d)$. For transparent shallow terrestrial waters, we can further simplify $F_{h\nu,S[IV]} \approx [S[IV]] \times d \times \int d\lambda \Phi_{S[IV]}(\lambda)\sigma_{S[IV]}(\lambda)\dot{E}(\lambda, 0) \approx [S[IV]] \times d \times \Delta\lambda \times \overline{\Phi_{S[IV]}}\,\overline{\sigma_{S[IV]}}\,\overline{\dot{E}(\lambda, 0)}$. Rearranging, for shallow terrestrial waters we have

$$[S[IV]] \approx \frac{\phi_{SO_2}}{d\Delta\lambda\,\overline{\Phi_{S[IV]}}\,\overline{\sigma_{S[IV]}}\,\overline{\dot{E}(\lambda, 0)}}$$

For a 1-m lake at basic pH at Earthlike outgassing, S[IV] is present as SO_3^{2-}, and we can estimate by eye from Figures S10-S15 that

$$[S[IV]] \approx \frac{3 \times 10^9 \mathrm{cm}^{-2}\mathrm{s}^{-1}}{100\mathrm{cm} \times 80\mathrm{nm} \times 0.2 \times 10^2 \mathrm{M}^{-1}\mathrm{cm}^{-1} \times 10^{12}\mathrm{cm}^{-2}\mathrm{s}^{-1}\mathrm{nm}^{-1}}$$
$$= \times 10^{-8}\mathrm{M}$$

which is the same order of magnitude as our detailed calculation (Figure 3, purple curve, $\frac{\phi}{\phi_0} = 0$).

If we instead assume acidic pH, such that S[IV] is present as HSO_3^-, we instead estimate

$$[S[IV]] \approx \frac{3 \times 10^9 \mathrm{cm}^{-2}\mathrm{s}^{-1}}{100\mathrm{cm} \times 100\mathrm{nm} \times 0.1 \times 10^1 \mathrm{M}^{-1}\mathrm{cm}^{-1} \times 10^{12}\mathrm{cm}^{-2}\mathrm{s}^{-1}\mathrm{nm}^{-1}}$$
$$= 10^{-7}\mathrm{M}$$

which recovers our finding that S[IV] can accumulate to higher concentrations when present as HSO_3^- at lower pH, consistent with environmental chemistry studies (Li et al., 2012).

For the ocean, assuming efficient S[IV] chemical loss, $n = 1$, disproportionation dominates loss, and $F_{sinks,S[IV]} \approx d \times [S[IV]] T_{disp,0}^{-1}$. Then, we estimate

$$[S[IV]] \approx \frac{\phi_{SO_2}}{dT_{disp,0}^{-1}}$$
$$\approx \frac{3 \times 10^9 \mathrm{cm}^{-2} s^{-1}}{3 \times 10^5 \mathrm{cm} \times (3 \times 10^7 \mathrm{s})^{-1}}$$
$$= 3 \times 10^{11} \mathrm{cm}^{-3}$$
$$= 10^{-9} \mathrm{M}$$

which is the same order of magnitude as our detailed calculation (Figure 2, yellow curve, $\frac{\phi}{\phi_0} = 0$).

If on the other hand S[IV] chemical loss is inefficient, then photolysis dominates S[IV] loss, as in the lake case. However, unlike the lake case, for the ocean the optically thin assumption is not valid; at depth, every incident photon will be absorbed by either S[IV] or seawater in proportion to their spectral absorbances. We can therefore write $\phi_{SO_2} \approx \overline{\Phi_{S[IV]}}(\Delta\lambda\overline{\dot{E}(\lambda,0)})\frac{[S[IV]]\overline{\sigma_{S[IV]}}}{\overline{a_{ocean}}+[S[IV]]\overline{\sigma_{S[IV]}}}$

Solving for [S[IV]], we find

$$\begin{aligned}[S[IV]] &\approx \frac{\overline{a_{ocean}}}{\overline{\sigma_{S[IV]}}(\frac{\Delta\lambda\overline{\dot{E}(\lambda,0)}\overline{\Phi_{S[IV]}}}{\phi_{SO_2}}-1)} \\ &= \frac{10^{-3}cm^{-1}}{10^2M^{-1}cm^{-1}(\frac{80nm\times10^{12}cm^{-2}s^{-1}nm^{-1}\times0.2}{3\times10^9cm^{-2}s^{-1}}-1)} \\ &= 10^{-8}M\end{aligned}$$

which is the same order of magnitude as our detailed calculation (Figure 2, green curve, $\frac{\phi}{\phi_0}=0$).

The above calculations are not accurate, because they consider only a few of the relevant processes and because they neglect the spectral shapes of the relevant variables and their interplay, and one should not read too much into them. However, that the general conclusions extracted from them broadly agree with the more detailed, accurate model strengthen our confidence in the general findings from the more accurate model.

Data Set S1. The Excel file sulfite_solution_phase_raw_processed_data_v5.xlsx gives the raw data from the solution-phase analytics of the long-term S[IV] experiment, and shows the processing applied to these data to generate the information presented in Table 6 of the main text.

References

Anbar, A. D., & Holland, H. D. (1992, July). The photochemistry of manganese and

the origin of banded iron formations. *Geochim. Cosmochim. Acta,*, *56*(7), 2595-2603. doi: 10.1016/0016-7037(92)90346-K

Beyad, Y., Burns, R., Puxty, G., & Maeder, M. (2014). A speciation study of sulfur (iv) in aqueous solution. *Dalton Transactions*, *43*(5), 2147–2152.

Claire, M. W., Sheets, J., Cohen, M., Ribas, I., Meadows, V. S., & Catling, D. C. (2012, September). The Evolution of Solar Flux from 0.1 nm to 160 μm: Quantitative Estimates for Planetary Studies. *Astrophysical Journal*, *757*, 95. doi: 10.1088/0004-637X/757/1/95

Cockell, C. S. (2002, January). Photobiological uncertainties in the Archaean and post-Archaean world. *International Journal of Astrobiology*, *1*, 31-38. doi: 10.1017/S1473550402001003

de Carvalho, L. M., & Schwedt, G. (2000). Sulfur speciation by capillary zone electrophoresis: conditions for sulfite stabilization and determination in the presence of sulfate, thiosulfate and peroxodisulfate. *Fresenius' journal of analytical chemistry*, *368*(2), 208–213.

Fischer, M., & Warneck, P. (1996). Photodecomposition and photooxidation of hydrogen sulfite in aqueous solution. *The Journal of Physical Chemistry*, *100*(37), 15111–15117.

Guekezian, M., Coichev, N., Suárez-Iha, M. E. V., & Neves, E. d. A. (1997). Stability of sulfur (iv) solutions in the presence of amines and the tendency of sulfite ions to disproportionate in stock solutions. *Analytical letters*, *30*(7), 1423–1436.

Hu, R., Seager, S., & Bains, W. (2012, December). Photochemistry in Terrestrial Exoplanet Atmospheres. I. Photochemistry Model and Benchmark Cases. *Astrophysical*

Journal, *761*, 166. doi: 10.1088/0004-637X/761/2/166

Hutchins, R. S., Molina, P., Alajarin, M., Vidal, A., & Bachas, L. G. (1994). Use of a guanidinium ionophore in a hydrogen sulfite-selective electrode. *Analytical Chemistry*, *66*(19), 3188–3192.

Karchmer, J. H. (1970). *Analytical chemistry of sulfur and its compounds*. Wiley-Interscience.

Li, X., Ma, J., Liu, G., Fang, J., Yue, S., Guan, Y., ... Liu, X. (2012). Efficient reductive dechlorination of monochloroacetic acid by sulfite/uv process. *Environmental science & technology*, *46*(13), 7342–7349.

Lian, R., Oulianov, D. A., Crowell, R. A., Shkrob, I. A., Chen, X., & Bradforth, S. E. (2006). Electron photodetachment from aqueous anions. 3. dynamics of geminate pairs derived from photoexcitation of mono-vs polyatomic anions. *The Journal of Physical Chemistry A*, *110*(29), 9071–9078.

Mack, J., & Bolton, J. R. (1999). Photochemistry of nitrite and nitrate in aqueous solution: a review. *Journal of Photochemistry and Photobiology A: Chemistry*, *128*(1-3), 1–13.

Meyer, B., Mulliken, B., & Weeks, H. (1980a). The reactions of ammonia with excess sulfur dioxide. *Phosphorus and Sulfur and the Related Elements*, *8*(3), 291–299.

Meyer, B., Mulliken, B., & Weeks, H. (1980b). The reactions of sulfur dioxide with excess ammonia. *Phosphorus and Sulfur and the Related Elements*, *8*(3), 281–290.

Meyer, B., Peter, L., & Ospina, M. (1979, September). Geochemical and cosmochemical cycles involving sulfur, sulfide, sulfite and sulfate. *Geochim. Cosmochim. Acta,*, *43*(9), 1579-1582. doi: 10.1016/0016-7037(79)90152-2

Millero, F. J., Hershey, J. P., Johnson, G., & Zhang, J.-Z. (1989). The solubility of so2 and the dissociation of h2so3 in nacl solutions. *Journal of atmospheric chemistry*, *8*(4), 377–389.

Neta, P., & Huie, R. E. (1985). Free-radical chemistry of sulfite. *Environmental health perspectives*, *64*, 209.

Ranjan, S., Kufner, C. L., Lozano, G. G., Todd, Z. R., Haseki, A., & Sasselov, D. D. (2022, March). UV Transmission in Natural Waters on Prebiotic Earth. *Astrobiology*, *22*(3), 242-262. doi: 10.1089/ast.2020.2422

Ranjan, S., & Sasselov, D. D. (2017, March). Constraints on the Early Terrestrial Surface UV Environment Relevant to Prebiotic Chemistry. *Astrobiology*, *17*, 169-204. doi: 10.1089/ast.2016.1519

Ranjan, S., Seager, S., Zhan, Z., Koll, D. D. B., Bains, W., Petkowski, J. J., ... Lin, Z. (2022, May). Photochemical Runaway in Exoplanet Atmospheres: Implications for Biosignatures. *Astrophys. J.,*, *930*(2), 131. doi: 10.3847/1538-4357/ac5749

Rugheimer, S., Segura, A., Kaltenegger, L., & Sasselov, D. (2015, June). UV Surface Environment of Earth-like Planets Orbiting FGKM Stars through Geological Evolution. *Astrophysical Journal*, *806*, 137. doi: 10.1088/0004-637X/806/1/137

Sauer, M. C., Crowell, R. A., & Shkrob, I. A. (2004). Electron photodetachment from aqueous anions. 1. quantum yields for generation of hydrated electron by 193 and 248 nm laser photoexcitation of miscellaneous inorganic anions. *The Journal of Physical Chemistry A*, *108*(25), 5490–5502.

Searcy, A. W. (1981). *Materials and molecular research division. annual report 1980* (Tech. Rep.). Lawrence Berkeley National Laboratory. Retrieved from `https://`

escholarship.org/uc/item/71d1h52c

Smith, R. C., & Baker, K. S. (1981). Optical properties of the clearest natural waters (200–800 nm). *Applied optics*, *20*(2), 177–184.

Toner, J. D., & Catling, D. C. (2020). A carbonate-rich lake solution to the phosphate problem of the origin of life. *Proceedings of the National Academy of Sciences*, *117*(2), 883–888.

Vincent, L., Colón-Santos, S., Cleaves, H. J., Baum, D. A., & Maurer, S. E. (2021). The prebiotic kitchen: A guide to composing prebiotic soup recipes to test origins of life hypotheses. *Life*, *11*(11), 1221.

Walton, C. R., Rimmer, P., & Shorttle, O. (2022, December). Can prebiotic systems survive in the wild? An interference chemistry approach. *Frontiers in Earth Science*, *10*, 1011717. doi: 10.3389/feart.2022.1011717

Zafiriou, O. C., & True, M. B. (1979). Nitrate photolysis in seawater by sunlight. *Marine Chemistry*, *8*(1), 33–42.

do not specify file extension

Notes

1. But not identical; care must be taken with the specific radiative quantity compared (Ranjan & Sasselov, 2017)

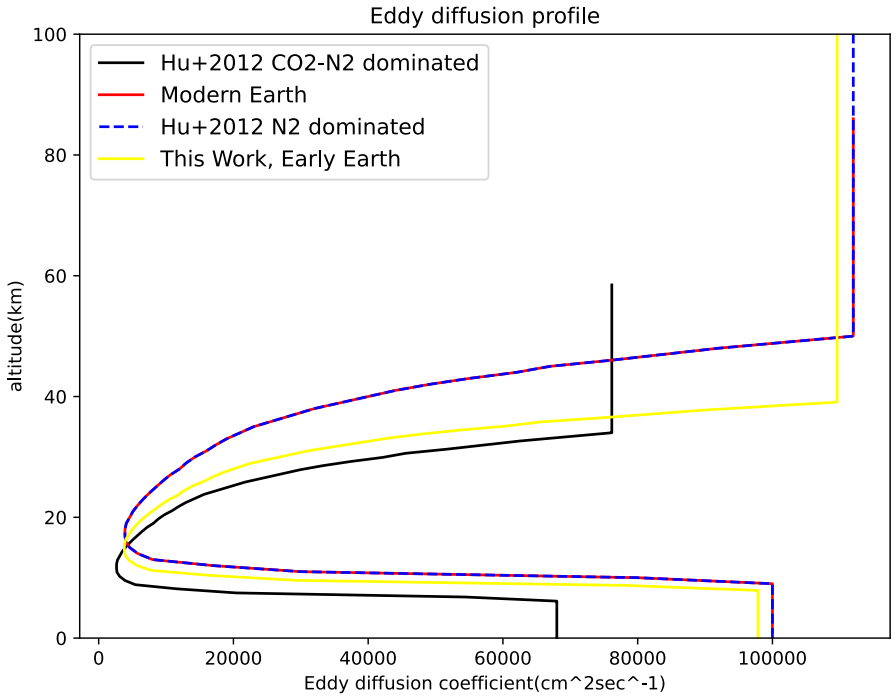

Figure S1. Eddy diffusion profile assumed in the photochemical calculation. Also shown for context are modern Earth eddy diffusion profile, and the eddy diffusion profiles in the Hu et al. (2012) CO_2-N_2 and N_2-dominated benchmark scenarios.

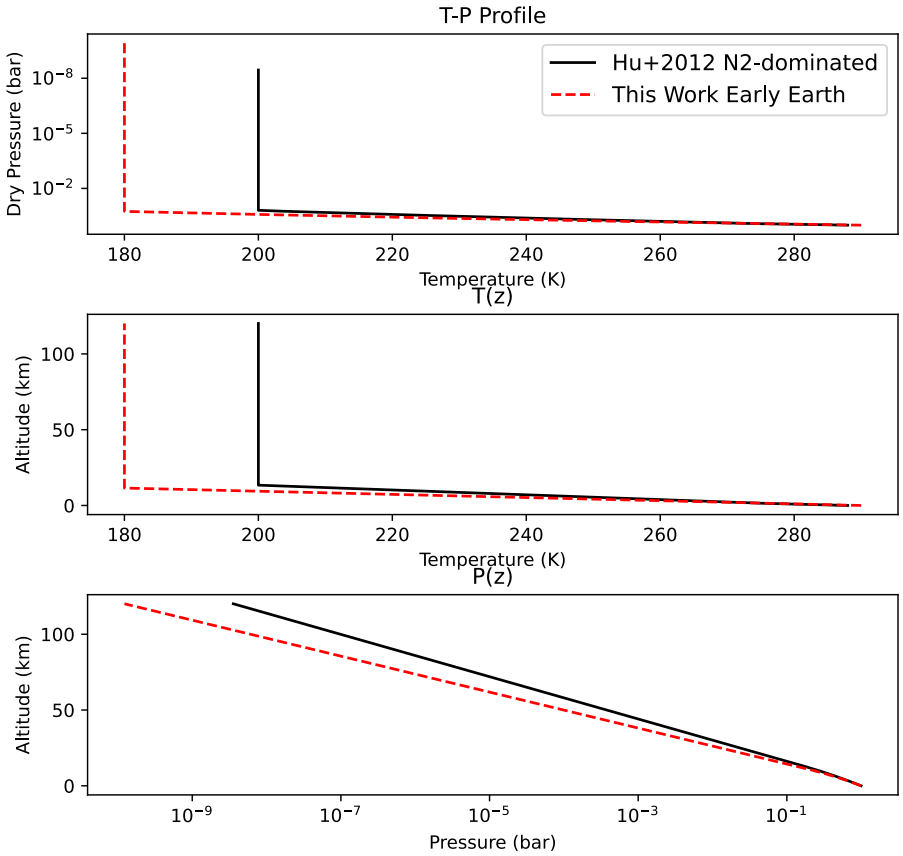

Figure S2. Temperature-pressure profile assumed in the photochemical calculation. Also shown for context is the temperature-pressure profile for the Hu et al. (2012) N_2-dominated benchmark scenario.

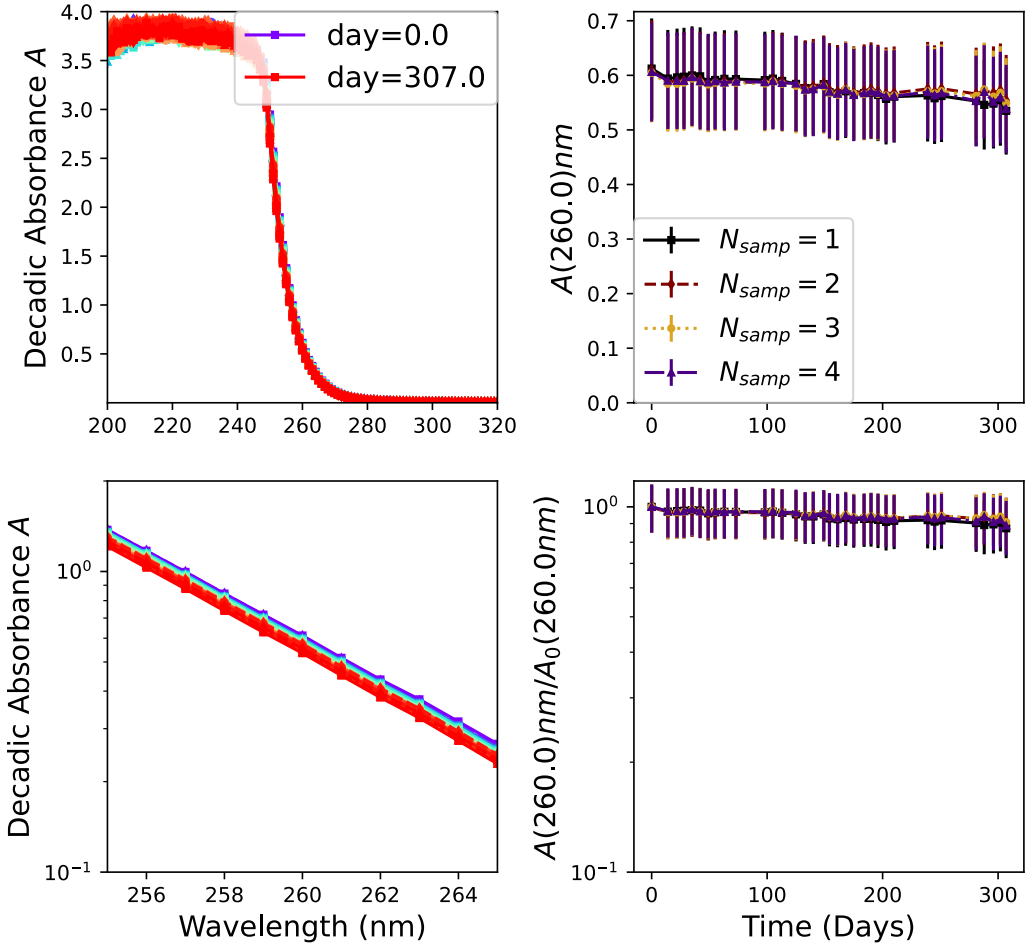

Figure S3. UV-VIS tracking of the 100 mM S[IV], $pH_0 = 7$ samples. Upper left: decadic absorbances (A) measured from the samples. The colorscale is rainbow, with more purple colors corresponding to earlier times and more red colors corresponding to later times. The different samples are demarcated with different linestyles, but are challenging to distinguish by eye. Error bars are omitted for clarity. Lower left: same as upper left, but zoomed in to the wavelength region around 260 nm, where A responds linearly to changes in concentration. Upper right: absorbance at 260 nm specifically as a function of time for the different samples at this experimental condition. In this plot, it is possible to distinguish the different samples; to facilitate this differentiation, in addition to different linestyles they are assigned different colors, which do not correspond to the color scheme of the left column. Lower right: same as upper right, except the absorbances are normalized to the absorbance on day 0 (showing relative change). This experimental condition shows very little change over 10 months, consistent with the solution analytics.

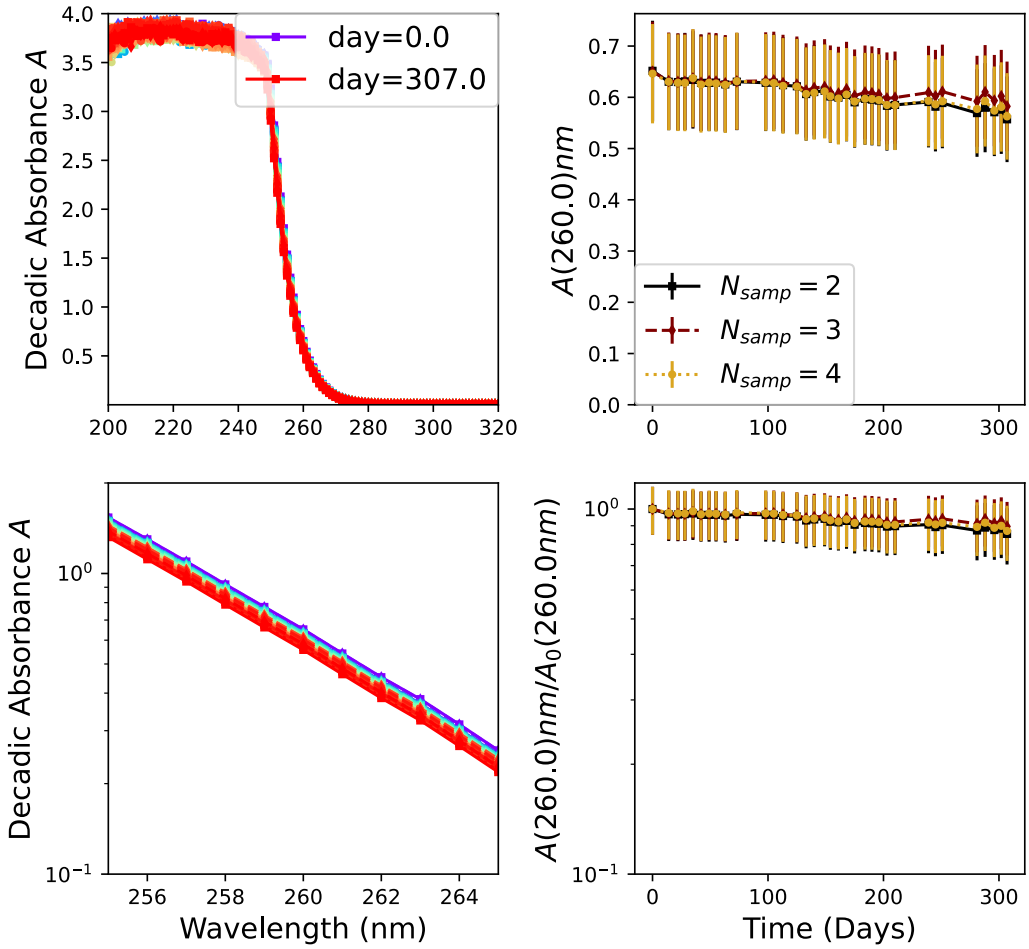

Figure S4. UV-VIS tracking of the 100 mM S[IV], pH-unadjusted samples. Upper left: decadic absorbances (A) measured from the samples. The colorscale is rainbow, with more purple colors corresponding to earlier times and more red colors corresponding to later times. The different samples are demarcated with different linestyles, but are challenging to distinguish by eye. Error bars are omitted for clarity. Lower left: same as upper left, but zoomed in to the wavelength region around 260 nm, where A responds linearly to changes in concentration. Upper right: absorbance at 260 nm as a function of time for the different samples at this experimental condition. In this plot, it is possible to distinguish the different samples; to facilitate this differentiation, in addition to different linestyles they are assigned different colors, which do not correspond to the color scheme of the left column. Lower right plot: same as upper right, except the absorbances are normalized to the absorbance on day 0 (showing relative change). This experimental condition shows very little change over 10 months, consistent with the solution analytics.

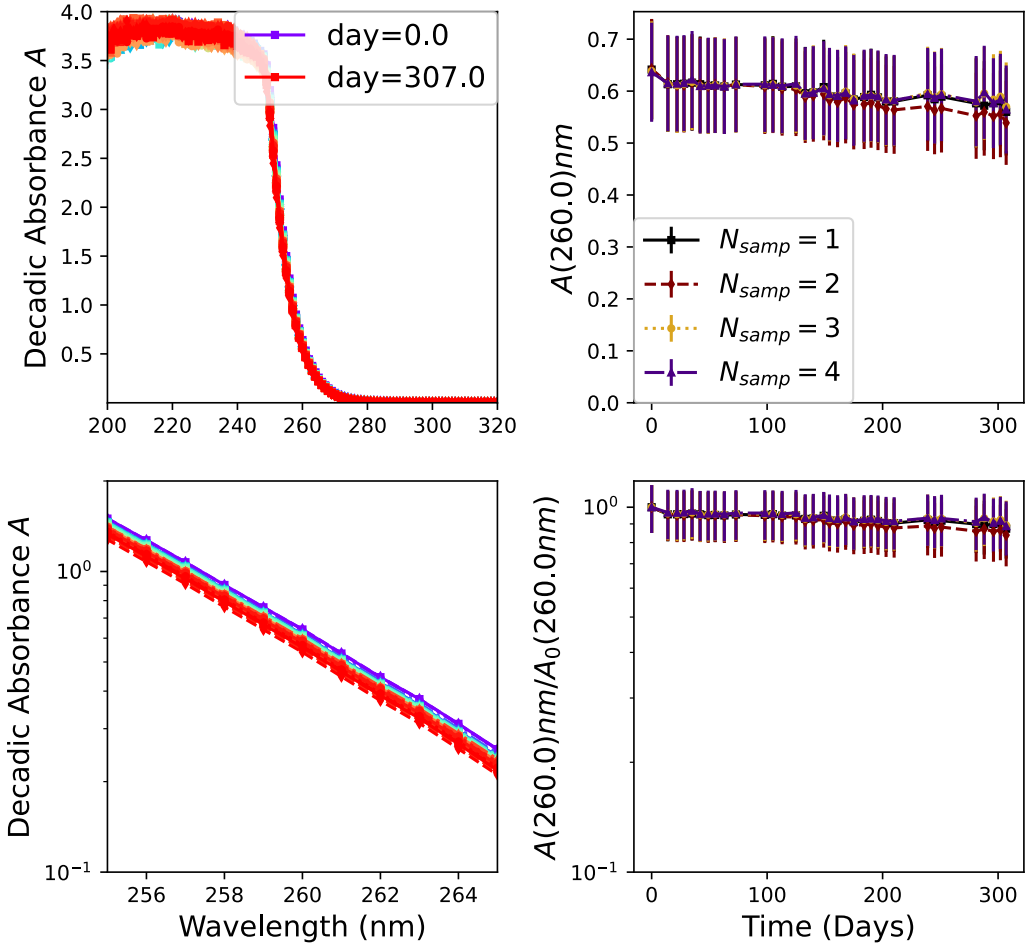

Figure S5. UV-VIS tracking of the 100 mM S[IV], $pH_0 = 13$ samples. Upper left plot: decadic absorbances (A) measured from the samples. The colorscale is rainbow, with more purple colors corresponding to earlier times and more red colors corresponding to later times. The different samples are demarcated with different linestyles, but are challenging to distinguish by eye. Error bars are omitted for clarity. Lower left: same as upper left, but zoomed in to the wavelength region around 260 nm, where A responds linearly to changes in concentration. Upper right: absorbance at 260 nm as a function of time for the different samples at this experimental condition. In this plot, it is possible to distinguish the different samples; to facilitate this differentiation, in addition to different linestyles they are assigned different colors, which do not correspond to the color scheme of the left column. Lower right: same as upper right, except the absorbances are normalized to the absorbance on day 0 (showing relative change). This experimental condition shows very little change over 10 months, consistent with the solution analytics but inconsistent with Guekezian et al. (1997).

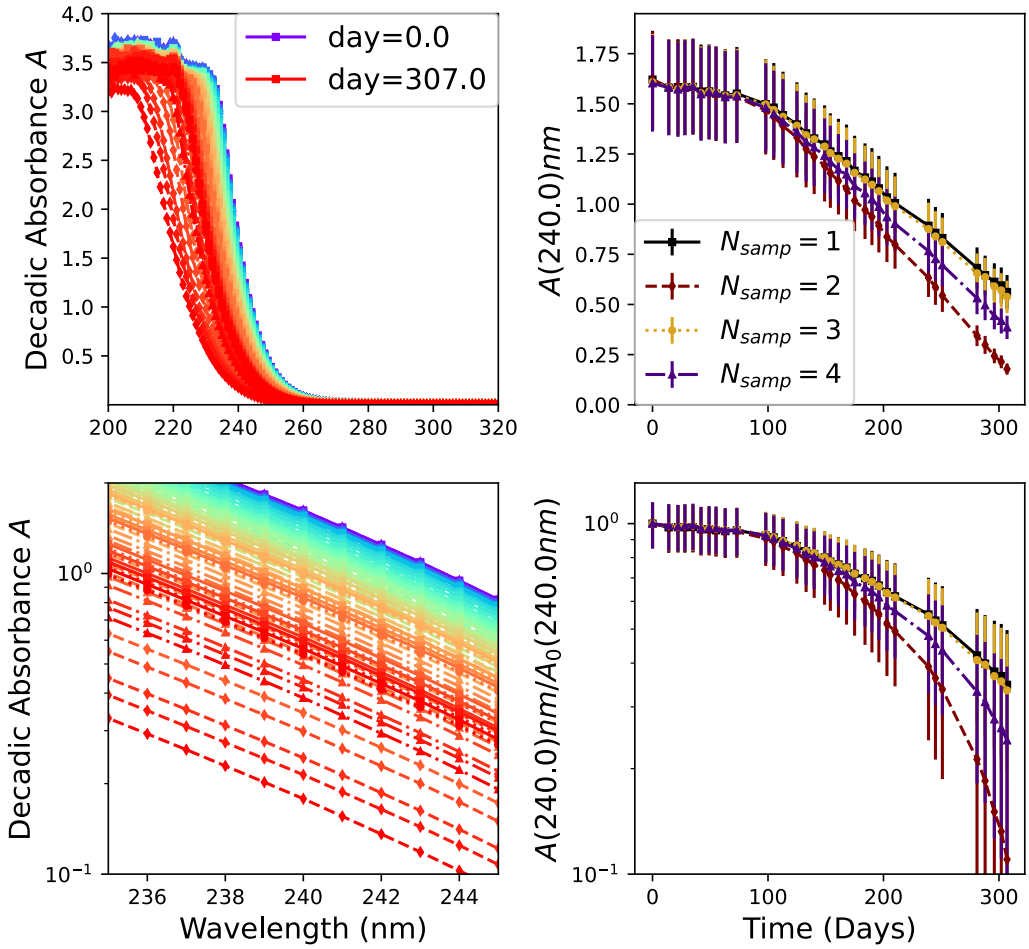

Figure S6. UV-VIS tracking of 10 mM S[IV], pH-unadjusted samples. Upper left: decadic absorbances (A) measured from the samples. The colorscale is rainbow, with more purple colors corresponding to earlier times and more red colors corresponding to later times. The different samples are demarcated with different linestyles, but are challenging to distinguish by eye. Error bars are omitted for clarity. Lower left plot: same as upper left, but zoomed in to the wavelength region around 240 nm, where A responds linearly to changes in concentration. Upper right: absorbance at 240 nm as a function of time for the samples at this experimental condition. In this plot, it is possible to distinguish the different samples; to facilitate this differentiation, in addition to different linestyles they are assigned different colors, which do not correspond to the color scheme of the left column. Lower right plot: same as upper right, except the absorbances are normalized to the absorbance on day 0 (showing relative change). This experimental condition shows significant change over 10 months. Samples 1, 3 and 4 are consistent with solution-phase analytics. Sample 2 indicates an absorbance that is a factor of ~ 3 lower than expected based

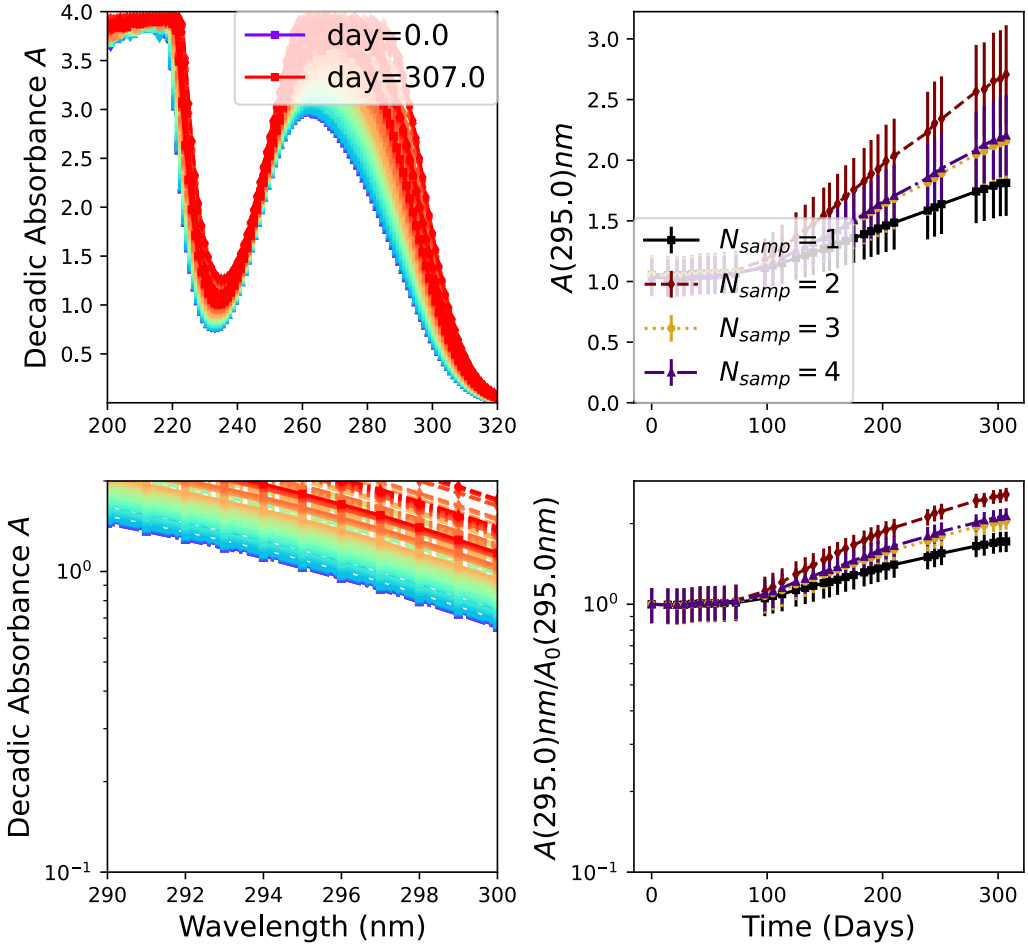

Figure S7. UV-VIS tracking of the 100 mM S[IV], $pH_0 = 4$ samples. Upper left: decadic absorbances (A) measured from the samples. The colorscale is rainbow, with more purple colors corresponding to earlier times and more red colors corresponding to later times. The different samples are demarcated with different linestyles, but are challenging to distinguish by eye. Error bars are omitted for clarity. Lower left: same as upper left, but zoomed in to the wavelength region around 295 nm, where A responds linearly to changes in concentration. Upper right: absorbance at 295 nm specifically as a function of time for the different samples. In this plot, it is possible to distinguish the samples; to facilitate this differentiation, in addition to different linestyles they are assigned different colors, which do not correspond to the color scheme of the left column. Lower right plot: same as upper right, except the absorbances are normalized to the absorbance on day 0 (showing relative change). This experimental condition shows different UV-VIS evolution than the non-acidic conditions, with an increase in absorbance with time and more rapid change. This different behaviour potentially aligns with reports indicating more efficient

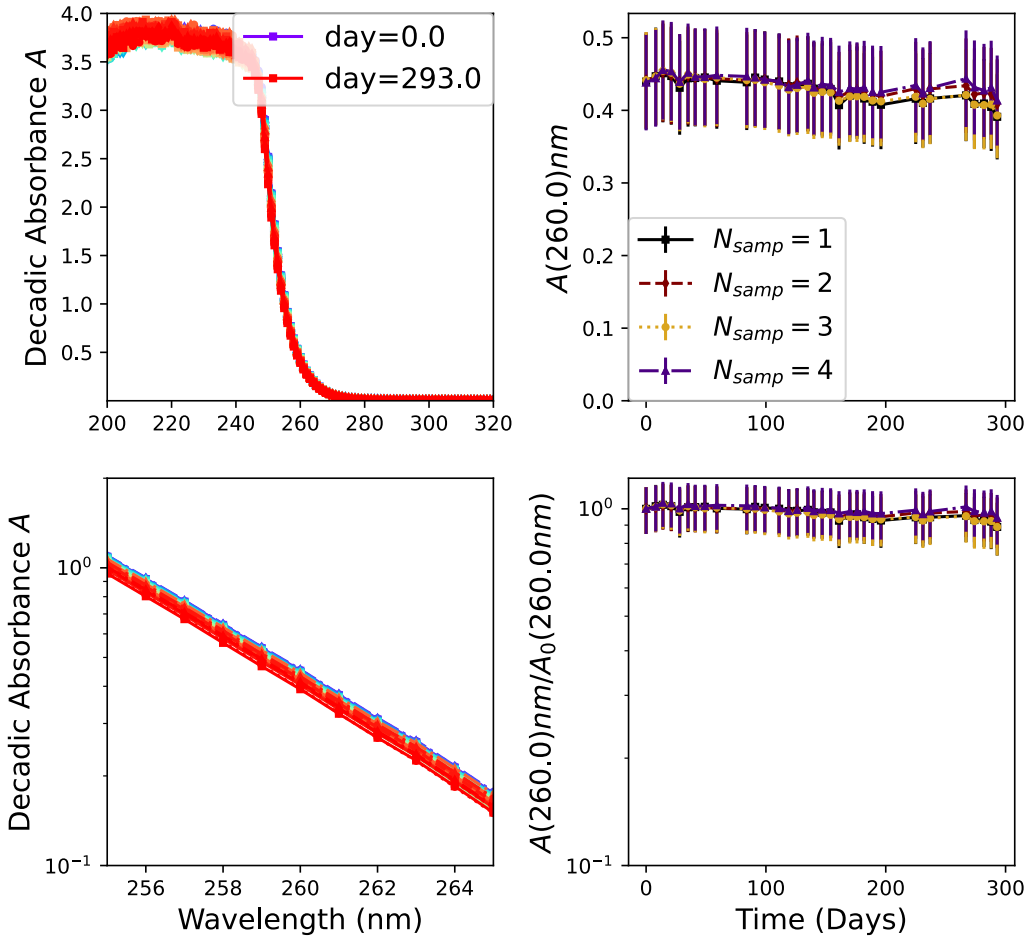

Figure S8. UV-VIS tracking of the 100 mM S[IV] samples in the low-concentration carbonate lake sensitivity test. Upper left: decadic absorbances (A) measured from the samples. The colorscale is rainbow, with more purple colors corresponding to earlier times and more red colors corresponding to later times. The different samples are demarcated with different linestyles, but are challenging to distinguish by eye. Error bars are omitted for clarity. Lower left: same as upper left, but zoomed in to the wavelength region around 260 nm, where A responds linearly to changes in concentration. Upper right: absorbance at 260 nm specifically as a function of time for the different samples. In this plot, it is possible to distinguish the samples; to facilitate this differentiation, in addition to different linestyles they are assigned different colors, which do not correspond to the color scheme of the left column. Lower right plot: same as upper right, except the absorbances are normalized to the absorbance on day 0 (showing relative change). This experimental condition behaves similarly to the non-acidic pH pure water experimental condition.

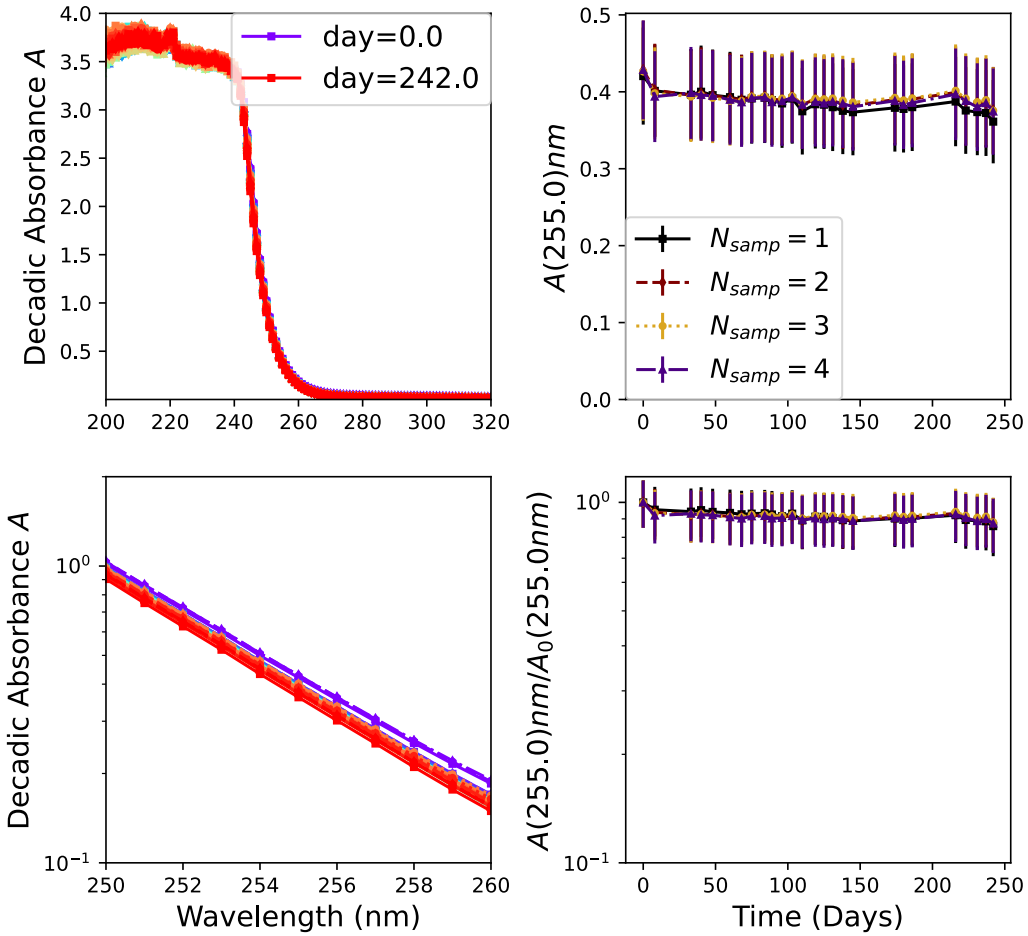

Figure S9. UV-VIS tracking of the 100 mM S[IV] samples in the high-concentration carbonate lake sensitivity test. Upper left: decadic absorbances (A) measured from the samples. The colorscale is rainbow, with more purple colors corresponding to earlier times and more red colors corresponding to later times. The different samples are demarcated with different linestyles, but are challenging to distinguish by eye. Error bars are omitted for clarity. Lower left: same as upper left, but zoomed in to the wavelength region around 255 nm, where A responds linearly to changes in concentration. Upper right: absorbance at 255 nm specifically as a function of time for the different samples. In this plot, it is possible to distinguish the samples; to facilitate this differentiation, in addition to different linestyles they are assigned different colors, which do not correspond to the color scheme of the left column. Lower right plot: same as upper right, except the absorbances are normalized to the absorbance on day 0 (showing relative change). This experimental condition behaves similarly to the non-acidic pH pure water experimental condition.

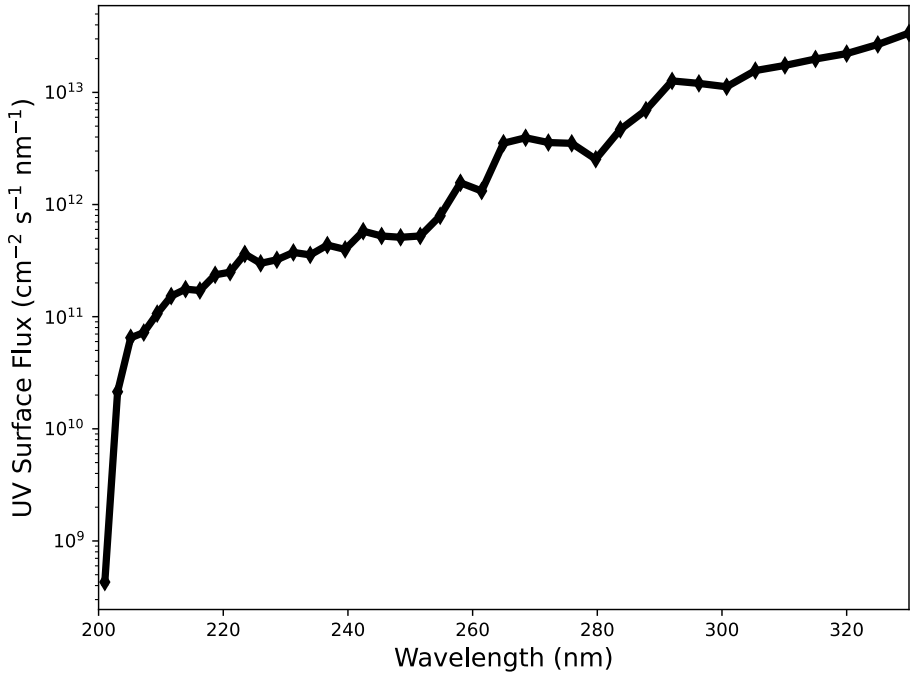

Figure S10. Surface UV irradiation (base of the atmosphere, but just above the water column). From (Ranjan & Sasselov, 2017), with atmospheric composition and conditions from Rugheimer et al. (2015).

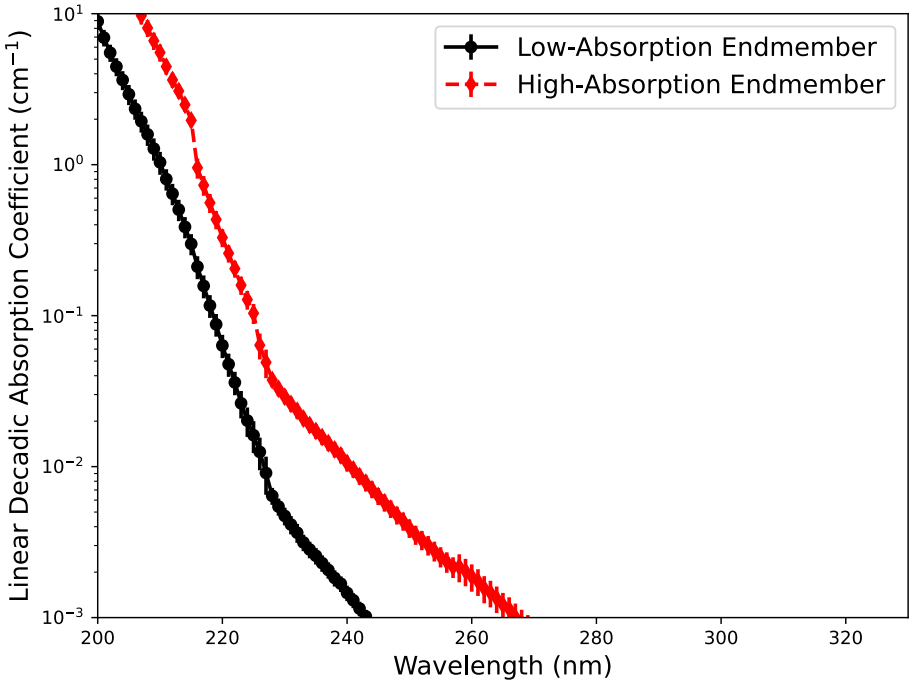

Figure S11. Low- and high-absorption endmember linear decadic absorption coefficients for the prebiotic ocean. Modified from Ranjan, Kufner, et al. (2022), with S[IV] species removed.

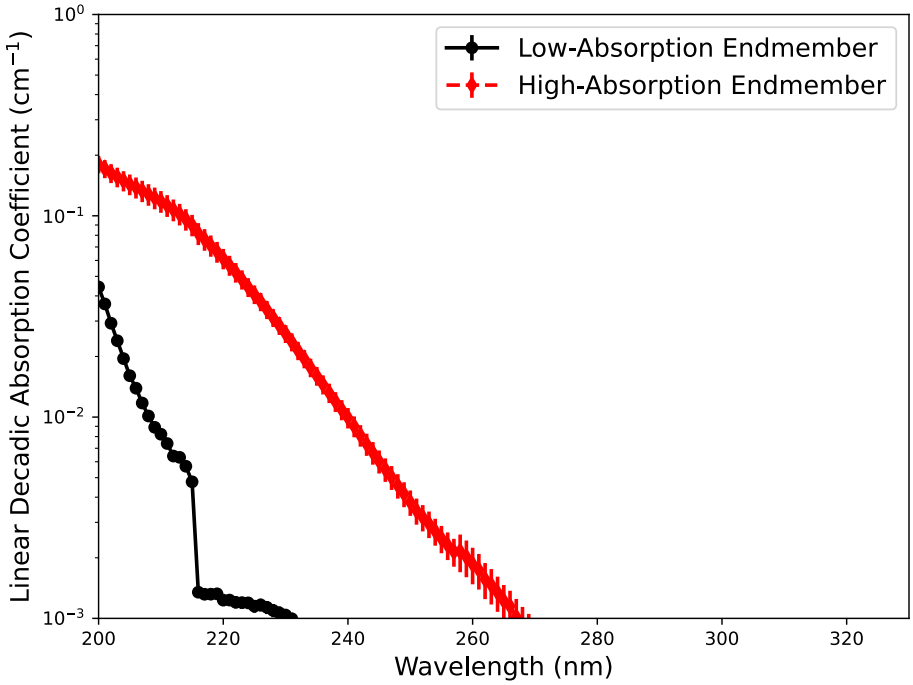

Figure S12. Low- and high-absorption endmember linear decadic absorption coefficients for prebiotic carbonate lakes. Modified from Ranjan, Kufner, et al. (2022), with S[IV] species removed.

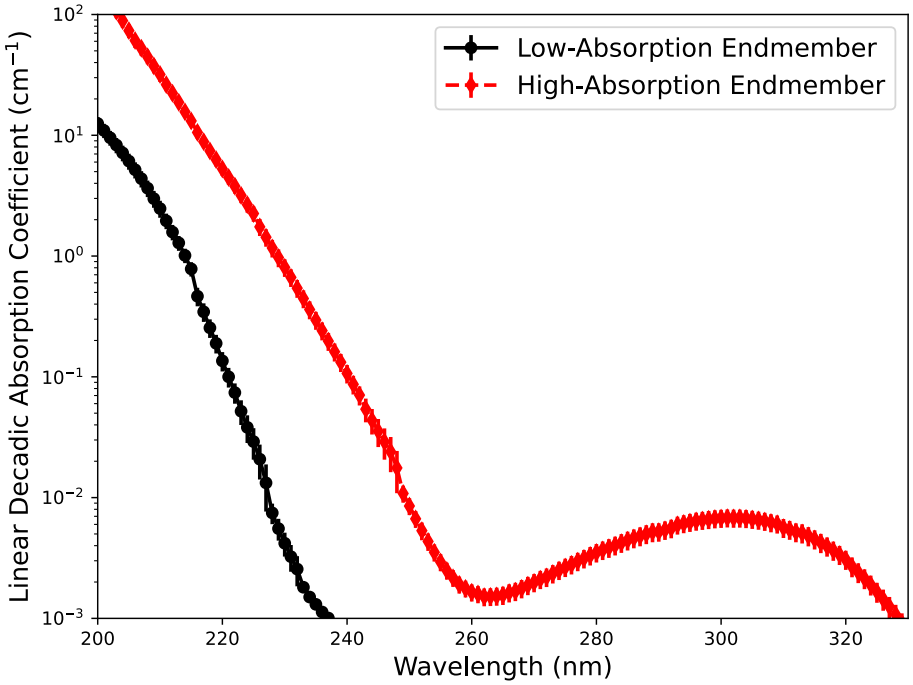

Figure S13. Low- and high-absorption endmember linear decadic absorption coefficients for prebiotic carbonate lakes. Modified from Ranjan, Kufner, et al. (2022), with S[IV] species removed.

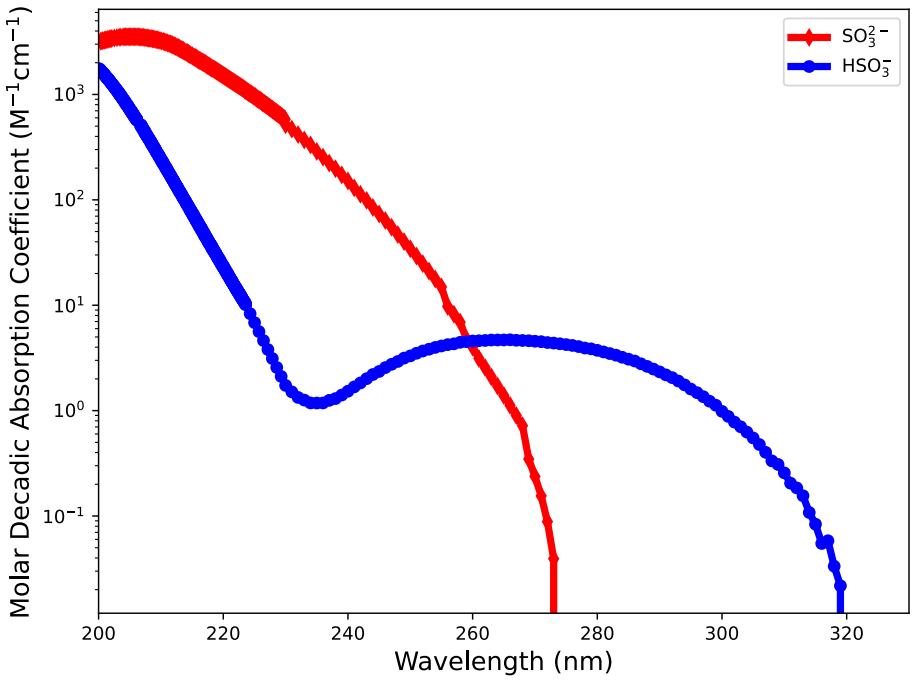

Figure S14. Absorption spectra of SO_3^{2-} and HSO_3^-, synthesized by Ranjan, Kufner, et al. (2022) from Fischer and Warneck (1996) and Beyad et al. (2014).

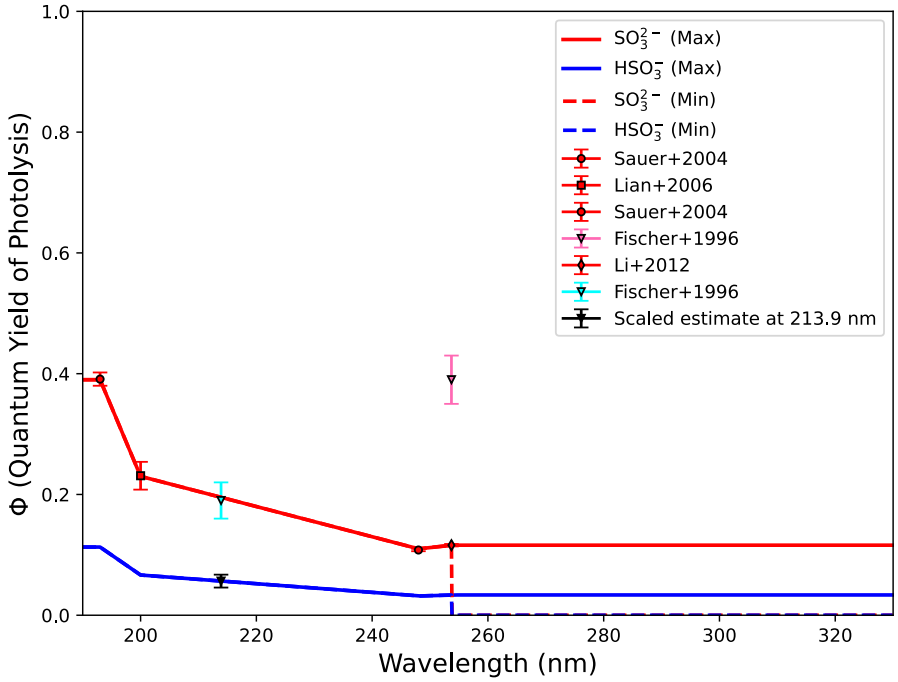

Figure S15. Prescribed S[IV] net photolysis quantum yields used in this work. The solid lines show the prescriptions assuming $\Phi(> 254\text{nm}) = \Phi(254\text{nm})$ (Max), and the dashed lines show the prescriptions assuming $\Phi(> 254\text{nm}) = 0$ (Min), which should span the uncertainty on $\Phi(> 254\text{nm})$. The red points indicate available experimental constraints on $\Phi_{SO_3^{2-}}$, which we extrapolate between to construct the prescription (Sauer et al., 2004; Lian et al., 2006; Li et al., 2012). The cyan and pink points indicate the upper bounds on $\Phi_{SO_3^{2-}}(254\text{nm})$ and $\Phi_{HSO_3^-}(214\text{nm})$ used to estimate $\Phi_{HSO_3^-}(214\text{nm})$ (black point). Overall, the quantum yields of S[IV] photolysis and especially bisulfite photolysis are extremely poorly constrained and should be prioritized for future study.

Table S1. Simulation Parameters For Planetary Scenario.

Parameter	Value
Reaction Network	As in Ranjan, Seager, et al. (2022). Excludes $C_{>2}$-chem
Stellar Irradiation	3.9 Ga Sun (Claire et al., 2012)
Semi-major axis	1 AU
Planet size	1 $M_\oplus$, 1 $R_\oplus$
Surface albedo	0.
Major atmospheric components	0.1 bar CO_2, 0.9 bar N_2
Surface temperature	290
Surface r_{H_2O} (lowest atmospheric bin)	0.01
Eddy Diffusion Profile	See Figure S1
Temperature-Pressure Profile	See Figure S2
Vertical Resolution	0-90 km, 1.8 km steps
Rainout	Earthlike; rainout turned off for H_2, CO, CH_4, NH_3, N_2, C_2H_2, C_2H_4, C_2H_6, and O_2 to simulate saturated ocean on abiotic planet
Atmospheric Redox Balance Checked	Yes
Global Redox Conservation Enforced	No

Table S2. Detailed species-by-species boundary conditions for photochemical modeling.

Species	Type[1]	Surface Flux[2] (cm^{-2} s^{-1})	Surface Mixing Ratio[2] *(relative to CO_2+N_2)*	v_{dep} (cm s^{-1})	TOA Flux[3] (cm^{-2} s^{-1})
N_2	C	–	0.9	0	0
CO_2	X	–	0.1	0	0
H_2O	X	–	0.01	0	0
NO	X	3E8	–	0.02	0
CO	X	$3E8+4E8\times\frac{\phi}{\phi_0}$	–	1×10^{-8}	0
CH_4	X	$3E8\times\frac{\phi}{\phi_0}$	–	0	0
SO_2	X	$3E9\times\frac{\phi}{\phi_0}$	–	1	0
H_2S	X	$3E8\times\frac{\phi}{\phi_0}$	–	0.015	0
H_2	X	$5E9\times\frac{\phi}{\phi_0}$	–	0	Diffusion-limited
H	X	0	–	1	Diffusion-limited
O	X	0	–	1	0
O(1D)	X	0	–	0	0
O_2	X	0	–	0	0
O_3	X	0	–	0.4	0

[1]"X": full continuity-diffusion equation is solved for the species."A" aerosol species; "C": chemically inert.

[2]For the bottom boundary condition, either a surface flux is specified, or a surface mixing ratio.

[3]TOA flux refers to the magnitude of outflow at the top-of-the-atmosphere (TOA). A negative number corresponds to an inflow.

Continuation of Table S2

Species	Type[1]	Surface Flux[2] (cm^{-2} s^{-1})	Surface Mixing Ratio[2] *(relative to CO_2+N_2)*	v_{dep} (cm s^{-1})	TOA Flux[3] (cm^{-2} s^{-1})
OH	X	0	–	1	0
HO_2	X	0	–	1	0
H_2O_2	X	0	–	0.5	0
CH_2O	X	0	–	0.1	0
CHO	X	0	–	0.1	0
C	X	0	–	0	0
CH	X	0	–	0	0
CH_2	X	0	–	0	0
$^1CH_2$	X	0	–	0	0
$^3CH_2$	X	0	–	0	0
CH_3	X	0	–	0	0
CH_3O	X	0	–	0.1	0
CH_4O	X	0	–	0.1	0
CHO_2	X	0	–	0.1	0
CH_2O_2	X	0	–	0.1	0
CH_3O_2	X	0	–	0	0
CH_4O_2	X	0	–	0.1	0
C_2	X	0	–	0	0
C_2H	X	0	–	0	0
C_2H_2	X	0	–	0	0
C_2H_3	X	0	–	0	0
C_2H_4	X	0	–	0	0
C_2H_5	X	0	–	0	0
C_2H_6	X	0	–	1×10^{-5}	0
C_2HO	X	0	–	0	0
C_2H_2O	X	0	–	0.1	0
C_2H_3O	X	0	–	0.1	0
C_2H_4O	X	0	–	0.1	0
C_2H_5O	X	0	–	0.1	0
S	X	0	–	0	0
S_2	X	0	–	0	0
S_3	X	0	–	0	0
S_4	X	0	–	0	0
SO	X	0	–	0	0
$^1SO_2$	X	0	–	0	0
$^3SO_2$	X	0	–	0	0
HS	X	0	–	0	0
HSO	X	0	–	0	0
HSO_2	X	0	–	0	0
HSO_3	X	0	–	0.1	0
HSO_4	X	0	–	1	0
H_2SO_4(A)	A	0	–	0.2	0
S_8	X	0	–	0	0

Continuation of Table S2					
Species	Type[1]	Surface Flux[2] (cm^{-2} s^{-1})	Surface Mixing Ratio[2] *(relative to CO_2+N_2)*	v_{dep} (cm s^{-1})	TOA Flux[3] (cm^{-2} s^{-1})
S_8(A)	A	0	–	0.2	0
OCS	X	0	–	0.01	0
CS	X	0	–	0.01	0
CH_3S	-	0	–	0.01	0
CH_4S	-	0	–	0.01	0

Table S3. Surface mixing ratio and wet deposition of SO_2 as a function of volcanic emission flux

$\frac{\phi}{\phi_0}$	ϕ_{SO_2} cm^{-2} s^{-1}	$r_{SO_2}(z=0)$	SO_2 wet deposition flux cm^{-2} s^{-1}
0.1	3×10^8	7×10^{-12}	3×10^7
0.3	9×10^8	2×10^{-11}	9×10^7
1	3×10^9	1×10^{-10}	4×10^8
3	9×10^9	3×10^{-10}	2×10^9
10	3×10^{10}	1×10^{-9}	5×10^9
30	9×10^{10}	3×10^{-9}	1×10^{10}

Table S4. Analytics of Discarded Aged S[IV] Sample

$[Na_2SO_3]_0^{\dagger}$ (mM)	$pH_0^{\dagger}$	Sample	$[SO_3^{2-}]_{f,tot}^{\ddagger,a}$ (mM)	$[SO_4^{2-}]_f^{\ddagger,b}$ (mM)	λ_m nm	$\frac{A_{\lambda_m,f}}{A_{\lambda_m,0}}$ ★
10	Unadjusted	2	3.4 ± 0.2	5.5 ± 0.2	240	0.11 ± 0.02

†Sample preparation (10/5/2021)
‡Cuvettes opened 8/20/2022
^{a}Electropotentiometry
^{b}Gravimetry
★UV-VIS last day 8/8/2022

Table S5. Construction of dilute carbonate lake solution sensitivity test.

Salt	Mass[a]	Na^+	K^+	Ca^{2+}	Mg^{2+}	Cl^-	Br^-	I^-	NO_3^-	PO_4^{3-}	B	SO_4^{2-}	S^{2-}+HS^-	CO_3^{2-}+HCO_3^-	SO_3^{2-}+HS
	(mg)	(M)	(M)	(M)	(M)	(M)	(M)	(M)	(M)	(M)	(M)	(M)	(M)	(M)	(M)
NaCl	116.88	0.1	0	0	0	0.1	0	0	0	0	0	0	0	0	0
KCl	44.73	0	0.03	0	0	0.03	0	0	0	0	0	0	0	0	0
$CaCl_2 \cdot 6H_2O$	0.44	0	0	1×10^{-4}	0	2×10^{-4}	0	0	0	0	0	0	0	0	0
$MgCl_2$	0.02	0	0	0	1×10^{-5}	2×10^{-5}	0	0	0	0	0	0	0	0	0
NaBr	2.06	1×10^{-3}	0	0	0	0	1×10^{-3}	0	0	0	0	0	0	0	0
NaI	1.2×10^{-4}	4×10^{-8}	0	0	0	0	0	4×10^{-8}	0	0	0	0	0	0	0
$NaNO_3$	8.5×10^{-6}	5×10^{-9}	0	0	0	0	0	0	5×10^{-9}	0	0	0	0	0	0
Na_2HPO_4	28.39	2×10^{-2}	0	0	0	0	0	0	0	1×10^{-2}	0	0	0	0	0
$Na_2B_4O_7$	4.02	2×10^{-3}	0	0	0	0	0	0	0	0	4×10^{-3}	0	0	0	0
Na_2SO_4	852.24	6×10^{-1}	0	0	0	0	0	0	0	0	0	3×10^{-1}	0	0	0
$Na_2S{\cdot}6H_2O$	4×10^{-5}	1.6×10^{-8}	0	0	0	0	0	0	0	0	0	0	8×10^{-9}	0	0
$NaHCO_3$	84.01	5×10^{-2}	0	0	0	0	0	0	0	0	0	0	0	5×10^{-2}	0
Na_2SO_3	252.08	2×10^{-1}	0	0	0	0	0	0	0	0	0	0	0	0	$1 \times 10^{-}$
Total		9.7×10^{-1}	3×10^{-2}	1×10^{-4}	1×10^{-5}	1.3×10^{-1}	1×10^{-3}	4×10^{-8}	5×10^{-9}	1×10^{-2}	4×10^{-3}	3×10^{-1}	8×10^{-9}	5×10^{-2}	$1 \times 10^{-}$

[a] Salts were added to 20 mL H_2O, and solution was adjusted to pH=9. No solids were observed after preparation.

Table S6. Construction of concentrated carbonate lake solution sensitivity test.

Salt	Mass[a]	Na^+	K^+	Ca^{2+}	Mg^{2+}	Cl^-	Br^-	I^-	NO_3^-	PO_4^{3-}	B	SO_4^{2-}	S^{2-}+HS^-	CO_3^{2-}+HCO_3^-	SO_3^{2-}+HSO_3^-
	(mg)	(M)	(M)	(M)	(M)	(M)	(M)	(M)	(M)	(M)	(M)	(M)	(M)	(M)	(M)
NaCl	2337.60	2.0	0	0	0	2.0	0	0	0	0	0	0	0	0	0
KCl	447.30	0	0.3	0	0	0.3	0	0	0	0	0	0	0	0	0
$CaCl_2 \cdot 6H_2O$	0.44	0	0	1×10^{-4}	0	2×10^{-4}	0	0	0	0	0	0	0	0	0
$MgCl_2$	0	0	0	0	0	0	0	0	0	0	0	0	0	0	0
NaBr	20.58	1×10^{-2}	0	0	0	0	1×10^{-2}	0	0	0	0	0	0	0	0
NaI	1.8×10^{-3}	6×10^{-7}	0	0	0	0	0	6×10^{-7}	0	0	0	0	0	0	0
$NaNO_3$	1.70	1×10^{-3}	0	0	0	0	0	0	1×10^{-3}	0	0	0	0	0	0
Na_2HPO_4	28.39	2×10^{-2}	0	0	0	0	0	0	0	1×10^{-2}	0	0	0	0	0
$Na_2B_4O_7$[b]	1207.32	0.6	0	0	0	0	0	0	0	0	1.2	0	0	0	0
Na_2SO_4	2840.80	2.0	0	0	0	0	0	0	0	0	0	1.0	0	0	0
$Na_2S{\cdot}6H_2O$	5×10^{-3}	2×10^{-6}	0	0	0	0	0	0	0	0	0	0	1×10^{-6}	0	0
$NaHCO_3$	168.02	1×10^{-1}	0	0	0	0	0	0	0	0	0	0	0	1×10^{-1}	0
Na_2SO_3	252.08	2×10^{-1}	0	0	0	0	0	0	0	0	0	0	0	0	1×10^{-1}
Total		4.93	3×10^{-1}	1×10^{-4}	0	2.3	1×10^{-2}	6×10^{-7}	1×10^{-3}	1×10^{-2}	1.20	1.00	1×10^{-6}	1×10^{-1}	1×10^{-1}

[a] Salts were added to 20 mL H_2O, and solution was adjusted to pH=7. Solids were observed after preparation, which we attribute to $Na_2B_4O_7$.

[b] Based on $Na_2B_4O_7$ solubility at 20°C.